Dynamics of Water and Hydrated Protons in Confinement

ISBN 978-90-801704-0-7

Cover design: Liyuan Liu

Dynamics of Water and Hydrated Protons in Confinement

ACADEMISCH PROEFSCHRIFT

ter verkrijging van de graad van doctor
aan de Universiteit van Amsterdam
op gezag van de Rector Magnificus
prof. dr. D. C. van den Boom
ten overstaan van een door het college voor promoties ingestelde
commissie, in het openbaar te verdedigen in de Agnietenkapel
op woensdag 28 oktober 2015, te 12:00 uur

door

Liyuan Liu
刘立媛

geboren te China

Promotiecommissie

Promotor:	prof. dr. H. J. Bakker
Overige leden:	dr. E. H. G. Backus
	prof. dr. A.M. Brouwer
	prof. dr. E.J. Meijer
	dr. Y. L. A. Rezus
	prof. dr. V. Subramaniam
	prof. dr. S. Woutersen

Faculteit der Natuurwetenschappen, Wiskunde en Informatica

The work described in this thesis was performed at the FOM Institute AMOLF, Science Park 104, 1098 XG Amsterdam, The Netherlands. This work is part of the research programme of the *Stichting Fundamenteel Onderzoek der Materie* (FOM), which is financially supported by the *Nederlandse Organisatie voor Wetenschappelijk Onderzoek* (NWO).

Voor Zhe en Peihan

This thesis is based on the following publications:

L. Liu, J. Hunger, and H. J. Bakker, Energy Relaxation Dynamics of the Hydration Complex of Hydroxide. *J. Phys. Chem. A 115*, 14593-14598 (2011). *(Chapter 4)*

L. Liu, and H. J. Bakker, Infrared-Activated Proton Transfer in Aqueous Nafion Proton Exchange Membrane Nanochannels. *Phys. Rev. Lett. 112*, 258301 (2014). *(Chapter 5)*

L. Liu, and H. J. Bakker, Vibrational Excitation Induced Proton Transfer in Hydrated Nafion Membranes. *J. Phys. Chem. B 119*, 2628-2637 (2015). *(Chapter 6)*

L. Liu, S. Lotze, and H.J. Bakker, Vibrational Dynamics of the Bending Mode of Hydrated Protons in Nafion Membranes. *To be submitted. (Chapter 7)*

N. Ottosson, L. Liu, and H. J. Bakker, Vibrational Relaxation of Aqueous Protons in Acetonitrile: Ultrafast Cluster Cooling and Vibrational Predissociation. *Submitted to J. Am. Chem. Soc. (Chapter 8)*

L. Liu, S. Strazdaite, and H.J. Bakker. Strong Isotope Effect in the Vibrational Response of the Hydration Shells of Hydrophobic Ions. *Submitted to J. Phys. Chem. C. (Chapter 9)*

Other publications by the same author:

J. Hunger, L. Liu, K. J. Tielrooij, M. Bonn, and H. J. Bakker, Vibrational and Orientational Dynamics of Water in Aqueous Hydroxide Solutions. *J. Chem. Phys 135*, 124517 (2011).

J. Hunger, T. Sonnleitner, L. Liu, R. Buchner, M. Bonn and H. J. Bakker, Hydrogen-Bond Dynamics in a Protic Ionic Liquid: Evidence of Large-Angle Jumps. *J. Phys. Chem. Lett. 3*, 3034-3038 (2012).

Contents

1

Introduction

The proton (H^+) plays a key role in many chemical and biological processes, for example in catalysis, atmospheric reactions, and in photosynthesis. Within a cell, proton transfer across membranes is used to create electrochemical gradients. The potential energy stored in the electrochemical gradient can be used for many processes such as ATP synthesis, photosynthesis, heat production, homeostasis and flagellar rotation. Proton transfer also plays an important role in industrial applications such as hydrogen fuel cells.

Proton Hydration Structure In water, protons are present in the form of hydrated complexes rather than bare H^+ ions, because bare protons strongly interact with the lone electron pairs of the water molecules, thus forming chemical bonds. In text books, the hydrated proton is often denoted as $H^+_{(aq)}$ or $H{\cdot}(H_2O)_n{}^+$. The value of n is not accurately defined because of the strong interaction of H^+ with water molecules and the rapid structural reorganization of the proton hydration complexes. There exist many different proton hydration complexes, but three limiting structures are frequently described and discussed in the literatures:

• $n = 1$, H_3O^+ Hydronium ion, as shown in Fig. 1.1 (a). In this structure the bare proton is connected to one water molecule thus forming H_3O^+ with three strong and equivalent covalent bonds.
• $n = 2$, $H_5O_2{}^+$ The Zundel ion, as shown in Fig. 1.1 (b). In the Zundel complex, the proton is flanked by two hydrogen-bonded water molecules.
• $n = 4$, $H_9O_4{}^+$ The Eigen ion, as shown in Fig. 1.1 (c). The Eigen ion possesses a hydronium core which is strongly hydrogen bonded to three surrounding water molecules [1].

The hydronium ion does not exist in its pure state in bulk water. Instead, the hydronium ion reorganizes into an Eigen or a Zundel ion. The calculated probability ratio of Eigen ions to Zundel ions in bulk liquid water is around 0.65:0.35 [2–4]. The cluster geometry of Eigen and Zundel ions has been investigated intensively with both X-ray structure determination and molecular dynamics simulations: For the Eigen ion, the O$\cdots$O separation at the first peak of the radial distribution functions is $\sim$2.51 $\mathring{A}$ and the O$\cdots$H separation is $\sim$1.04 $\mathring{A}$. For the Zundel ion, the O$\cdots$O separation is $\sim$2.39-2.43 $\mathring{A}$ and the O-H separation is $\sim$1.20 $\mathring{A}$ [4–7].

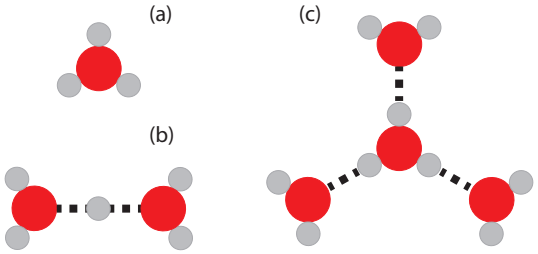

FIGURE 1.1. Schematic pictures of (a) the hydronium ion, (b) the Zundel ion and (c) the Eigen ion. The red-filled circles represent oxygen atoms and the gray-filled circles represent hydrogen atoms. The dashed black lines denote the hydrogen bonds.

TABLE 1.1. Limiting ion conductivity in water at 298 K

Cations	$\lambda_+{}^0$/mS m^{2}Mol^{-1}	Anions	$\lambda_-{}^0$/mS m^{2}Mol^{-1}
H^+	34.96	OH^-	19.91
Li^+	3.869	Cl^-	7.634
Na^+	5.011	Br^-	7.84
K^+	7.350	I^-	7.68
Mg^{2+}	10.612	SO_4^{2-}	15.96
Ca^{2+}	11.900	NO_3^-	7.14
Ba^{2+}	12.728	$CH_3CO_2^-$	4.09

PROTON TRANSFER IN AQUEOUS MEDIA In aqueous solution, the proton H^+ and the hydroxide ion OH^- exhibit anomalously high conductivity values, as indicated in Table 1.1. In water, the mobility of the proton is approximately seven times larger than that of the Na^+ ion, and the hydroxide ion possesses an approximately three times larger mobility than the Cl^- ion. Normal ions like Na^+ and Cl^- diffuse as particles (mass and charges are transfered together) in water due to random thermal motions, i.e. Brownian motion. This is the *"vehicle mechanism"*. The anomalously high mobility of the proton indicates that the proton gets transferred in aqueous system by a different mechanism. A detailed knowledge of the origin of the unusually high mobility of the proton in water is crucial for a molecular-level understanding of reactions and processes involving proton transfer. The high mobility of the proton can be explained by *"Grotthuss mechanism"*, which is a conduction process of the proton charge that strongly relies on the structural and dynamical properties of the 3D hydrogen-bond network of liquid water.

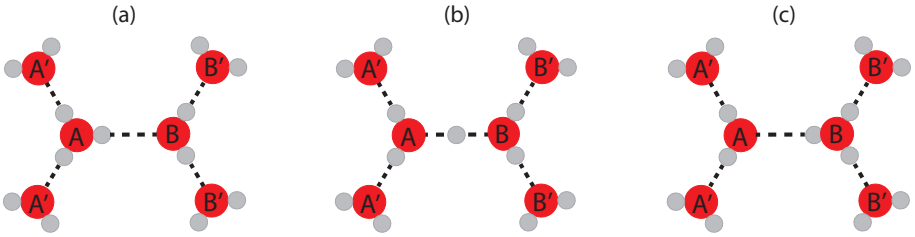

FIGURE 1.2. Schematic representation of the structural interconversion between Eigen and Zundel proton hydration structures constituting the "Grotthuss mechanism".

GROTTHUSS MECHANISM The Grotthuss mechanism was invented for a different system by Theodor von Grotthuss in 1806 [8]. *Ab initio* molecular dynamics simulations [4, 9–20] and experiments [21–24] showed that the Grotthuss mechanism involves the structural interconversion between Eigen and Zundel complexes ("Eigen-Zundel-Eigen"(EZE) scenario), as illustrated in Fig. 1.2. In the first step, the proton charge located in the hydronium core of an Eigen complex migrates towards one of the three neighboring water molecules as a consequence of the hydrogen bond fluctuations in the solvation shell of the Eigen complex. As a result, a Zundel complex is formed, in which the proton is flanked by two water molecules. This step is shown by Fig. 1.2 (a) to (b). In the second step, the proton in the Zundel complex returns to the initial Eigen complex, indicated by Fig. 1.2 (b) to (a), or can further migrate and form a new Eigen complex, indicated by Fig. 1.2 (b) to (c). In the latter case, the proton charge has moved from position A to B. Whether the proton returns to the initial complex or migrates further depends on the collective rearrangement of the hydration shells of the Zundel complex. In the first step, the Eigen complex is not exactly symmetric [11], one of the hydrogen bond (between A and B in Fig. 1.2 (a)) is shorter than the other two (between A and A') and forms the so called "special pair"[18, 19]. The proton migrates along this shorter hydrogen bond and forms a Zundel complex [5]. In the second step, the proton can move further to B, provided that the A to B hydrogen bond becomes weaker (longer) and the hydrogen bonds between B and B' become stronger (shorter), see Fig. 1.2 [25]. The transfer between structure Fig. 1.2 (a) and (b) happens on a time scale of tens of femto-seconds ($1fs$=$10^{-15}s$) [21]. The formation of a new Eigen structure takes longer, as this process requires the surrounding water molecules to reorient in such a way that the positive charge of the proton is stabilized at the new position. It has been shown that the proton transfer involves the rearrangement of around 20 surrounding water molecules [13, 26]. For the hydroxide ion a similar type of conduction and structural diffusion mechanism has been proposed [16, 27–29]. It should be noted that the EZE mechanism is not the only possible mechanism of aqueous proton transfer. Vuilleumier and Borgis proposed that aqueous proton transfer involves a "Zundel-Zundel"(ZZ) scenario. Reed and co-authors argued that the most stable proton hydration structure is formed by $H_{13}O_6^+$, which is a Zundel structure in which each of

FIGURE 1.3. Model of the vehicle mechanism (top) and structure diffusion mechanism (bottom) [32]. As explained in text, in vehicle mechanism both charge (indicated by $\oplus$) and mass (indicated by matchstick men) are transfered as a group. While, for proton only the charge is transfered rather than the mass.

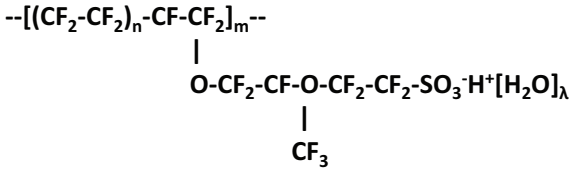

FIGURE 1.4. Molecular formula of Nafion which consists of a Teflon back bone and a sulfonic side group. The sulfonic side groups self-organize into arrays of hydrophilic water channels of several nanometers, through which small ions can be easily transported. λ indicates the hydration level of Nafion, which is defined as the number of water molecules per sulfonic side group.

the flanking H_2O molecules is hydrogen bonded to two other H_2O molecules. This highly symmetric structure has a relatively large central $O\cdots O$ distance of 2.57 $\mathring{A}$ [30, 31]. Notwithstanding the disagreement on the details of the structural diffusion mechanism, it is generally agreed that in aqueous proton transfer the charge rather than the mass of the proton is transported, while for normal cations like Na^+ the mass and charge are transported together. This difference between a vehicle mechanism and a structure diffusion mechanism is similar to the difference between individual work and team work, which is vividly described by the cartoon in Fig. 1.3 [32].

PROTON TRANSFER IN NANO-CONFINEMENT As illustrated by the Grotthuss mechanism, proton transfer in aqueous solution is strongly coupled to the structural and dynamical properties of the three-dimensional hydrogen-bond network of water, which in turn depends on the environment of the aqueous system. In highly ordered hydrogen-bond networks, proton transfer can be much faster than in solution. For example, proton transfer through a "water wire" formed in a carbon nano-tube can be up to 40 times faster than in bulk liquid water [33, 34], proteins [35].

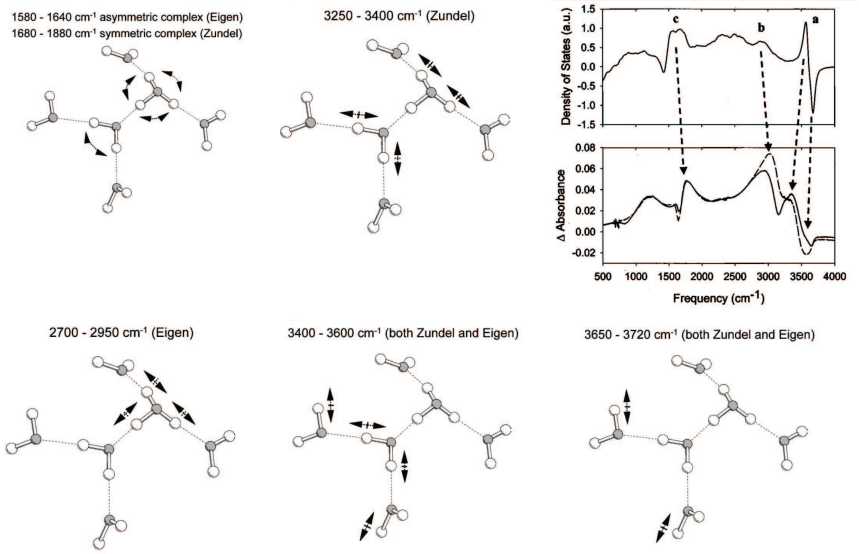

FIGURE 1.5. Schematic illustration of proton hydration structures and corresponding vibrational spectra [37].

NAFION This thesis focuses on the dynamics of aqueous proton transfer in different hydrophilic confinements, including the nano-channels of Nafion membranes and water nano-clusters dissolved in acetonitrile. Nafion constitutes the most widely used separator membrane material in proton exchange membrane (PEM) fuel cells. Nafion consists of a hydrophobic polytetrafluoroethylene (Teflon) backbone functionalized with hydrophilic sulfonic acid ($-SO_3H$) terminated side groups, see Fig. 1.4. The combination of the Teflon back bone and the sulfonic side chains provides Nafion with a high proton conductivity, chemical stability and thermal stability (operating temperature up to 190^oC). The sulfonic side chains can be hydrated (λ, the number of water molecules per sulfonic group indicates the hydration level of the membrane), thus forming hydrophilic domains which have characteristic dimensions of only a few nanometers [36]. The connected hydrophilic domains enable the long-range transport of protons through the membrane.

VIBRATIONAL SPECTRA OF PROTON HYDRATION COMPLEXES Extensive experimental and theoretical efforts have been made to determine the vibrational spectrum of proton hydration complexes. In the liquid phase, the vibrational spectrum of the proton hydration complexes strongly overlaps with the spectrum of bulk water and water molecules associated with the counter anions. Experimentally, the vibrational spectrum of proton hydration complexes in bulk liquid water has been obtained by spectral subtraction [30, 37–41]. The spectrum of the anion associated water molecules can be subtracted using the spectrum of the corresponding alkali salt solution. In the gas phase, the vibrational

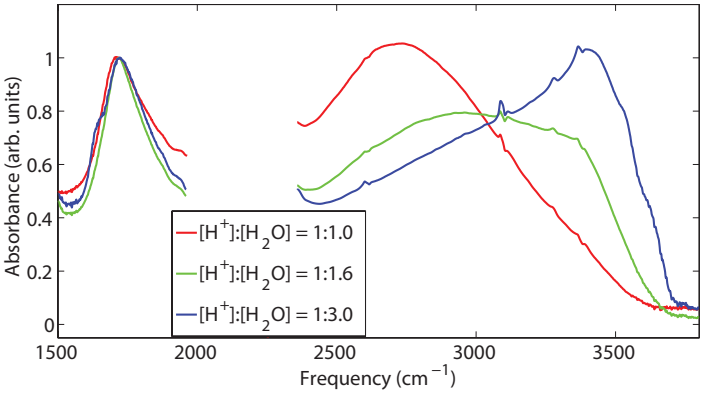

FIGURE 1.6. Normalized infrared spectra of mixture of water, triflic acid and deuterated acetonitrile. The ratio of proton to water $[H^+]$:$[H_2O]$ varies from 1:1 to 1:3, and the ratio of water to acetonitrile is fixed as $[H_2O]$:[ACN]=1:25. The background from acetonitrile is subtracted.

spectra of different proton hydration complexes can be recorded precisely [42–52]. Numerical simulation also forms a powerful method to predict the vibrational spectra of proton hydration complexes. Numerical calculations have been performed with a number of hydrating water molecules up to 100. This latter case is expected to correspond to the vibrational spectrum of the proton in bulk liquid water [43, 44, 48, 53–57]. Kim and co-authors compare the experimental results obtained for a solution of HCl in water with the calculation results from molecular dynamic (MD) simulation [37]. The resulting difference spectrum showed four distinct absorption bands in the frequency regions of 3250-3400 cm^{-1}, 2700-2950 cm^{-1}, 1580-1880 cm^{-1} and 1000-1200 cm^{-1}, on top of an extremely broad continuous band extending from 1000 cm^{-1} to 3800 cm^{-1}. The assignments of the absorption bands in the difference infrared spectra and the corresponding hydration structures are shown in Fig. 1.5.

To study the dependence of the vibrational response of the hydrated proton on the number of hydrating water molecules, we measured vibrational spectra of acid water nano-clusters in acetonitrile. The sample is a mixture of triflic acid and water diluted in deuterated acetonitrile with a molar ratio of acetonitrile to water of 25:1. The water content is indicated by the ratio of proton to water, which we varied from 1:1 to 1:3. Pines and co-workers have found that the strong acids such as hydroiodic acid (HI) and triflic acid (CF_3SO_3H) can completely dissociate in aqueous clusters in acetonitrile [58]. The spectra are shown in Fig. 1.6. For low water content $[H^+]$:$[H_2O]$=1:1, the spectrum (red curve) shows a strong absorption at ~2700 cm^{-1}, which we assign to the O-H stretch modes of hydronium ions. When the water content is increased to $[H^+]$:$[H_2O]$=1:3, the spectrum (blue curve) becomes broader and the maximum of the absorption band shifts to ~3450 cm^{-1}. This latter response can be assigned to the O-H

stretch vibrations of water molecules flanking the proton in a Zundel structure. For $[H^+]$:$[H_2O]$=1:2, the spectrum is shown in green. Obviously, the amplitude of the two bands at $\sim$2700 cm^{-1} and $\sim$3450 cm^{-1} are comparable, showing the gradual evolution of the proton hydration structure from a hydronium ion to a Zundel complex. The absorption bands in the frequency region from 1500-2000 cm^{-1} do not change dramatically when the water content is increased. There are two possible assignments for the absorption band at $\sim$1730 cm^{-1}. The first is to the bending modes of the hydronium core [40]. The other is to the bending vibration of the water molecules flanking the Zundel proton, coupled to the stretch vibration of the Zundel proton [58, 59]. The bending mode absorption band does not change when the water content is increased. When the water-proton ratio is increased to 3, a new absorption band on the red side ($\sim$1640 cm^{-1}) of the $\sim$1730 cm^{-1} band rises. This lower-frequency band can be assigned to the bending mode of water molecules in the second hydration shell of the Zundel proton.

OUTLINE This thesis focuses on the study of the vibrational dynamics of proton and hydroxide hydration complexes using polarization-resolved infrared pump-probe spectroscopy. Chapter 2 gives a theoretical basis of the light-mater interaction (including linear and nonlinear interactions). The nonlinear spectroscopy setups that were used in the experiments are described in Chapter 3. Chapter 4 subsequently discusses the dynamics of the vibrational relaxation of hydroxide hydration complexes. The following 3 chapters discuss the vibrational dynamics of the proton hydration complexes in Nafion nano-channels. In Chapter 5 and Chapter 6, we study infrared activated proton transfer in hydrated Nafion nano-channels. In Chapter 7, we present a study of the vibrational dynamics of the bending mode of hydrated proton in Nafion membrane. In Chapter 8 we report on the dynamics of proton transfer and vibrational relaxation of proton hydration complexes within water nano-clusters in acetonitrile. Finally, in Chapter 9, we present the observation of isotope effect in the vibrational response of a strong the hydration shell of hydrophobic ions on aqueous surfaces.

2

Theory

2.1 Light Matter Interaction

Molecule is the smallest chemical compound and in general case contains two or more atoms that are held together by chemical bonds forming as a result of the sharing electrons among atoms.

In many molecules the centers of positive and negative charge do not coincide. When two point charges $+q$ and $-q$ are at a mutual distance d they form an *electrical dipole moment* $\mu_0 = qd$. A molecule with a permanent dipole moment is called *polar*. A well-known example of a polar molecule is water. The oxygen atom of the water molecule attracts more electrons than the two hydrogen atoms, resulting in a charge separation and a permanent electrical dipole moment. Molecules that have no permanent dipole moment are called *nonpolar*. Examples are oxygen, carbon dioxide, and carbon tetrachloride. For both polar ($\mu_0 \neq 0$) and nonpolar ($\mu_0 = 0$) molecules, a dipole moment may be induced by an electric field. The magnitude of the induced dipole moment depends on the frequency of the applied field, because the molecular motions that respond to the external field have particular resonant frequencies. The molecular vibrations, i.e. the *oscillations* of the nuclei around their equilibrium position, have resonance frequencies in the infrared region of the light spectrum.

2.1.1 Light and Matter Interaction

When a molecule is exposed to an external electric field, the positive charges move in the direction of the field, while the negative charges move in the opposite direction. This displacement of the positive and negative charges corresponds to an *induced electrical dipole moment*. The magnitude of the induced dipole moment μ_{ind} depends on the amplitude of the external electric field $\overrightarrow{E}(\omega)$ and the polarizability $\alpha(\omega)$ of the molecule[a]:

$$\overrightarrow{\mu_{ind}}(\omega) = \alpha(\omega) \cdot \overrightarrow{E}(\omega) \tag{2.1}$$

[a]For polar molecules, an applied electric field can also cause an *orientation polarization*, as a result of the alignment of the permanent dipole moments with the electric field [60]

The induced dipole moment and the external electric field are vectors, the polarizability $\alpha(\omega)$ is a second-rank tensor.[b] The polarizability $\alpha(\omega)$ represents the ease with which an external electric field displaces the positive charges with respect to the negative charges. In an atom or a molecule with spherical symmetry, the induced dipole moment μ_{ind} is in the same direction as the external field, and thus the polarizability $\alpha(\omega)$ is a scalar. For molecules lacking spherical symmetry, the direction of $\mu_{ind}(\omega)$ depends on the direction of the electric field relative to the axis of the normal modes. Thus, $\alpha(\omega)$ is a second-rank tensor.

When the external electric field is comparable with the electric field that electrons experience in a molecule, the response to the field will become nonlinear in the amplitude of the field. We can expand the induced dipole moment in the applied electric field:

$$\overrightarrow{\mu_{ind}} = \alpha \cdot \overrightarrow{E} + \beta \vdots \overrightarrow{E}^2 + \gamma \vdots \overrightarrow{E}^3 + \cdots \tag{2.2}$$

where β and γ are second-order and third-order non-linear polarizabilities, which are third-rank and fourth-rank tensors, respectively.

Macroscopically, the response of the medium to the external electric field $\overrightarrow{E}(\omega)$ is described by the bulk polarization $\overrightarrow{P}(\omega)$. Most materials have a zero static polarization, so we consider only the polarization induced by an oscillating external electric field. The polarization $\overrightarrow{P}(\omega)$ can be written as:

$$\begin{aligned} \overrightarrow{P} &= \epsilon_0[\chi^{(1)} \cdot \overrightarrow{E} + \chi^{(2)} \vdots \overrightarrow{E}^2 + \chi^{(3)} \vdots \overrightarrow{E}^3 + \cdots] \\ &= \overrightarrow{P}^{(1)} + \overrightarrow{P}^{(2)} + \overrightarrow{P}^{(3)} + \cdots . \end{aligned} \tag{2.3}$$

where ϵ_0 is the permittivity of free space and $\chi^{(n)}$ is known as the n^{th}-order susceptibility, which is an (n+1)-rank tensor. Each non-linear polarization $\overrightarrow{P}^{(i)}$ has specific symmetry properties. The second-order polarization $\overrightarrow{P}^{(2)}$ is only nonzero in non-centrosymmetric media such as crystals that do not possess inversion symmetry, and at the interface of two media. The third-order non-linear polarization $\overrightarrow{P}^{(3)}$ is nonzero in both centrosymmetric and non-centrosymmetric media [61]. The work described in this thesis is related to the first three terms in Eq. (2.3):

- $\overrightarrow{P}^{(1)}$: represents the response measured in linear infrared spectroscopy.
- $\overrightarrow{P}^{(2)}$: represents the response used in IR pulse generation (including optical-parametric amplification, second-harmonic generation and difference-frequency generation) and the response measured in surface sum-frequency generation (SFG) probing the response of molecular vibrations at interfaces.
- $\overrightarrow{P}^{(3)}$: represents the response measured in polarization-resolved infrared saturation (pump-probe) spectroscopy.

[b] In this thesis, vectors are indicated by an arrow →.The tensor character of the polarizabilities and susceptibilities is not indicated to preserve the clarity of equations.

2.1.2 OPTICAL NONLINEARITY

The susceptibility $\chi^{(n)}$ is related to the microscopic structure of the medium. For many systems $\chi^{(n)}$ can potentially be evaluated with quantum-mechanical calculations. The mechanistic origin of a non-linear optical response can be illustrated with relatively simple models such as the anharmonic oscillator model and the free electron gas model. Here we discuss the nonlinear optical response of a medium in terms of the anharmonic oscillator model. The equation of motion of a driven anharmonic oscillator in one dimension x is given by:

$$\ddot{x} + \Gamma\dot{x} + \omega_0^2 x + ax^2 = \frac{1}{m}F \tag{2.4}$$

where Γ is the damping constant, a the anharmonicity, m the reduced mass of the oscillator, and F the driving force. The resonance frequency ω_0 of the harmonic part of the oscillator can be expressed as $\omega_0 = \sqrt{k/m}$, in which k is the linear force constant. If the oscillator possesses a charge q, it can be driven by an electric field:

$$F = q\overrightarrow{E}(t) \tag{2.5}$$

The applied force can result from the sum of two monochromatic oscillating electric fields at frequencies ω_1 and ω_2:

$$\begin{aligned}\overrightarrow{E}(t) =& \overrightarrow{E}_1(t) + \overrightarrow{E}_2(t)\\ =& \overrightarrow{E}_1(e^{-i\omega_1 t} + e^{+i\omega_1 t}) + \overrightarrow{E}_2(e^{-i\omega_2 t} + e^{+i\omega_2 t})\end{aligned} \tag{2.6}$$

If the anharmonicity a is small and the electric fields are not very strong, then the solution to Eq. (2.4) can be expanded as:

$$x = x^{(1)} + x^{(2)} + x^{(3)} + \cdots \tag{2.7}$$

The solution to Eq. (2.4) can be found in detail in Ref. 61.

The first-order solution is given by:

$$\begin{aligned}x^{(1)} =& x^{(1)}(\omega_1) + x^{(1)}(\omega_2)\\ x^{(1)}(\omega_i) =& \frac{q}{m}\frac{1}{(\omega_0^2 - \omega_i^2 - i\omega_i\Gamma)}\overrightarrow{E}_i(t)\\ =& \frac{q}{m}\frac{1}{D(\omega_i)}\overrightarrow{E}_i(t)\end{aligned} \tag{2.8}$$

where we introduce the complex denominator function $D(\omega_i)$:

$$D(\omega_i) = \omega_0^2 - \omega_i^2 - i\omega_i\Gamma \tag{2.9}$$

The second-order solution is given by:

$$x^{(2)} = x^{(2)}(2\omega_1) + x^{(2)}(2\omega_2) + x^{(2)}(\omega_1 + \omega_2) + x^{(2)}(\omega_1 - \omega_2) + x^{(2)}(0) \tag{2.10}$$

$$
\begin{aligned}
x^{(2)}(2\omega_i) =& \frac{-aq^2}{m^2}\frac{1}{D(2\omega_i)\cdot D^2(\omega_i)}(\overrightarrow{E}_i(t))^2 && (SHG)\\
x^{(2)}(\omega_1+\omega_2) =& \frac{-2aq^2}{m^2}\frac{1}{D(\omega_1+\omega_2)\cdot D(\omega_1)\cdot D(\omega_2)}\overrightarrow{E}_1(t)\overrightarrow{E}_2(t) && (SFG)\\
x^{(2)}(\omega_1-\omega_2) =& \frac{-2aq^2}{m^2}\frac{1}{D(\omega_1-\omega_2)\cdot D(\omega_1)\cdot D(-\omega_2)}\overrightarrow{E}_1(t)\overrightarrow{E}_2^*(t) && (DFG)\\
x^{(2)}(0) =& \frac{-2aq^2}{m^2}\{\frac{1}{D(0)\cdot D(\omega_1)\cdot D(-\omega_1)}\overrightarrow{E}_1(t)\overrightarrow{E}_1^*(t)\\
&+\frac{1}{D(0)\cdot D(\omega_2)\cdot D(-\omega_2)}\overrightarrow{E}_2(t)\overrightarrow{E}_2^*(t)\} && (2.11)
\end{aligned}
$$

The non-linear susceptibility of a material can be used to generate light at new frequencies, such as $2\omega_1$, $2\omega_2$, $\omega_1+\omega_2$ and $\omega_1-\omega_2$.

In case the interactions between different oscillators can be neglected, the induced polarization of the medium can be written as:

$$
\begin{aligned}
P =& Nqx\\
=& Nq(x^{(1)}+x^{(2)}+x^{(3)}+\cdots) && (2.12)
\end{aligned}
$$

By comparing Eq. (2.12) with Eq. (2.3), we get an expression of the n^{th}-order susceptibility. In the condensed phase, the interaction between molecules is usually considerable. In that case the macroscopic nonlinear susceptibility of the medium is not merely the sum of the microscopic polarizabilities of single molecule. The macroscopic susceptibility of a condensed-phase system can often be derived through full quantum-mechanical calculations [62, 63].

2.2 First-order Linear Polarization

2.2.1 Linear Absorption Spectroscopy

In this section, we discuss linear absorption spectroscopy in the frequency domain. When low intensity light propagates through a medium, the electromagnetic field $\overrightarrow{E}_{in}(\omega)$ induces an oscillating linear polarization $\overrightarrow{P}^{(1)}(\omega)$. The induced polarization $\overrightarrow{P}^{(1)}(\omega)$ serves as a radiation source of a new electric field $\overrightarrow{E}_{rad}(\omega)$ which propagates out of phase with the incident field $\overrightarrow{E}_{in}(\omega)$.

The emitted light $\overrightarrow{E}^{(1)}_{rad}(\omega)$ is 90 degrees out of phase with the induced polarization of which the magnitude depends linearly on the incident light field [63]:

$$
\overrightarrow{E}^{(1)}_{rad}(\omega) \propto i\overrightarrow{P}^{(1)}(\omega) = i\varepsilon_0\chi^{(1)}(\omega)\overrightarrow{E}_{in}(\omega) \qquad (2.13)
$$

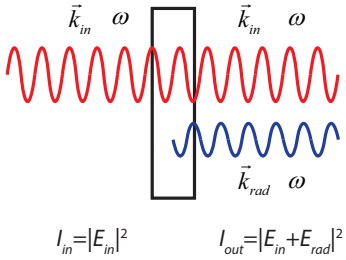

FIGURE 2.1. Schematic picture of linear absorption as a result of the destructive interference of the incident and the emitted (radiated) electric field.

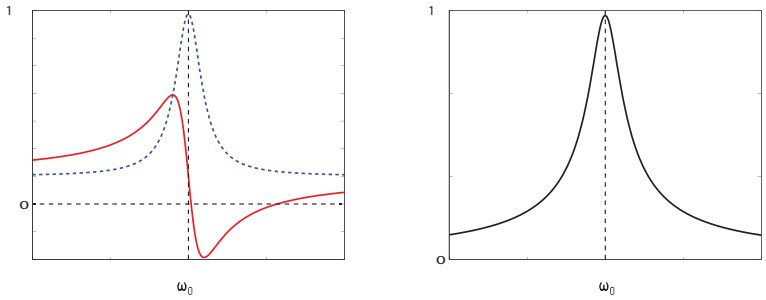

FIGURE 2.2. Frequency dependence of the first-order susceptibility $\chi^{(1)}(\omega)$. The red and blue dashed lines in the left panel represent the real and imaginary parts, respectively. The right panel shows the absolute value of $\chi^{(1)}(\omega)$

The first-order susceptibility $\chi^{(1)}(\omega)$ can be derived from Eq. (2.8), Eq. (2.12) and Eq. (2.3):

$$\chi^{(1)}(\omega) = \frac{Nq^2}{\varepsilon_0 m} \frac{1}{(\omega_0^2 - \omega^2 - i\omega\Gamma)} \tag{2.14}$$

Fig. 2.2 shows the frequency dependence of the first-order susceptibility $\chi^{(1)}$. As shown in the left panel, if the driving field $\overrightarrow{E}_{in}(\omega)$ is resonant with the oscillator, the imaginary part $Im|\chi^{(1)}|$ has the largest amplitude, while the real part is close to zero. Hence, at the resonance frequency the induced polarization is exactly 90 degrees out of phase with the driving field $\overrightarrow{E}_{in}(\omega)$. Thus at resonance the phase of the emitted field $\overrightarrow{E}_{rad}(\omega)$ is opposite to that of the incident field $\overrightarrow{E}_{in}(\omega)$. The emitted electric field $\overrightarrow{E}^{(1)}_{rad}(\omega)$ propagates in the same direction as the incident electric field $\overrightarrow{E}_0(\omega)$. As a result, the two electric fields $\overrightarrow{E}_0(\omega)$ and $\overrightarrow{E}^{(1)}_{rad}(\omega)$ interfere destructively, as shown in Fig. 2.1.

The absorbance is defined as:

$$A(\omega) = -log(\frac{I_{out}(\omega)}{I_{in}(\omega)}) = -log(\frac{|\overrightarrow{E}_{in}(\omega) + \overrightarrow{E}_{rad}(\omega)|^2}{|\overrightarrow{E}_{in}(\omega)|^2}) \tag{2.15}$$

The absorbance is also equal to:

$$A(\omega) = \alpha(\omega)l \tag{2.16}$$

where $\alpha(\omega)$ is the absorption coefficient of medium as a function of frequency, and l is the thickness of sample. Taking these equations together we obtain Lambert-Beers law:

$$I_{out}(\omega) = I_{in}(\omega)e^{-\alpha(\omega)l} \tag{2.17}$$

2.2.2 Spectral Line Shape

The absorption coefficient $\alpha(\omega)$ is defined by the spectral line shape and the absorption cross section:

$$\alpha(\omega) = Sf(\omega - \omega_0) \tag{2.18}$$

where S is the absorption cross section and $f(\omega - \omega_0)$ is the spectral line shape function. The line shape function $f(\omega - \omega_0)$ can often be approximated as a convolution of a Lorentz profile $f_L(\omega)$ and a Gaussian profile $f_G(\omega)$. The Lorentz profile is usually associated with homogeneous line-broadening mechanisms like lifetime broadening and pure dephasing. The population of an excited (molecular) state exponentially decays back to the ground state with a population relaxation time constant of T_1. Rapid fluctuations of the oscillator frequency cause a loss of coherence between oscillators at the same central resonance frequency ω_0. This process is characterized by a coherence loss time constant T_2^*. The lifetime broadening and the pure dephasing lead to a decay of the polarization with time constant T_2 ($1/T_2 = 1/(2T_1) + 1/(T_2^*)$, thus broadening of the spectrum.

The Lorentz line shape is:

$$f_L(\omega) \propto \frac{1/T_2}{(\omega - \omega_0)^2 + 1/(T_2)^2} \tag{2.19}$$

The full width at half maximum (FWHM) of the Lorentz profile function is $\Delta\omega_L = 1/(\pi T_2)$. The Gaussian profile function $f_G(\omega)$ refers to the broadening effect that results from the inhomogeneity of the system. For most systems the oscillators experience different local environments and therefore have different resonance frequencies. The resonance frequencies are often distributed as a Gaussian function with a central frequency of ω_0 and a standard deviation σ:

$$f_G(\omega) \propto exp(-\frac{(\omega - \omega_0)^2}{2\sigma^2}) \tag{2.20}$$

The FWHM of the Gaussian profile function is $\Delta\omega_G = 2\sqrt{2ln(2)}\sigma$. The line-shape of the absorption band is often the convolution of a Gaussian function and a Lorentzian function which is denoted as a Voigt profile:

$$f_{Voigt}(\omega) = \int_{-\infty}^{\infty} f_L(\omega')f_D(\omega - \omega')d\omega' \tag{2.21}$$

Usually it is difficult to distinguish homogeneous and inhomogeneous broadening effects in the linear spectrum. These different contribution can be distinguished using nonlinear spectroscopic techniques like pump-probe saturation spectroscopy, which will be discussed in section 2.4.

2.3 Second-order Non-linear Polarization

We consider the case that the incident electric field is the sum of two oscillating fields with distinct frequencies ω_1 and ω_2:

$$\begin{aligned}\overrightarrow{E}(t) =& \overrightarrow{E}_1(t) + \overrightarrow{E}_2(t) \\ =& \overrightarrow{E}_1(e^{-i\omega_1 t} + e^{+i\omega_1 t}) + \overrightarrow{E}_2(e^{-i\omega_2 t} + e^{+i\omega_2 t})\end{aligned} \tag{2.22}$$

The second-order polarization $\overrightarrow{P}^{(2)}(\omega)$ is given by:

$$\overrightarrow{P}^{(2)} = \varepsilon_0 \chi^{(2)} \overrightarrow{E}^2 \tag{2.23}$$

In case the medium does not contain resonances (negligible dispersion), this expression can be directly transferred to the time domain:

$$P^{(2)}(t) = \varepsilon_0 \chi^{(2)} \overrightarrow{E}^2(t) \tag{2.24}$$

Substituting the electric field of Eq. (2.22) gives:

$$\begin{aligned}\overrightarrow{P}^{(2)}(t) = \varepsilon_0\chi^{(2)}[&E_1^2(e^{-i2\omega_1 t} + e^{i2\omega_1 t}) && (SHG) \\ &+E_2^2(e^{-i2\omega_2 t} + e^{i2\omega_2 t}) && (SHG) \\ &+2E_1E_2(e^{-i(\omega_1+\omega_2)t} + e^{i(\omega_1+\omega_2)t}) && (SFG) \\ &+2E_1E_2(e^{-i(\omega_1-\omega_2)t} + e^{i(\omega_1-\omega_2)t}) && (DFG) \\ &+2(E_1^2 + E_2^2)] && (DC)\end{aligned} \tag{2.25}$$

It is clearly seen that the induced polarization contains light at newly created frequencies: light at frequencies of $2\omega_1$ and $2\omega_2$ (second harmonic generation, SHG), light at a frequency of $\omega_1 + \omega_2$ (sum-frequency generation, SFG) and light at a frequency of $|\omega_1 - \omega_2|$ (difference frequency generation, DFG), and a DC field (optical rectification).

To generate new light as a result of the second-order non-linear polarization the medium needs to possess a non-zero $\chi^{(2)}$ which requires the medium to be

non-centrosymmetric. The generation of light at new frequencies is strongly enhanced in case the nonlinear optical process is phase matched, which implies that the wave vector of the incoming light fields match with the wave vector of the generated light field, e.g. $\overrightarrow{k}(\omega_1+\omega_2) = \overrightarrow{k}(\omega_1)+\overrightarrow{k}(\omega_2)$ for the SFG process. The phase matching condition will be discussed in the following section 2.3.1.

2.3.1 IR PLUSE GENERATION: NONRESONANT $\chi^{(2)}$

In our experiments, we use ultrashort mid-infrared pulses (<75 fs) in the wavelength region of 3.3-6 μm (3000-1700 cm^{-1}). There exists no laser that directly delivers intense <100 fs pulses in this frequency region. Hence the ultrashort mid-infrared pulses are generated from intense femtosecond light pulses at a shorter wavelength, e.g. 800 nm pulses (at 12500 cm^{-1}) through a series of second-order non-linear optical processes including second harmonic generation (SHG) and difference-frequency generation (DFG) in non-linear optical crystals.

The intensity of the generated light at ω_3 strongly depends on the wave vector mismatch Δk between the generated light field and the incident light fields at frequencies ω_1 and ω_2. For instance for the DFG generation process (the non-linear optical process that is commonly used to generate mid-infrared pulses, as described in section 3.1) in which $\omega_3 = \omega_1 - \omega_2$:

$$\begin{aligned}\Delta k =& k_1 - k_2 - k_3 \\ =& n(\omega_1)\omega_1 - n(\omega_2)\omega_2 - n(\omega_3)\omega_3,\end{aligned} \tag{2.26}$$

Where $n(\omega_i)$ is the refractive index at frequency ω_i.

The deteriorating effect of a phase mismatch ($\Delta k \neq 0$) can be understood as follows. The incident electric fields create a second-order polarization at every point in the propagation direction in the medium. This induced polarization emits light at the new frequency (as described by Eq. (2.25)). Because the refractive index depends on frequency, a phase difference between the newly generated light and the two incident fields will accumulate during the propagation. As a result the new light generated at the beginning of the crystal can get out of phase with the new light that is generated further on in the crystal (of which the phase is set by the propagated incident light fields).

In case the frequency conversion leads to negligible depletion of the incident fields, the intensity of the generated field can be written as:

$$I \propto sinc^2(\frac{\Delta k \cdot L}{2}) = (\frac{sin(\Delta k \cdot L/2)}{\Delta k \cdot L/2})^2, \tag{2.27}$$

With L the length of the medium.

Fig. 2.3 shows that the efficiency of the DFG generation is maximized when Δk=0. It is also seen that for non-zero Δk, the intensity of the emitted light decreases as L increases. For a length $L_c = 2\pi/\Delta k$ the destructive interference is complete, meaning that there is no net light generation. $\Delta k = 0$ is called phase matching condition.

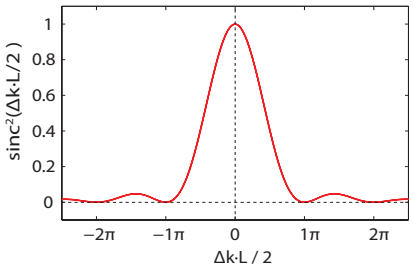

FIGURE 2.3. Difference-frequency generation (DFG) efficiency as a function of the product of the wavevector mismatch and the medium length.

In optically isotropic materials, the phase matching condition is hard to realize. In optically anisotropic crystals, for which the refractive index depends on the polarization direction of the light fields, the phase matching condition can be satisfied by variation of the polarization components of at least one of the interacting fields along the crystal axes. In the case of a uniaxial birefringent crystal (single optical axis for which the refractive index differs from the refractive indices of the other two crystal axes) tuning of the polarization components can be achieved by rotating the crystal around an axis perpendicular to the plane spanned by the optical axis and the light propagation direction. By varying the effective refractive index of one of the interacting fields we can tune Δk to 0, thereby strongly enhancing the generation of the new light field. The refractive indices of crystals are often very sensitive to the temperature. Hence for stable infrared generation the temperature in the laboratory has to be constant.

2.3.2 VIBRATIONAL SFG SPECTROSCOPY: RESONANT $\chi^{(2)}$

The second-order non-linear susceptibility $\chi^{(2)}(\omega)$ can be non-zero at the interface of two centrosymmetric media, as at this position the centrosymmetry is broken. Thanks to this property we can selectively study the response of vibrations of molecules located at interfaces with second-order nonlinear optical techniques. The surface specific second-order nonlinear technique employed in this thesis is vibrational sum-frequency generation (SFG) spectroscopy. Here, we give a brief discussion on vibrational SFG spectroscopy, a detailed description can be found in Refs. 62, 64–67. To study the vibrations of molecules on surfaces with vibrational SFG spectroscopy, one of the incident beams should be in the infrared region of the spectrum to be resonant with the vibrations. The other beam can be non-resonant and can have a frequency in the visible or near infrared region of the spectrum. In our experiment we employ the 800 nm beam of the femtosecond Ti:sapphire laser system as the non-resonant beam. The two fields $\overrightarrow{E}_{VIS}(\omega_{VIS})$ and $\overrightarrow{E}_{IR}(\omega_{IR})$ create a second-order polarization

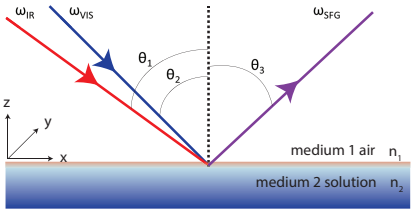

FIGURE 2.4. Geometry of an SFG experiment at an air/solution interface. The incident angles of the IR beam and the 800 nm beam are θ_1 and θ_2, respectively. The angle of the reflected SFG beam is θ_3. The dashed line shows the surface normal. For clarity, the reflected and the transmitted IR and visible beams are not shown in the plot. The SFG beam that is generated in transmission is also not shown.

at their sum frequency at the interface:

$$\overrightarrow{P}^{(2)}(\omega_{SFG}) = \varepsilon_0 \chi^{(2)}_{eff}(\omega_{SFG} = \omega_{VIS} + \omega_{IR}) : E_{VIS}(\omega_{VIS}) E_{IR}(\omega_{IR}) + c.c \tag{2.28}$$

where $\chi^{(2)}_{eff}(\omega_{SFG} = \omega_{VIS} + \omega_{IR})$ is the effective second-order non-linear susceptibility of the interface.

The SFG term of Eq. (2.11) shows that the second-order susceptibility and thus the generated SFG field is enhanced if the frequency of one of the interacting fields (the two incident fields or the SFG field) is in resonance with an oscillator at the surface. Hence by tuning the frequency of the infrared light and monitoring the produced SFG light we can measure the vibrational spectrum of the molecules at the interface.

Fig. 2.4 shows the geometry of the SFG experiments of this thesis. The reflected angle θ_3 of the SFG beam follows from the conservation of momentum in the x direction (parallel to the surface):

$$\begin{aligned} k_{SFG,x} &= k_{IR,x} + k_{VIS,x} \\ \omega_{SFG} sin(\theta_3) &= \omega_{IR} sin(\theta_1) + \omega_{VIS} sin(\theta_2) \end{aligned} \tag{2.29}$$

In our experiment, $\theta_1 = 50^o$, $\theta_2 = 45^o$ and $\theta_3 = 46^o$.

The induced non-linear polarization at the interface $\overrightarrow{P}^{(2)}(\omega_{SFG})$ generates a surface electric field $\overrightarrow{E}_{rad}(\omega_{SFG})$:

$$\begin{aligned} \overrightarrow{E}_{rad}(\omega_{SFG}) &\propto i\overrightarrow{P}^{(2)}(\omega_{SFG}) \\ &= i\varepsilon_0 \chi^{(2)}_{eff}(\omega_{SFG} = \omega_{VIS} + \omega_{IR}) \overrightarrow{E}_{IR}(\omega_{IR}) \overrightarrow{E}_{VIS}(\omega_{VIS}) \end{aligned} \tag{2.30}$$

The intensity of the SFG signal is given by [68]:

$$I(\omega_{SFG}) = \frac{8\pi^3 \omega^2_{SFG} sec^2\theta_3}{c^3 n_1(\omega_{IR}) n_1(\omega_{VIS})} |\chi^{(2)}_{eff}|^2 I_{IR} I_{VIS} \tag{2.31}$$

where $n_1(\omega_i)$ is the refractive index of air (medium 1) at frequency ω_i. The spectral shape of the measured SFG signal depends on the configuration (angles) of the beams for the following reasons. In the first place, the contributions of the different tensor elements of the second-order susceptibility depend on the incident angle of the IR beam. Second, the local electric IR field depends on Fresnel factors that in turn depend on the frequency and the incident/reflected angle. Thus the spectrum of the same sample measured under different angles can be slightly different [69]. In order to obtain the actual second-order susceptibility $\chi^{(2)}$, the measured SFG spectra have to be corrected for the frequency dependence of the Fresnel factors. In the case of the water/air interface, this is a small correction.

The second-order susceptibility $\chi^{(2)}(\omega_{SFG} = \omega_{VIS} + \omega_{IR})$ that is probed in surface vibrational SFG spectroscopy contains both resonant and non-resonant terms:

$$\chi^{(2)} = \chi^{(2)}_{NR} + \sum_{q=1}^{n} \chi^{(2)}_{R,q} \tag{2.32}$$

In dielectric media the non-resonant component is quite small and can be neglected. However, in metals the amplitude of the non-resonant component can be quite significant because of electronic contributions. These contributions show little dependence on the IR frequency. The non-resonant contribution can also be large in dielectric materials that lack inversion symmetry like quartz. In the vibrational SFG experiment we use the non-resonant SFG signal from gold or quartz as a reference to normalize the measured SFG spectra for the spectral dependence of the incident IR beam.

Each resonant component in Eq. (2.32) can be written as:

$$\begin{aligned} \chi^{(2)}_{R,q} =& \frac{1}{\omega_q - \omega_{IR} - i\Gamma_q} \\ =& \frac{\omega_q - \omega_{IR}}{(\omega_q - \omega)^2 + \Gamma_q^2} + i\frac{\Gamma}{(\omega_q - \omega)^2 + \Gamma_q^2} \end{aligned} \tag{2.33}$$

where Γ is the damping constant of the vibration oscillator and gives the vibrational life time of the resonance.

The macroscopic susceptibility $\chi^{(2)}$ is related to the molecular hyperpolarizability β by the structure and orientational distribution of the molecules at the surface. The measured $\chi^{(2)}$, in combination with calculations of the molecular hyperpolarizability, provides important information on the structural properties and the orientational distribution of molecules at interfaces [70].

In a conventional SFG experiment, the intensity of the measured SFG light is proportional to $|\chi^{(2)}|^2$. Hence, conventional SFG does not provide information on the sign and phase of $\chi^{(2)}$. Yet this information is important, as the resonant contributions can interfere with each other and with a non-resonant term, leading to complex SFG spectra. Moreover, the sign of $\chi^{(2)}$ gives information on the orientation of the probed molecular vibrations and thereby on the molecular structure of the surface. This shortcoming can be remedied by interfering

the SFG signal from the sample with a non-resonant SFG signal from a local oscillator (quartz or gold) with a well-known and well-defined phase [71, 72]. This technique is denoted as phase-sensitive SFG spectroscopy, and allows one to determine the real and imaginary parts of $\chi^{(2)}_{R,q}$. The sign of $Im(\chi^{(2)}_{R,q})$ is directly related to orientation of the probed molecular vibration at the surface [70]. For water surfaces it has been shown that a positive $Im(\chi^{(2)}_{R,q})$ of the OH stretch vibrations implies that the OH groups of the water molecules have a net orientation pointing away from the water phase (to the other medium), a negative $Im(\chi^{(2)}_{R,q})$ implies that the OH groups have a net orientation towards the water phase.

2.4 Third-order Non-linear Polarization: Pump-Probe Spectroscopy

As mentioned in Section 2.2.2 to obtain dynamic information of vibrational modes, one needs to employ non-linear spectroscopy technique, such as pump-probe spectroscopy. For bulk centrosymmetric media, the lowest-order non-linear optical response is formed by the third-order $\chi^{(3)}(\omega)$ response. In third-order non-linear spectroscopy, two or three beams are overlapped in the medium and the molecules interact three times with the incident fields. The induced polarization is:

$$\overrightarrow{P}^{(3)} = \varepsilon_0 \chi^{(3)} \vdots \overrightarrow{E}^3 \tag{2.34}$$

where $\chi^{(3)}$ is the (fourth-rank) third-order susceptibility tensor and $\overrightarrow{E}$ the incident electric field, which can be a sum of electric fields at different frequencies and with different wave vectors (propagation directions). The incident electric field can comprise an excitation (pump) pulse and a delayed (by time τ relative to the pump) probing pulse:

$$\begin{aligned}\overrightarrow{E}(t) =& \overrightarrow{E}_1(t) + \overrightarrow{E}_2(t) \\ =& E_1(e^{-i\omega_1 t} + e^{+i\omega_1 t}) + E_2(e^{-i\omega_2 t} + e^{+i\omega_2 t})\end{aligned} \tag{2.35}$$

where the subscripts 1 and 2 represent the pump and probe fields, respectively.

The contributions to the third-order polarization $\overrightarrow{P}^{(3)}$ for which the electric fields are not resonant can be obtained by substituting Eq. (2.35) into Eq. (2.34). It is clear that the third-order induced polarization $\overrightarrow{P}^{(3)}$ contains

eight combinations of the incident fields:

$$\begin{aligned}\overrightarrow{P}^{(3)} = \varepsilon_0\chi^{(3)}[&E_1E_1E_1(e^{-i3\omega_1 t}+e^{i3\omega_1 t})\\ &+E_2E_2E_2(e^{-i3\omega_2 t}+e^{i3\omega_2 t})\\ &+3E_1E_1E_2(e^{-i(2\omega_1+\omega_2)t}+e^{i(2\omega_1+\omega_2)t})\\ &+3E_1E_1E_2(e^{-i(2\omega_1-\omega_2)t}+e^{i(2\omega_1-\omega_2)t})\\ &+3E_1E_2E_2(e^{-i(\omega_1+2\omega_2)t}+e^{i(\omega_1+2\omega_2)t})\\ &+3E_1E_2E_2(e^{-i(\omega_1-2\omega_2)t}+e^{i(-\omega_1+2\omega_2)t})\\ &+(3E_1E_1E_1+6E_1E_2E_2)(e^{-i\omega_1 t}+e^{i\omega_1 t})\\ &+(3E_2E_2E_2+6E_1E_1E_2)(e^{-i\omega_2 t}+e^{i\omega_2 t})]\end{aligned} \tag{2.36}$$

The effect of the third-order polarization is often measured as a change in intensity in the probe direction k_2. Both terms $3E_2E_2E_2(e^{-i\omega_2 t}+e^{i\omega_2 t})$ with $k_{rad} = k_2-k_2+k_2 = k_2$ and $6E_1E_1E_2(e^{-i\omega_2 t}+e^{i\omega_2 t})$ with $k_{rad} = k_1-k_1+k_2 = k_2$ propagate in the same direction as the probe pulse. When the intensity of the probe beam is much lower than that of the pump, the term $3E_2E_2E_2(e^{-i\omega_2 t}+e^{i\omega_2 t})$ can be neglected. Hence, in the pump-probe experiments presented in this thesis, the detected field is $6E_1E_1E_2(e^{-i\omega_2 t}+e^{i\omega_2 t})$ which implies that the electric field of the pump pulse has two interactions with the medium and the electric field of the probe pulses only one interaction.

For the resonant contributions to the third-order polarization $\overrightarrow{P}^{(3)}$ we cannot simply substitute Eq. (2.35) into Eq. (2.34), because the elements of the third-order susceptibility $\chi^{(3)}(\omega_2)$ strongly depend on frequency. In this thesis we investigate the vibrational dynamics of O-H of water molecules or proton hydration complex using IR pump-probe spectroscopy where the incident fields are strongly resonant with O-H vibrations which means that the third-order susceptibility $\chi^{(3)}(\omega_2)$ indeed strongly depends on frequency. In this case the third-order induced polarization $\overrightarrow{P}^{(3)}$ is obtained by successive time integration of the third-order response function $S^{(3)}(t_3,t_2,t_1)$:

$$\begin{aligned}\overrightarrow{P}^{(3)} = &\int_0^\infty dt_3\int_0^\infty dt_2\int_0^\infty dt_1 S^{(3)}(t_3,t_2,t_1)\\ &E(t-t_1)E(t-t_1-t_2)E(t-t_1-t_2-t_3)\end{aligned} \tag{2.37}$$

The details of this treatment can be found in text books Refs. 63 and 73. The induced polarization radiates an electric field:

$$\overrightarrow{E}_{rad}(\omega,t) \propto i\overrightarrow{P}^{(3)}(\omega,t) \tag{2.38}$$

In pump-probe spectroscopy, we measure the pump-induced absorption change of the sample as a function of frequency and delay time between the pump and probe pulses. This absorption change results from the interference of the electric field radiated by the third-order polarization $\overrightarrow{P}^{(3)}$ and the electric field

of the probe pulse:

$$\Delta\alpha(\omega,t) = 1 - \frac{I}{I_0} = 1 - \frac{|\overrightarrow{E}_2(\omega) + \overrightarrow{E}_{rad}(\omega,t)|^2}{|\overrightarrow{E}_2(\omega)|^2}$$
$$\Delta\alpha(\omega,t) \propto \frac{2Im(\overrightarrow{P}^{(3)}(\omega,t)\overrightarrow{E}_2(\omega))}{|\overrightarrow{E}_2(\omega)|^2} \tag{2.39}$$

In the following, we present a more phenomenological description of polarization-resolved infrared pump-probe spectroscopy. We define a molecular vibration with a fundamental resonance frequency of ω_{01} and a ground state population of N_0. In the absence of the pump pulse, all the vibrational oscillators will be in the ground state and the absorbance α_0 of the probe light is:

$$\alpha_0 = \sigma_{01} N_0 \tag{2.40}$$

where σ_{01} is the absorption cross section of the absorbing molecule from ground state to the first excited state. The spectrum is indicated by the dashed line in Fig. 2.5 (b).

As a result of the interaction with the intense pump pulse, a number of vibrational oscillators N_1 are resonantly excited from the ground state $\upsilon = 0$ to the first excited state $\upsilon = 1$. As a consequence, the population of the ground state $\upsilon = 0$ is depleted to $N_0 - N_1$, whereas the population at first excited state $\upsilon = 1$ is increased by N_1. The oscillators in the first excited state can be excited further to the second excited state by absorbing light at frequency ω_{12} (as the red arrow shown in Fig. 2.5(a)). These excited oscillators can also be pumped back to the ground state by stimulated emission of light at ω_{10} (as the green arrow shown in Fig. 2.5(a)). Hence, the resulting absorption spectrum α of the excited sample is:

$$\alpha = \sigma_{01}(N_0 - N_1) - \sigma_{01}N_1 + \sigma_{12}N_1 \tag{2.41}$$

The absorption changes caused by the intense pump pulse contains three terms:

$$\Delta\alpha = \alpha - \alpha_0 = \underbrace{-\sigma_{01}N_1}_{\text{Depletion}} \quad \underbrace{-\sigma_{01}N_1}_{\text{Stimulated Emission}} \quad \underbrace{+\sigma_{12}N_1}_{\text{Induced Abs.}} \tag{2.42}$$

where $\omega_{01} = \omega_{10} \neq \omega_{12}$, due to the anharmonicity of the vibration potential (indicated in Fig. 2.5 (a)). The absorption changes $\Delta\alpha$ generally contains a negative change in absorption (bleaching) due to the depletion of the ground state and stimulated emission out of the first excited state, and a positive change in absorption (induced absorption) due to excited state absorption. The bleaching and induced absorption signals are indicated in blue and red respectively in Fig. 2.5 (c).

The pump induced population N_1 is short lived, because the excited molecules will relax back to the vibrational ground state. The population of

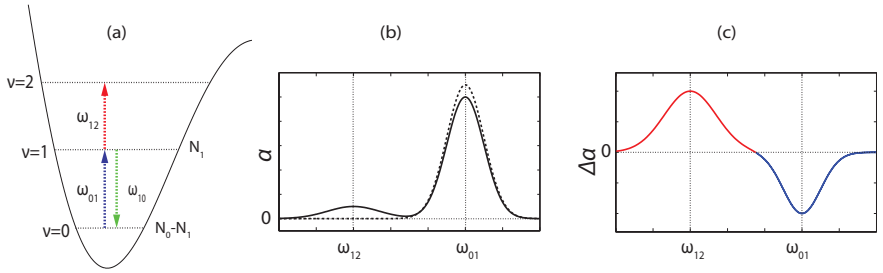

FIGURE 2.5. Schematic picture of pump-probe spectroscopy. (a) Potential energy diagram of a molecular vibration. Without pump pulse, the population of the ground state ($\nu = 0$) equals N_0. An intense IR pulse with a frequency ω_{01} excites N_1 oscillators to the first excited $\nu = 1$ state, as indicated with the blue arrow. The oscillators in the $\nu = 1$ state will absorb light at frequency ω_{12} (transition from $\nu = 1$ to $\nu = 2$ state, indicated by the red arrow). The oscillators in the $\nu = 1$ state can also be stimulated back to $\nu = 0$ state and emit light at the fundamental frequency ω_{10} (indicated by the green arrow). (b) The absorption spectrum of the probe beam after pump excitation (α_1, solid line) and before (without) pump excitation (α_0, dashed line) pump. (c) Difference spectrum $\Delta\alpha = \alpha_1 - \alpha_0$. The blue band at ω_{01} represents the absorption decrease (bleaching), while the red band at ω_{12} represents the induced absorption.

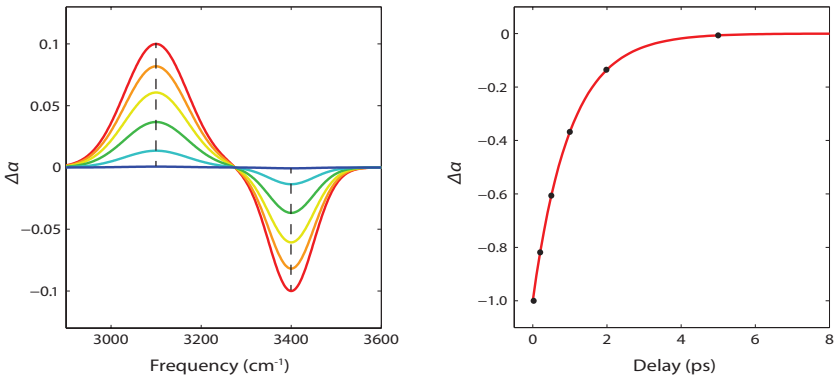

FIGURE 2.6. (a) Pump-probe transient spectroscopy, spectral evolution of $\Delta\alpha$ at different delay times between the pump and probe pulses. (b) Delay trace of $\Delta\alpha$ at ω_{01} as a function of delay time.

the excited state decays exponentially with a time constant of T_1 to the ground state, $N_1(t) = N_1(0)e^{-t/T_1}$. In case the population relaxes back to the ground state the time-dependent absorption change is given by:

$$\Delta\alpha(\omega, t) = (-2\sigma_{01}(\omega) + \sigma_{12}(\omega))N_1(0)e^{-t/T_1} \tag{2.43}$$

The time and frequency dependence of $\Delta\alpha(\omega, t)$ are illustrated in Fig. 2.6(a). By measuring the absorption difference $\Delta\alpha(\omega, t)$ at different time delay between

the pump and probe pulses, we determine the time constant of the vibrational relaxation of the excited oscillators. A delay trace at the central frequency of ω_{01} is shown in Fig. 2.6(b).

For an oscillator with its transition dipole moment at an angle θ with respect to the pump polarization, the excitation probability is proportional to $cos^2(\theta)$. The excitation thus leads to an anisotropic distribution of excited oscillators. The absorbance change for probe light that is polarized parallel to the pump polarization is stronger than that for probe light that is polarized perpendicular to the pump polarization, $(\Delta\alpha_{\parallel}(\omega,t) > \Delta\alpha_{\perp}(\omega,t))$.

The orientation of the excited oscillators will randomize as a result of molecular reorientation, and thus the difference between parallel $\Delta\alpha_{\parallel}$ and perpendicular $\Delta\alpha_{\perp}$ will decay. When the rotational relaxation is complete, the two components will be equal, $\Delta\alpha_{\parallel}(\omega,\infty) = \Delta\alpha_{\perp}(\omega,\infty)$.

In polarization-resolved pump-probe spectroscopy, we measure both the parallel and perpendicular components, and we can construct the isotropic signal $\Delta\alpha(\omega,t)$ and the anisotropic signal $R(\omega,t)$:

$$\begin{aligned}\Delta\alpha_{iso}(\omega,t) &= \frac{\Delta\alpha_{\parallel}(\omega,t) + 2\Delta\alpha_{\perp}(\omega,t)}{3} \\ R(\omega,t) &= \frac{\Delta\alpha_{\parallel}(\omega,t) - \Delta\alpha_{\perp}(\omega,t)}{\Delta\alpha_{\parallel}(\omega,t) + 2\Delta\alpha_{\perp}(\omega,t)}\end{aligned} \tag{2.44}$$

The prefactor of 2 can be understood from the fact that in a three-dimensional system there are two independent directions perpendicular to the polarization of the pump. The isotropic signal $\Delta\alpha(\omega,t)$ decays only as a result of vibration relaxation and spectral relaxation. The anisotropy parameter $R(\omega,t)$ decays due to the reorientation of the molecules and resonant energy transfer between differently oriented oscillators (Förster energy transfer). The anisotropy is proportional to the second-order orientational correlation function:

$$\begin{aligned}R(t) =& \frac{2}{5}C_2(t) \\ =& \frac{2}{5}\langle P_2(cos\theta_r)\rangle \\ =& \frac{2}{5}\langle(3cos^2(\theta_r) - 1)/2\rangle\end{aligned} \tag{2.45}$$

where θ_r is the angle between the initial and the final orientation of the excited molecule, and $\langle\cdots\rangle$ represents a statistical average.

Often the anisotropy decay due to orientational diffusion can be described as a mono-exponential function:

$$R(t) = \frac{2}{5}e^{(-t/\tau_{or})} \tag{2.46}$$

For some systems, the anisotropy not only decays as a result of molecular reorientation, but also as a result of resonant energy transfer between oscillators that are oriented at different angle with respect to the pump polarization. Resonant energy transfer becomes an important contribution to the anisotropy decay

in case the transition dipole moment of the vibration is large and the oscillators are closely spaced. These conditions are fulfilled for pure water or in proton hydration structures, containing a high concentration of strongly absorbing O-H stretch vibrations (as discussed in Chapter 5).

Often the system under study contains several distinct vibrational components that all contribute to the measured pump-probe signal. As a result, the isotropic signal is the sum of the contributions of all components and the anisotropy is the weighted average of the anisotropy values of each component:

$$\begin{aligned} \Delta\alpha_{iso,total}(\omega,t) =& \sum_n \Delta\alpha_{iso,n}(\omega,t) \\ R(\omega,t) =& \sum_n a_n(\omega,t) R_n(\omega,t) \\ a_n(\omega,t) =& \frac{\Delta\alpha_{iso,n}(\omega,t)}{\Delta\alpha_{iso,total}(\omega,t)} \end{aligned} \tag{2.47}$$

where $a(\omega,t)$ is a weight factor defined as the ratio of the isotropic signal of each component to the total isotropic signal. A correct signal analysis thus requires a detailed decomposition of the spectrum and the population dynamics of each vibrational component, see Chapter 7 and Chapter 8.

3

Experiment

The rate and mechanism of aqueous proton transfer can be well investigated via the structural and dynamical properties of the O-H stretch modes of the proton hydration complexes. The O-H vibrations strongly absorb light in the infrared region of the spectrum. Hence, the properties of these vibrations can be well studied with ultrashort and intense infrared light pulses. In this thesis, we used two experimental methods: polarization-resolved femtosecond infrared pump-probe spectroscopy and vibrational sum-frequency generation spectroscopy. The details of these two experimental methods are explained in this chapter.

3.1 Generation of Femtosecond Mid-Infrared Pulses

The infrared pulses are generated via optical parametric amplification (OPA) processes (TOPAS, HE-TOPAS and home-built OPA) that are pumped by the intense 800 nm pulses delivered by commercial Titanium:sapphire laser systems. The scheme of the home-built OPA is presented in the blue region of Fig. 3.1. This OPA is based on the design of the group of Peter Hamm. 1 mJ of 800 nm light (with a time duration of 45 fs) is used to pump the OPA. The incident 800 nm light is split into two parts. The part B1 that is reflected from the first beam splitter (BS1) (a few percent of the total 800 nm light) is used to generate white light by focusing the beam in a sapphire plate. Stable white-light generation depends critically on the incident intensity of the 800 nm pulse. To optimize the intensity, the 800 nm beam B1 is sent through a half-wave plate and a cubic polarizer. The transmitted *p*-polarized 800 nm beam is focused by a lens (L1) into a sapphire plate to generate white light. The 800 nm beam that is transmitted by BS1 is sent into a delay stage D1 and split by BS2 into B2 (around 10%, used for the first amplification step) and B3 (used for the second amplification step). The 800 nm beam B2 and the white light are sent together into the BBO crystal C2 (which is $\sim$1 mm thick) in spatial and temporal overlap. The temporal overlap is realized with delay stage D1. In this process signal and idler pulses are generated. The frequencies of the signal

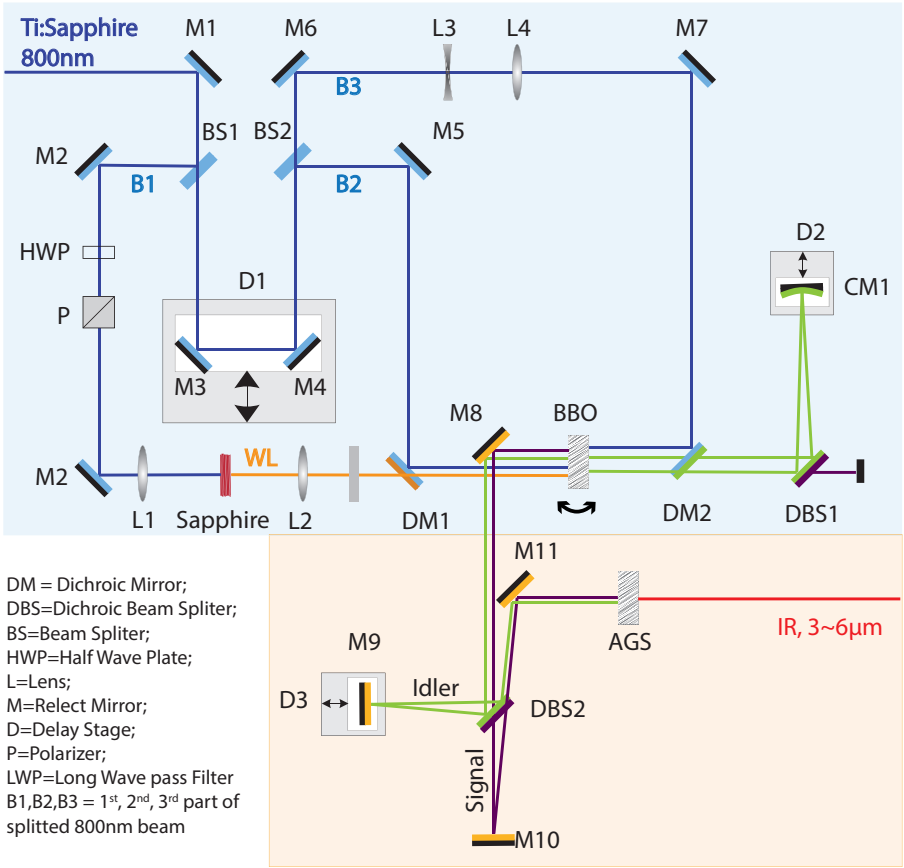

FIGURE 3.1. Schematic picture of the setup used to generate the infrared probe pulses that are used in the two-color polarization-resolved pump-probe setup (fs-IR). Blue region: home-built optical parametric amplifier (OPA). Orange region: difference-frequency generation (DFG) set-up where mid-IR light is generated via difference frequency generation of the signal and idler (created by the OPA) in a $AgGaS_2$ crystal.

(ω_S) and the idler (ω_I) are determined by the phase-matching condition, which depends on the temperature and the angle between the incident pump laser and the optical axis of the crystal, see section 2.3.1. The generated signal pulses pass through the dichroic beam splitter DBS1 and are stopped by a beam blocker. The generated idler pulses are reflected by the dichroic beam splitter DBS1 to a curved mirror CM1 that is put on delay stage D2. The back reflected idler pulses are focused by CM1 on the BBO crystal and spatially and temporally overlapped with the 800 nm beam B3. The idler pulses are amplified and the signal pulses are regenerated. The sum of the pulse energies of signal and idler is ~200 μJ.

The generated signal and idler are used in a difference frequency generation

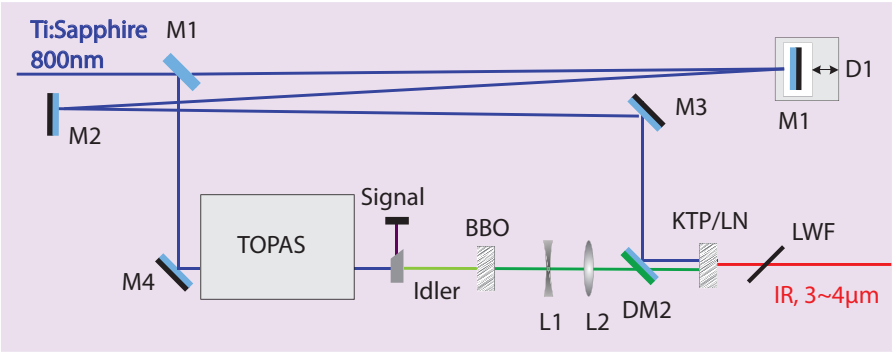

FIGURE 3.2. Schematic of infrared pump pulse generation parts of the two-color polarization-resolved pump-probe setup (fs-IR).

(DFG) process in a silver gallium disulphide ($AgGaS_2$) crystal, as illustrated in the orange region of Fig. 3.1. To obtain spatial and temporal overlap in the $AgGaS_2$ crystal, the signal and idler are first spatially separated with a dichroic beam splitter (DBS2), that transmits the signal and reflects the idler. The reflected idler is sent over a delay stage (D3) to obtain temporal overlap. The frequency of the mid-IR pulses generated in the DFG process is equal to the difference frequency of signal and idler (ω_{IR}=ω_S-ω_I) and tunable in a frequency region of 1600-3700 cm^{-1}. The generated infrared pulses have a full width at half maximum (FWHM) of 300 cm^{-1} and a time duration of ~75 fs. Typical pulse energies are 4 μJ. The generated mid-IR pulses are used as probe and reference in a two-color pump-probe experiment. The pump pulses of the two-color pump-probe experiments presented in this thesis are generated via difference frequency mixing of an intense 800 nm pulse and a frequency-doubled idler pulse. The idler pulses are generated by a commercial parameteric generation and amplification device (TOPAS (Light-Conversion)) that is pumped with a ~1 mJ 800 nm pulse. The seed pulse for the parametric amplification process is created via parametric generation (super-fluorescence) which starts from quantum noise. As a result, the generated signal and idler pulses are less stable than the pulses that are generated by white-light seeded OPA. A schematic of the setup used to generate the infrared pump pulses is shown in Fig. 3.2. The signal generated by the TOPAS is filtered out by a dichroic mirror. The idler is frequency doubled with a BBO crystal. Subsequently the frequency-doubled idler is difference-frequency mixed with an 800 nm pulse (~1.3 mJ) in a potassium-titanyl-phosphate crystal (KTP, to generate 3 μm IR pulses) or a lithiumniobate crystal (LN, to generate 4 μm IR pulses). After the crystal, the residual idler and doubled idler are removed using a long wave pass filter (LWF). The frequency of the generated mid-infrared pulses is equal to the difference frequency of the 800 nm pulse and the doubled idler pulse: ω_{IR}=ω_{vis}-2·ω_I. The duration and spectral bandwidth of the infrared pulses largely depends on the thickness of the BBO and LN (or KTP) crystals. In the experiments presented in this thesis, the pump infrared

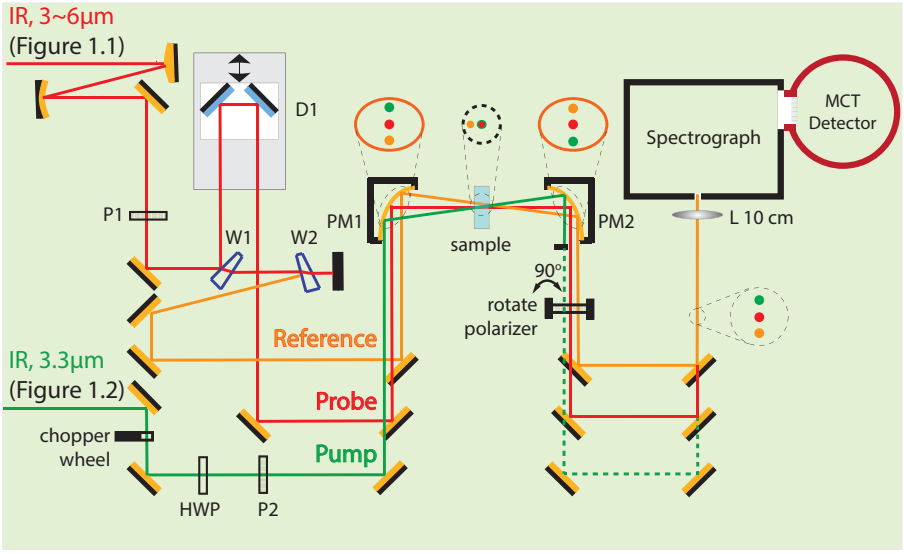

FIGURE 3.3. Schematic picture of the two-color infrared polarization-resolved pump-probe setup (fs-IR). The pump, probe and reference beams are indicated with green, red and orange lines. The probe and the reference originate from the same infrared pulse (generated by the home-built OPA). The relative positions of the pump, probe and reference beams on the parabolic mirrors and the sample are indicated in the solid and dashed circles.

pulses have a spectral bandwidth with a FWHM of ∼150 cm^{-1}, a pulse energy of ∼15 μJ and a pulse duration of ∼100 fs.

The home-built OPA (described in Fig. 3.1) delivers pulses with a broad tunability but low pulse intensity, making it ideal to generate probe pulses. The mixing of the 800 nm beam with the doubled idler leads to IR pulses with less tunability but leads to higher infrared pulse energies, which makes this approach ideally suited to generate pump pulses.

3.2 INFRARED PUMP-PROBE SPECTROSCOPY

3.2.1 TWO-COLOR PUMP-PROBE SETUP

The polarization-resolved two-color infrared pump-probe setup used in the experiments is illustrated in Fig. 3.3. The infrared pulses generated with the setup that is illustrated in Fig. 3.1 serve as probe and reference pulses. The beam first goes through a telescope to increase the beam size by a factor of 2.5 (to obtain a tighter focus in the sample). The polarization of the pulses is cleaned up with a wire grid polarizer P1. Around 10% of the IR beam is reflected from the front side of the first wedge W1 (ZnSe, 4^o), and used as the probe. Around 10% of the transmitted part is reflected on the second wedge W2 and used as

the reference. The probe pulses are sent into a delay stage D1 to vary the delay time between the pump and probe pulses. The infrared pulses generated in the process illustrated in Fig. 3.2 are used as the pump. The polarization of the pump pulses is rotated to an angle of 45° with respect to the polarization of the probe/reference pulses with a $\lambda/2$ plate. After this rotation the polarization is cleaned up with wire grid polarizer P2. Every second pump pulse is blocked by a chopper.

The pump, probe and reference pulses are propagated in parallel to a gold coated parabolic mirror PM1 and focused into the sample. The pump and probe are spatially overlapped in the sample. After the sample, all three beams are re-collimated with the second parabolic mirror PM2. After this mirror, the probe and reference pulses are sent through a 90° rotatable wire grid polarizer to select a polarization component parallel or perpendicular with respect to the polarization of the pump pulses. The pump pulses are blocked before the polarizer.

The probe and reference beams are dispersed with a spectrograph and detected with a mercury-cadmium-telluride (MCT) 3×32 pixel detector. In the experiment we measure the pump-induced change in the transmission of the probe pulses as a function of the delay time and the probe frequency. The transmission of the reference pulses is also measured as a function of frequency and used for a pulse-to-pulse normalization of the probe pulse energy. The normalized, pump-induced transmission changes of the transmission of the probe provide essential information on the energy-relaxation and reorientation dynamics of the molecular vibrations in the sample, as expressed in equation 2.44.

3.2.2 One-Color Pump-Probe Setup

We also performed one-color pump-probe experiments, meaning that the pump, probe and reference pulses are all derived from the same mid-infrared light pulse. In one of the used set-ups, we generate 4 μm pulses via nonlinear frequency conversion processes that are pumped by the pulses that are delivered by a Ti:sapphire laser system (Hurricane, Spectra-Physics). This laser generates 800 nm pulses with a pulse duration of ∼100 fs and a pulse energy of ∼900 μJ. The infrared pulses are generated in the same way as described in Fig. 3.2. However, instead of a parametric generation based OPA, we use a white-light seeded OPA (Spectraphysics). The idler is frequency doubled in a BBO crystal and difference-frequency mixed with a second part of the 800 nm beam in a lithium niobate (LN) crystal. In this process, infrared pulses are generated with a frequency that is tunable between 2300 cm^{-1} and 2800 cm^{-1}. The infrared pulses have a pulse duration of ∼120 fs, a spectral bandwidth with a FWHM of 100 cm^{-1}, and a pulse energy of ∼5 μJ. The pump, probe and reference beams are split from the same infrared pulse with a CaF_2 wedge. The reflection from the front side is used as the probe, the reflection from the back side is used as the reference, and the transmitted beam serves as the pump. In another one color pump-probe experiment we generate pulses at 6 μm using a high-power Ti:sapphire laser system (Coherent Legend Duo) that delivers 800

nm pulses with a pulse duration of ∼35 fs a pulse energy of ∼7.5 μJ. The 6 μm infrared pulses are generated by a commercial HE-TOPAS (high-energy TOPAS) which integrates a white-light seeded OPA (triple amplification) and a DFG stage. The HE-TOPAS generates high intensity (∼60 μJ) and broad band (∼300 cm^{-1}) infrared pulses with frequencies that are tunable in the region of 1200-3700 cm^{-1}.

3.3 Sum Frequency Generation Spectroscopy

Vibrational sum-frequency generation (VSFG) spectroscopy is a powerful method to study the vibrational response of water molecules at water-air interfaces. In this technique a narrow-band visible beam and a broad-band infrared beam are combined at the surface to generate light at the sum-frequency. The sum-frequency generation process will be enhanced in case the infrared light is resonant with a molecular vibration, see section 2.3.2. The SFG setup makes use of the pulses of an amplified Ti:Sapphire laser system (Coherent Legend Elite). The 800 nm pulses have a pulse duration of 45 fs and a pulse energy of ∼3.5 mJ. The 800 nm beam is split into two parts. The first part, ∼1 mJ, is used to pump a home-built OPA. To obtain high-energy signal and idler pulses, this OPA has three amplification stages instead of two. The signal and idler pulses generated by this OPA have a total energy of ∼0.65 mJ. The signal and idler pulses are subsequently used in a difference-frequency mixing process in a $AgGaS_2$ crystal to generate mid-infrared pulses (see Fig. 2.3) that are tunable from 2-10 μm. The generated infrared pulses have a pulse energy of 10-20 μJ and a spectral bandwidth with a FWHM of ∼400 cm^{-1}. The second part of the 800 nm beam serves as the visible beam in the SFG process. Fig. 3.4 shows a schematic picture of the VSFG spectroscopy setup. The 800 nm beam is sent through an etalon to narrow its bandwidth to 15 cm^{-1} and then sent into a delay stage D1 to ensure temporal overlap of the visible pulses and the infrared pulses. In this thesis, all VSFG spectra are recorded with *ssp* polarization (*s*-polarized SFG, *s*-polarized 800 nm, and *p*-polarized infrared light). The 800 nm pulses are sent into a cubic polarizer P1 to clean up their polarization. The infrared pulses are sent to a combination of a $\lambda/2$ plate HWP and a wire grid polarizer P2 to adjust the polarization and intensity of the infrared pulses. The narrow-band 800 nm and broad-band infrared pulses are focused on the sample surface by lenses L1 and L2 with focal lengths of 20 cm and 10 cm, respectively. The two pulses are in temporal and spatial overlap and generate light at their sum frequency. The height of the sample can be adjusted with a translation stage. After the sample the 800 nm beam is removed by filter F1. The generated sum-frequency light is re-collimated with lens L3 (20 cm) and then spectrally dispersed by a monochromator and detected with an Electron-Multiplied Charge Coupled Device (EMCCD, Andor Technologies). To correct the VSFG spectra for the spectral dependence of the intensity of the infrared light pulse, the measured VSFG spectra are divided by the spectrum of the sum-frequency light that is generated by a reference z-cut quartz crystal. The

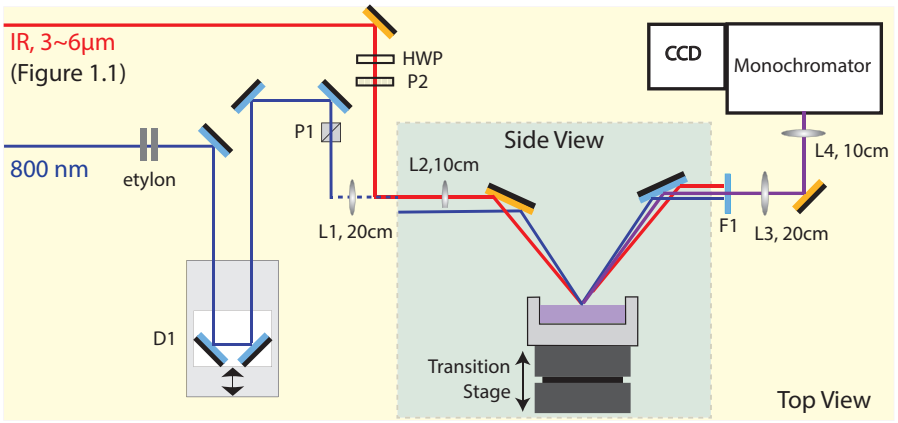

FIGURE 3.4. Schematic picture of the SFG setup. The broad-band infrared and narrow-band 800 nm pulses are focused onto the sample surface. The two pulses are in temporal and spatial overlap and generate light at their sum frequency. The sum-frequency light is sent into a monochromator and detected with a CCD camera. The yellow region shows a view of the setup from the top, while the grey region shows a side view of the SFG generation process.

sum-frequency generation in this crystal is a non-resonant process, meaning that its $\chi^{(2)}$ does not depend on the infrared frequency. Hence, the spectrum of the sum-frequency light generated by the quartz crystal only depends on the intensity spectrum of the infrared pulses and can thus be used to normalize the VSFG signal generated by the sample[74].

3.4 SAMPLES

All samples used in this thesis contain normal and/or heavy water. H_2O was purified with Millipore. D_2O was purchased from Cambridge Isotope Laboratories (with purity >99.6%). The other compounds like sodium hydroxide solution (in Chapter 4), sodium triflate, sodium ethanesulfonate, sodium butanesulfonate, sodium perchlorate (in Chapter 9) and deuterated acetonitrile and trifluoromethanesulfonic acid (in Chapter 8) were all purchased from Sigma Aldrich and used without further purification. In the experiment on aqueous solutions we used a conventional sample cell. This cell consists of two pieces of 4 mm thick CaF_2 windows. The two windows are separated by a Teflon spacer with a well-defined thickness. The thickness of the spacer is varied such that we obtain an infrared absorbance of ∼1 OD.

Nafion membranes (in Chapter 5, Chapter 6 and Chapter 7) were purchased from Alpha Aesar and purified as follows: firstly the membranes were boiled in 3% H_2O_2 solution to get rid of organic contaminations, secondly they were boiled in water, and then in a 1 M H_2SO_4 solution to ensure that all sulfonate groups in the membranes are binding protons. Finally, the membranes were put

in deionized water. In each step, Nafion membranes were boiled at least for one hour[75, 76]. To control the ratio of proton (H^+) and sodium (Na^+) ions in the membranes, the protonated membranes were soaked in a mixed solution of HCl and NaCl with the desired ratio of $[H^+]$:$[Na^+]$ for 24 hours[76]. In the last step the membranes are rinsed with deionized water.

TABLE 3.1. Equilibrium relative humidities (R.H.%) of saturated salt solutions and the resulting hydration levels (λ) of the Nafion membranes

Saturated Salt Solution	R.H.% at 25 ^{o}C.	Hydration Level λ
CsF	3	3
LiBr	6.3	7
LiCl	11.7	9
CH_3COOK	22.5	12
$MgCl_2$	32.8	16

To vary the hydration level, the prepared Nafion membranes were placed in a chamber sealed between two CaF_2 windows. Through channels in the wall of chamber, the membranes were exposed to a large volume of an aqueous saturated salt solution at room temperature. The character of the salt solution determines the relative humidity of the air interacting with the Nafion membranes which in turn determines the hydration level of the membranes. We let the membranes equilibrate for a week to obtain a well-defined hydration level. The used saturated salt solutions and their corresponding relative humidities and hydration levels (λ=$[H_2O]/[SO_3{}^-]$) are summarized in Table 3.1. [77–80] To avoid sample degradation caused by the repeated exposure to the intense pump pulses during the measurements, the sealed chamber with the hydrated Nafion membrane was mounted on a rotation stage and constantly rotated during the IR pump-probe experiments.

4

Dynamics of the Hydration Complex of Hydroxide

We use polarization-resolved mid-infrared pump-probe spectroscopy to study the dynamics of the hydration shells of hydroxide ions (OH^-). We excite the O–H stretch vibrations of H_2O molecules solvating the OH^- ion and observe that this excitation decays with a relaxation time constant T_1 of 200 fs. This relaxation is followed by a thermalization process that becomes slower with increasing concentration of OH^-. The pre-thermalized state is observed to be anisotropic, showing that the energy of the excited O–H stretch vibrations is dissipated within the hydration complex. The anisotropy of the pre-thermalized state decays both as a result of the reorientation of the OH^- hydration complex and heat diffusion from the excited complexes to unexcited complexes. Modeling the anisotropy data at different concentrations allows for an accurate determination of the number of water molecules in the hydration shell of OH^-, the reorientation dynamics of the OH^- hydration complex, and the molecular-scale heat diffusivity.

4.1 Introduction

The hydroxide ion OH^- and the hydronium ion H_3O^+ both form strong hydrogen bonds with their surrounding water molecules. Experimental and theoretical investigations indicate that these hydrogen bonds are rapidly exchanged with the chemical bonds of the surrounding water molecules [81–84]. This exchange results in a transfer of the charge of the proton and the hydroxide ion to the solvating water molecules, and thus effectively in the transport of the proton and hydroxide ion. Hence, these ions are not transported as particles, as in conventional Stokes diffusion, but only their charge is being conducted. This structural diffusion mechanism is highly efficient and explains the anomalously high mobility of protons and hydroxide ions in liquid water. The mechanism is often referred to as Grotthuss conduction [8].

Density functional calculations indicate that there are two somewhat different mechanisms by which the hydroxide ion is transported through liquid water. One of these mechanisms is denoted as the "dynamical hypercoordination" mechanism, [27, 29] which involves reduction of coordination number of OH^- complex. In this mechanism $OH^-(H_2O)_4$ breaks an accepting hydro-

gen bond between its oxygen and a water molecule in the first hydration shell, and then donates a hydrogen bond transiently to another water molecule. The other mechanism is the so-called "mirror image" mechanism [83, 85, 86], in which $H_7O_4^-$ ions are converted to $H_3O_2^-$ ions by cleavage of a second shell hydrogen bond. This mechanism is quite similar to the transfer mechanism of protons in liquid water, thus explaining the name "mirror image" mechanism.

The dynamics of the O–H stretch vibrations of protons and hydroxide ions in water has been investigated using femtosecond mid-infrared spectroscopy of isotopically diluted systems. For a solution of OD^- and HDO in D_2O, it was found that for part of the HDO molecules the absorption spectrum of the OH stretch vibration is broadened and shifted to lower frequencies [87–89]. This spectral component shows a very rapid relaxation with a time constant of 120-160 femtoseconds. The amplitude of the fast component scales with the concentration of OD^-, and is thus assigned to HDO molecules hydrating the OD^- ions. The fast relaxation has been interpreted in two different ways. In one interpretation, the fast relaxation was assigned to HDO molecules of which the OH group is hydrogen-bonded to an OD^- ion that is showing deuteron exchange with a D_2O molecule [87]. The exchange will lead to a strong modulation of the strength of the O-H$\cdots$O hydrogen bond as this bond changes from a bond to an OD^- to a bond to a D_2O molecule. The modulation leads to a fast decay of the vibrational excitation of the HDO molecule that is a spectator at the deuteron transfer. In the other interpretation the fast relaxation component is assigned to the second excited vibrational state of a DO$\cdots$H$\cdots$OD Zundel complex [88]. This Zundel complex forms a transition state in the transfer of the proton from HDO to OD^-. The fast vibrational relaxation is explained from the short lifetime of this transition state complex.

In this chapter, we use polarization-resolved pump-probe infrared spectroscopy to investigate the energy and reorientation dynamics of the hydration complex of the OH^- ion in H_2O. We study the energy relaxation dynamics of the O–H vibrations that are strongly hydrogen bonded to the OH^- ion. We also study the structural relaxation dynamics of the liquid following the fast local dissipation of heat and the heat diffusion from the excited hydration complexes to the surroundings.

4.2 EXPERIMENT

The experiments were performed with the one-color pump-probe setup described in Section 3.2.2. We excite the OH stretch vibrations of H_2O molecules hydrating the OH^- ions with intensive pump pulses ($\sim$4 μJ) with a central frequency of 2650 cm^{-1} and a FWHM of 120 cm^{-1}. The absorption changes caused by the intense pump pulses are monitored by the time-delayed probe pulses.

The experiments were performed on $NaOH/H_2O$ solutions at ten concentrations ranging from 0.5 to 10 M. The stock NaOH solution was purchased from Sigma-Aldrich. The solutions were held in a sample cell with two 4 mm thick CaF_2 windows separated by Teflon spacers of 50 μm (for 0.5 and 1.0 M), 25 μm

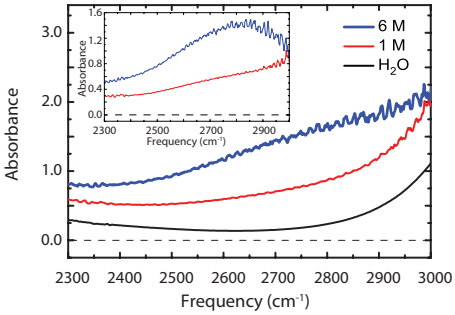

Figure 4.1. Absorption spectra of H_2O (black line) and $NaOH/H_2O$ solutions of 1 M (red line) and 6 M (blue line). The inset shows the spectra of the hydroxide solutions after subtraction of the pure H_2O spectrum.

(for 2.0 and 3.0 M) and 12 μm (for 4.0, 5.0, 6.0, 7.0, 8.6 and 10.0 M).

4.3 Results and Discussion

Fig. 4.1 shows the linear absorption spectra of $NaOH/H_2O$ solutions with two different hydroxide concentrations. It is clear that the spectra show an increasing red-shifted absorption with increasing NaOH concentration. This red-shifted absorption is assigned to the O-H stretch vibrations of water molecules that are hydrogen bonded to hydroxide ions. The hydrogen bonds between H_2O molecules and the OH^- ion are much stronger than the hydrogen bonds between H_2O molecules. As a result, the (uncoupled) vibrational frequency of these oscillators is strongly red-shifted with respect to the other vibrations in the liquid making these vibrations relatively well localized. This assignment agrees with the results of some recent studies by the group of Tokmakoff [88, 89]. In these latter studies it was shown that the broad, red-shifted OH stretch vibrational spectrum of OH groups bonded to OH^- comprises both $0\rightarrow2$ transitions to Zundel states for (nearly) symmetric $O\cdots H\cdots O$ systems and $0\rightarrow1$ transitions of OH groups that are strongly hydrogen bonded to OH^-, but that are asymmetric in the sense that the hydrogen atom is much closer to one of the oxygen atoms.

4.3.1 Vibrational Relaxation

We excite the OH stretch vibrations of H_2O molecules hydrating the OH^- ions. At all concentrations, we use pump and probe pulses with a central frequency of 2650 cm^{-1}. In Fig. 4.2 we show transient absorption spectra at three different delay times, 0.4 ps, 1.2 ps and 40 ps, for solutions of 2 M, 4 M and 6 M. At early delays, the transient spectra show a negative absorption change throughout the whole frequency region. This negative absorption change is due to the bleaching of the ground state and the stimulated emission from the excited OH stretch

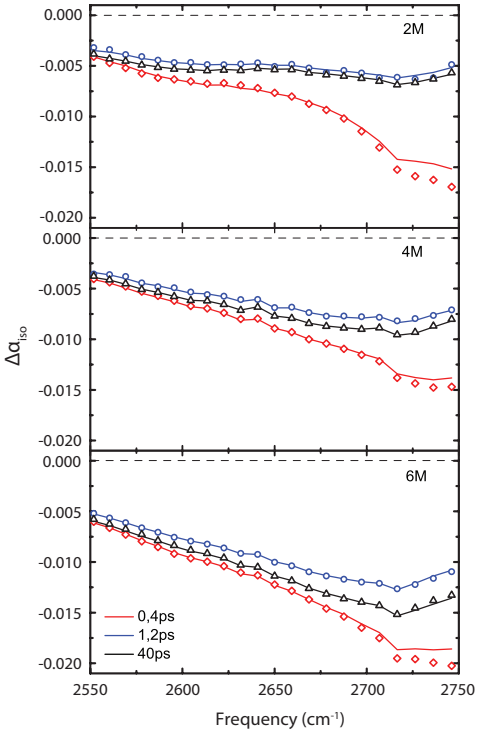

FIGURE 4.2. Transient spectra of three different NaOH solutions at pump-probe delay times of 0.4 ps (⋄), 1.2 ps (○) and 40 ps (△). The solid lines show the fitted result with the consecutive relaxation model.

vibration. It is seen that the amplitude of the bleaching decays rapidly at short delay time, but it increases again at later delay times.

In Fig. 4.3 (a) the isotropic absorption change $\Delta\alpha_{\mathrm{iso}}$ at the center frequency 2650 cm^{-1} is shown as a function of delay for three NaOH concentrations. At zero time delay, the pump excitation results in a bleaching signal that rapidly relaxes on a time scale of a few hundred femtoseconds. After reaching a minimum, the bleaching rises again on a much longer time scale. The signal no longer changes after ∼5 picoseconds. At this time the energy that was put in by the excitation is completely thermal over the focus. The transient minimum in the bleaching implies that the vibrational relaxation does not immediately lead to a thermalization of the excitation energy. Fig. 4.3 (a) shows that the equilibration process becomes slower with increasing NaOH concentration, which makes the bleaching minimum more pronounced.

The isotropic signals were fitted by least-square method with a consecutive relaxation model [90]. In this model, the excited state relaxes with a time constant T_1 to an intermediate state. This intermediate state relaxes to the final thermal equilibrium with a time constant T_{eq}. The fitted results are represented

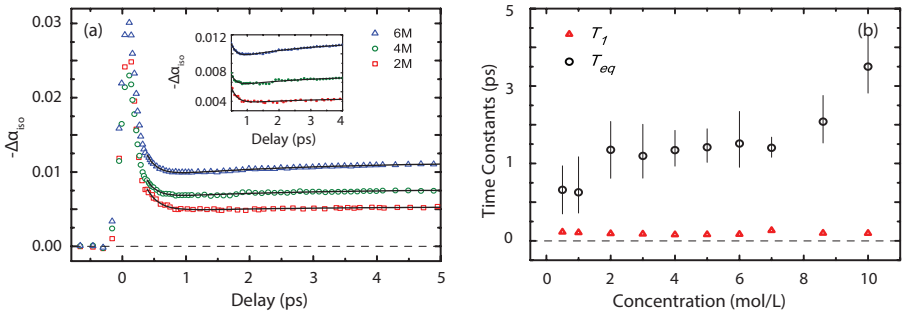

FIGURE 4.3. (a) Isotropic absorption change $-\Delta\alpha_{iso}$ as a function of delay time for three different concentrations of NaOH, measured at frequency of 2650 cm^{-1}. The solid lines represent fits to the data with the consecutive relaxation model. Inset, zoom-in from 0.5 ps to 4 ps. (b) Vibrational lifetime constant T_1 and equilibration time constant T_{eq} as a function of concentration. The error bars of T_{eq} are estimated by increasing the chi-square up to 10% of the minimum. The error bars of T_1 are comparable with the triangle size

by the solid lines in Fig. 4.2 and Fig. 4.3 (a). The time constants T_1 and T_{eq} resulting from the fit are plotted as a function of concentration in Fig. 4.3 (b). As shown in Fig. 4.3 (b), the concentration dependencies of T_1 and T_{eq} are quite different.

The transient spectrum of the intermediate state has the form of a thermal difference spectrum, which means that the fast relaxation process corresponds to the vibrational relaxation of the O–H stretch vibration of H_2O molecules hydrating OH^-. The time constant T_1 has a value of 200 fs, and is independent of OH^- concentration (see Fig. 4.3 (b)). The lack of concentration dependence of T_1 indicates that the vibrational relaxation is a local process in which the energy of the excited O–H stretch vibration relaxes to lower-frequency degrees of freedom within the same OH^- hydration complex. The value of T_1 is quite similar to the relaxation time constant T_1 of the O-H stretch vibrations in pure H_2O [91, 92]. The relaxation time of 200 fs is also quite similar to the time constant of 120-160 fs that was observed for HDO hydrating an OD^- ion [87–89].

The character of the intermediate state (being a local heated state) differs from that of the intermediate state of the relaxation observed in studies of isotopically diluted water, i.e. for the O–D/O–H stretch vibration of HDO molecules in H_2O/D_2O [93]. The intermediate state of the latter relaxation process does not have an associated transient spectrum, and its relaxation likely represents the delayed adaptation of the coordinates of the hydrogen bond network to the higher energy content of the low-frequency modes (librations, hydrogen-bond stretch and bend vibrations) that results from the relaxation of the O–D/O–H stretch vibration.

The equilibration time strongly varies with concentration, and increases from

1.3±0.5 ps at low concentrations to 4.5±0.7 ps for a solution of 10 M NaOH. The lack of concentration dependence of T_1 indicates that the vibrational relaxation is a local process in which the energy of the excited O–H stretch vibration relaxes to other vibrations within the same OH^- hydration complex. In contrast, the equilibration time T_{eq} is a more global parameter and very sensitive to the structural dynamics of the hydrogen bond network of the solution. For higher OH^- concentrations the restructuring takes more time, probably as a result of the stiffer hydrogen-bond network.

The intermediate state relaxes with an equilibration time constant that increases from 1.3±0.5 ps at low concentrations to 4.5±0.7 ps for a solution of 10 M NaOH. This strong concentration dependence can be understood from the fact the equilibration time T_{eq} is not a local parameter and will be strongly related to the collective structural dynamics of the hydrogen bond network of the solution. At higher OH^- concentrations the hydrogen-bond network will be stiffer, which will make the restructuring and thus full equilibration of the solution slower.

4.3.2 Anisotropy Dynamics

Fig. 4.4 shows the anisotropy decay for five different concentrations (0.5, 1.0, 2.0, 4.0, and 6.0 M). At time zero the anisotropy signals are roughly 0.35. The initial partial decay of this anisotropy from 0.4 to 0.35 may be due to rapid resonant intermolecular energy transfer between OH vibrations within the OH^- hydration complex and/or due to librational motions. The anisotropy dynamic shows a rapid initial drop (200 fs) followed by a much slower decay on a time scale of ∼10 ps. With increasing NaOH concentration the initial drop becomes larger and the subsequent decay becomes faster. In view of the short T_1 of the relaxation of the O–H stretch vibrations of 200 fs, it is clear that the signal conserves its anisotropy after the vibrational relaxation is complete, which implies that the influence of the heat resulting from the vibration relaxation on the transient spectral response is anisotropic. After the fast vibrational relaxation, the resulting localized heat primarily affects the originally excited O-Hs whose transition dipole moments direction have not changed during this short time. Therefore the transient spectrum resulting from this local heating effect is anisotropic. In fact, if the heating effect resulting from the vibrational relaxation would only influence the absorption spectrum of the originally excited OH vibration, the anisotropy of the original excitation would be conserved fully. However, the dissipated heat will also affect the absorption spectra of other O–H vibrations in the same hydration complex of the OH^- ion that will have different orientations. Nevertheless, as the number of O–H vibrations absorbing at 2650 cm^{-1} within the complex will be limited, a net non-zero anisotropy is retained.

The ultrafast excitation and vibrational relaxation of the OH vibrations result in a strongly heated OH^- hydration complex that is hotter than its surroundings. Hence, the complex itself is in (hot) thermal equilibrium but the whole solution is in a non-equilibrium state. The complex then cools via heat

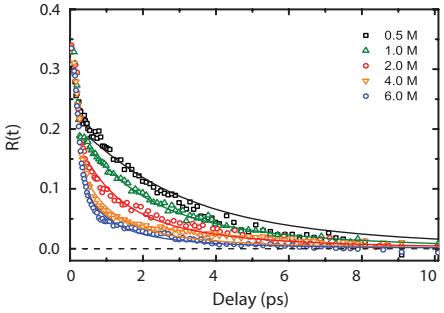

FIGURE 4.4. Anisotropy as a function of delay for five different concentrations of NaOH. The data are measured at a frequency of 2650 cm^{-1}. The solid lines are fits to the data of the heat diffusion model.

diffusion to its surroundings. Given the probe frequency of 2650 cm^{-1}, we only observe the effects of heat reaching other excited and unexcited hydration complexes. Over time the unexcited complexes will become heated and, as the solvating water OH groups in these complexes have different (random) orientations, the overall distribution of the thermally affected O-H vibrations becomes isotropic.

The anisotropy dynamics of hydroxide solutions have been studied before for isotopically diluted solutions of HDO in D_2O/OD^- [87]. In this latter study, the dynamics of the isotropic signal contained a strong slow component associated with the vibrational relaxation of HDO molecules that are not directly interacting with OD^- ions. In addition, the heating effect of the vibrational relaxation was much smaller, because the probed hydroxyl groups are isotopically diluted. As a result, the anisotropy dynamics observed in Ref.10 were dominated by the orientational dynamics of the still excited OH vibrations of HDO molecules that are not in the first hydration shell of the hydroxide ion. In this chapter the anisotropy dynamics are dominated by the heat diffusion and reorientation of the hot OH^- hydration complexes.

To calculate the anisotropy decay due to heat diffusion, we assume that the hydration complex of OH^- is a sphere with radius R and we neglect the interactions between different excited complexes. Under these assumptions, the time-dependent distribution of the temperature inside and outside the hot complex is expressed by the following equation [94], that describes the heat diffusion from a hot sphere to an infinitely large cold environment without any source:

$$T(R,r,t) = T_{\max} \cdot \left\{ \frac{1}{r}\sqrt{\frac{\chi}{\pi}t}[\exp(-\varepsilon_+^2) - \exp(-\varepsilon_-^2)] + \frac{1}{2}[\mathrm{erf}(\varepsilon_+) + \mathrm{erf}(\varepsilon_-)] \right\} \tag{4.1}$$

where $\varepsilon_{\pm}(R,r,t)=(R\pm r)/(2\sqrt{\chi t})$, $\mathrm{erf}(x)$ is the Gaussian error function, $T_{\max}$ denotes the initial temperature of the hot sphere, χ represents the thermal diffusivity of the medium surrounding the complex respectively, and r is the distance away from the center of the hot complex.

The thermal energy that diffuses out of the excited complex will heat other unexcited complexes and solvent water molecules. The fraction f of the thermal energy contained in these other complexes is equal to the volume fraction of the OH^- hydration complex $f=4\pi\rho R^3/3$, where ρ is the number density expressed in number of hydration complexes per nm^3. After the vibrational relaxation, the thermal energy still present in the excited complex and the thermal energy contained in the other complexes is governed by following equations:

$$E_{\mathrm{in}}(t) = \int_0^R 4\pi r^2 T(R,r,t)dr \tag{4.2}$$

$$E_{\mathrm{out}}(t) = f \cdot \int_R^\infty 4\pi r^2 T(R,r,t)dr \tag{4.3}$$

The anisotropy due to the heating effect $R_{\mathrm{h}}(t)$ is proportional to the ratio of the part of the excitation energy that is still in the excited complex $E_{\mathrm{in}}(t)$, and the total dumped energy contained in all OH^- hydration complexes which is the sum of the energy in the excited complex and the energy contained in all other complexes outside the excited complex E_{out}:

$$R_{\mathrm{h}}(r,t) = a \cdot \frac{E_{\mathrm{in}}(t)}{E_{\mathrm{in}}(t) + E_{\mathrm{out}}(t)} \tag{4.4}$$

where a is a scaling factor. Substituting the expressions for $E_{\mathrm{in}}(t)$ and $E_{\mathrm{out}}(t)$ we obtain:

$$R_{\mathrm{h}}(r,t) = \frac{a \cdot \int_0^R r^2 T(R,r,t)dr}{\int_0^R r^2 T(R,r,t)dr + f \cdot \int_R^\infty r^2 T(R,r,t)dr} \tag{4.5}$$

The anisotropy not only decays as a result of heat diffusion but as a result of the reorientation of the OH^- hydration complexes. These anisotropy dynamics $R_{\mathrm{r}}(t)$ are described by an exponential function:

$$R_{\mathrm{r}}(t) = e^{-\frac{t}{t_{\mathrm{r}}}} \tag{4.6}$$

As the total anisotropy dynamics of the hydroxide complexes is described by $R(t) = R_{\mathrm{h}}(t)R_{\mathrm{r}}(t)$, we obtain:

$$R(t) = \frac{a \cdot \int_0^R r^2 T(R,r,t)dr}{\int_0^R r^2 T(R,r,t)dr + f \cdot \int_R^\infty r^2 T(R,r,t)dr} \cdot e^{-\frac{t}{t_{\mathrm{r}}}} \tag{4.7}$$

The three parameters R, χ and t_{r} that enter Eq. (4.7) are assumed to be independent of concentration, which is not necessarily true. However, it was shown in neutron scattering studies that the spatial distribution of water molecules

hydrating hydroxide remains the same, even at very high concentrations, which indicates that the radius R of hydration complex is quite independent of concentration [95, 96]. Likewise, the thermal diffusivity of aqueous salt solutions shows very little dependence on the salt concentration: the χ of pure water is 0.1435 nm^2/ps and the χ of 6 M $NaOH/H_2O$ is 0.1495 nm^2/ps both at 25 °C [97].

We fitted the anisotropy signals globally, and find that the heat diffusion model provides a very good description of the anisotropy decay at all hydroxide concentrations, as illustrated by the solid lines in Fig. 4.4. The speed up of the anisotropy decay with concentration can thus be well explained from the fact that with increasing NaOH concentration the nearest unexcited hydration complexes are located at smaller values of r. From the fitting we obtain a=0.22±0.02, R=0.36±0.03 nm, χ=0.05±0.01 nm^2/ps and t_r=12±2 ps. The errors are estimated when chi-square increases up to 1.5 times the minimum value.

The a value of 0.22±0.02 represents the anisotropy of the heated excited complex, which is smaller than the initial value of the anisotropy of 0.4. This decrease in anisotropy can be explained from the presence of other differently oriented O–H groups with the excited hydration complex that are also hydrogen-bonded to the OH^- ions. The absorption frequencies of these other O–H groups can be close to ∼2650 cm^{-1}, and the heating of these other differently oriented O–H groups results in an anisotropy of the heated excited complex that is smaller than 0.4. In view of this picture the a value of 0.22±0.02 may be considered to be relatively high. However, it should be noted that the anisotropy will only decay due to the heating of O–H groups that possess a non-negligible absorption at the probe frequency of 2650 cm^{-1}. The transfer of energy to O–H groups that do not absorb at 2650 cm^{-1} will decrease the magnitude of the isotropic (heating) signal at 2650 cm^{-1}, but not its anisotropy. Nevertheless, the high value of a of 0.22±0.02 indicates that the initially excited O–H strongly contributes to the heated excited complex that results directly after the vibrational relaxation.

Using the radius R of the complex of 0.36±0.03 nm and the average volume of water molecule at room temperature, we calculate the number of water molecules contained in the hydration complex to be ∼4.5. This value agrees well with the results of *ab*−initio molecular dynamic (MD) simulations that found respective coordination numbers of 4.2, 4.8 and 4.7 respectively for mirror mechanism, dynamical hypercoordination mechanism and static hypercoordination mechanism [29]. The thermal diffusivity of 0.05 nm^2/ps is approximately three times lower than the macroscopic thermal diffusivity [98]. This difference may be due to the different character of the excitations of which the energy has to be transferred. The reorientation time constant t_r of the hydration complex of 12±2 ps is significantly longer than the reorientation time constant of 2.5 ps of O–D groups of HDO molecules in H_2O [90, 93]. This larger reorientation time constant indicates that the reorienting hydration complex forms a relatively large and rigid structure that has to reorient as a whole [99].

4.4 CONCLUSIONS

We study the vibrational relaxation dynamics and anisotropy dynamics of the hydration shells of OH^- ions with polarization-resolved femtosecond vibrational spectroscopy. We study the dynamics for solutions of NaOH in H_2O with concentrations ranging from 0.5 to 10 M. The relaxation of O–H stretch vibrations of water molecules hydrating the OH^- ion is observed to proceed via two subsequent processes. In the first process, the excited O–H vibrations relax to an intermediate state with a concentration independent time constant 200 fs. The intermediate state represents a state in which the relaxed energy of the excited O–H vibration has led to a local heating of the hydration complex. In the second process, the intermediate state decays to a final thermal equilibrium in which the energy is thermally distributed over the focus of the exciting laser pulse. The time constant of the equilibration process rises with increasing concentration, from 1.2 ps for a 0.5 M solution to 4.5 ps for a 10 M solution.

The locally heated hydration complex possesses a significant nonzero anisotropy which shows that this state contains a large contribution of the initially excited O–H group. We describe the decay of the anisotropy of the intermediate state with a model in which we include the heat diffusion from the excited hydration complexes to non-excited complexes and the reorientation of the hydration complexes. We find that this model provides a quantitative description of the anisotropy decay at all measured concentrations using concentration independent values for the initial anisotropy a of the intermediate state, the radius R of the hydration complex, the heat diffusivity χ, and the reorientation time t_r of the hydration complex. We find a=0.22±0.02, R=0.36±0.03 nm, χ=0.05±0.01 nm^2/ps, and t_r=12±2 ps.

The initial anisotropy a of the intermediates state of 0.22±0.02 is relatively high, which indicates that there is no resonant energy transfer within the H_2O molecule to which the excited O–H group belongs [100]. This result shows that the two O–H groups of this H_2O molecule are shifted far out of resonance, because only one of the O–H groups is hydrating the OH^- ion. The high value of a also implies that the intermediate state possesses a strong contribution of the initially excited O–H group, which means that the initial heating is truly a very local effect and/or there are very little O–H vibrations within the hydration complex absorbing near 2650 cm^{-1}. The value of R corresponds to a hydration shell of 4.5 water molecules, in excellent agreement with the results of *ab*−initio molecular dynamics calculations. The reorientation time of the hydration complex is significantly longer than the reorientation time of 2.5 ps of water molecules in bulk liquid water, which indicates that this complex forms a relatively large and rigid structure.

5

Infrared Activated Proton Transfer in Aqueous Nafion

We report on the observation of a strong reorganization of the proton hydration structure in hydrated Nafion membranes following single-quantum excitation of a proton vibration with ∼4 μm light pulses. The reorganization takes place with a time constant of 170±20 fs and leads to a strong red-shift of the excited proton vibration and the rise of new water-like O–H stretch absorption bands. These observations can be explained from a vibrational-excitation induced change of the proton-hydration structure that involves transfer of the proton charge. The results are consistent with the results of recent quantum molecular dynamics simulations of proton transfer in Nafion membranes.

5.1 Introduction

Light-induced chemical reactions are extremely widespread and important. Examples are photosynthesis and the formation of ozone. In most cases the reaction is induced by excitation of an electronic degree of freedom of the molecule that leads to a weakening of one or more chemical bonds. The triggering of a chemical reaction by excitation of a molecular vibration is much less common, and usually requires multi-quantum excitation to a highly excited vibrational state [101–103].

Single-quantum vibrational excitation is usually not sufficient to trigger a chemical reaction. However, for some reactive systems, single-quantum vibrational excitation can increase the rate of a particular reaction channel, as has been demonstrated for bi-molecular reactions between small molecules and radicals in the gas phase [104, 105]. In the condensed phase the triggering of a chemical reaction by vibrational excitation is more complicated, as the intermolecular interactions can lead to dissipation of the energy of the excited vibration before the reaction can take place. Up to now, the only example of a such a condensed-phase reaction is the cis-trans isomerization of nitrous acid (HONO) following excitation of the O–H stretch vibration [106, 107]. For this IR driven reaction to occur, the molecule has to be embedded in a rare-gas matrix at low temperatures to limit the intermolecular interactions that would lead to dissipation.

Intermolecular interactions can also have a positive effect in enabling a light-driven chemical reaction. The groups of Hynes and Ando [108, 109] predicted that the strong coupling between an excited vibration and surrounding water molecules can lead to proton transfer. They calculated that the excitation of the H–F vibration of HF in water would lead to transfer of a proton from HF to a neighboring water molecule. Up to now this type of vibrational-excitation induced proton transfer has eluded experimental observation.

In this chapter, we find evidence for the activation of proton transfer by single-quantum vibrational excitation in the nanochannels of a hydrated Nafion membrane at room temperature. Nafion is a sulfonated tetrafluoroethelyne (Teflon)-based fluoropolymer and forms the most widely used proton exchange membrane (PEM) in hydrogen fuel cells [110]. Nafion possesses hydrophilic sulfonated perfluorovinyl side chains that form nanoscaled hydrophilic domains. The counter cations of the negatively charged sulfonate groups can be formed by protons, and in case the Nafion is hydrated, meaning that the membrane channels contain water molecules, the protons become mobile [111]. The introduction of protons leads to a broad-band absorption between 1500 and 3100 cm^{-1} (see Section 5.4.1). Recent quantum molecular dynamics simulations of Nafion employing the self-consistent multi-state empirical valence bond method showed that the hydrated proton in Nafion acquires similar proton hydration structures as in liquid water, i.e. the proton can be hydrated in an Eigen-like structure or in a Zundel-like structure [112–114]. The Eigen hydration structure is formed by an H_3O^+ ion of which the three O–H groups are strongly hydrogen bonded to three neighboring oxygen atoms, thus forming an $H_9O_4{}^+$ structure. In the Zundel structure the proton is flanked by two water molecules, thus forming an $H_5O_2{}^+$ structure. The quantum molecular dynamics simulations show that the proton hydration structure is Zundel-like in the first hydration shell of the sulfonate counterion, and Eigen-like at larger distances from this ion [112, 113].

5.2 Experiment

We study the properties of water molecules and protons in hydrated nafion nanochannels using polarization-resolved femtosecond vibrational spectroscopy employing independently tunable excitation and detection pulses. The experiments were performed with the two-color pump-probe setup described in Section 3.2.1. The frequency ν_{exc} of the excitation pulse is tuned from 2850 to 3700 cm^{-1}, and the detection frequency ν_{det} is tuned from 1500 to 3600 cm^{-1}. We use a relatively narrow-band excitation pulse (with a bandwidth of $\sim$110 cm^{-1}) to ensure the selective excitation of molecular vibrations of water molecules or proton hydration structures. In the experiment we monitor the excitation-induced absorption changes $\Delta\alpha$ and the anisotropic signal R as a function of the central excitation frequency, the detection frequency, and the time delay between the excitation and the detection pulses.

We obtain the 2D-IR spectra (Fig. 5.1) by tuning the frequency ν_{exc} of the

excitation pulse from 2850 to 3600 cm^{-1} (2.6 to 3.5 μm), and by combining isotropic transient spectra that are measured with broadband detection pulses centered at different wavelengths.

The Nafion is purchased as 180 μm thick membranes in the proton terminated form and purified in the way described in Section 3.4. To get enough transmission of infrared light, the purified membranes are treated with 1 M mixture of HCl and NaCl (H^+:Na^+=1:9) to replace 10% of the Na^+ ions by protons. The membranes are placed in a desiccator containing saturated CsF solution to control the number of water molecules per Nafion sulfonate group. The membranes are transferred to the cuvette just before the measurement. The cuvette is a gastight chamber, ensuring a constant humidity of the Nafion membranes during the experiment. The proton and water content of the Nafion samples are checked by measuring linear IR spectra of the samples with a dual beam Perkin-Elmer 881 spectrometer.

5.3 Results and Discussion

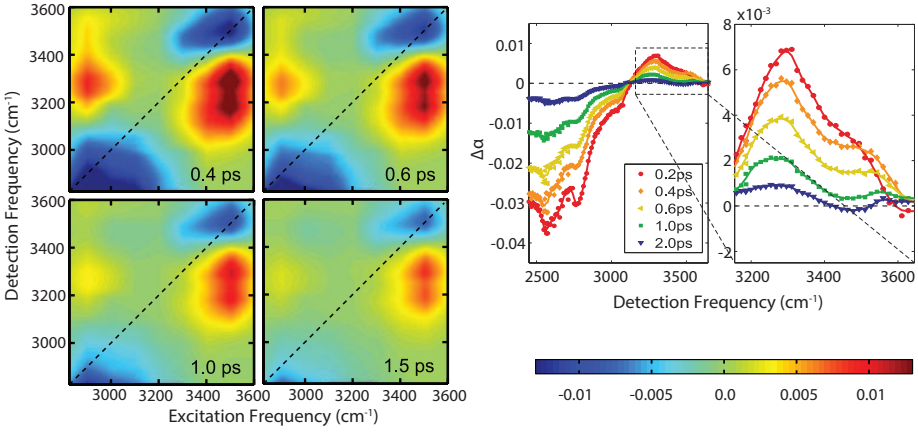

Figure 5.1. Left panel: isotropic two-dimensional infrared (2D-IR) spectra of Nafion membranes at a hydration level of 3 water molecules per sulfonate group. The spectra show strong diagonal signals at the water vibrations (∼3500 cm^{-1}) and the Eigen proton vibrations (∼2900 cm^{-1}), and cross-peak signals between the proton and the water vibrations. Right panel: cuts at ν_{exc}=2900 cm^{-1} of 2D-IR spectra at different delay times. The induced absorption bands at 3270 and 3520 cm^{-1} are also shown enlarged.

Fig. 5.1 shows two-dimensional infrared (2D-IR) spectra of hydrated Nafion nanochannels for four different time delays between the excitation and the detection pulses. For ν_{exc}=3500 cm^{-1}, ν_{det}=3500 cm^{-1} we observe a bleaching signal of the fundamental v=0→1 absorption of the water O–H stretch vibra-

tions. The induced absorption signal observed for ν_{exc}=3500 cm^{-1}, ν_{det}=3300 cm^{-1} results from the v=1→2 excited-state absorption of the water O–H stretch vibrations. The 2D-spectra at different time delays illustrate that the excited water O–H stretch vibrations decay relatively slowly, much slower than the O–H stretch vibrations of bulk H_2O for which T_1 is ∼250 fs [91]. This finding agrees with the results of a previous study of the vibrational relaxation of isotopically diluted water in nafion membranes [115].

For ν_{exc}=2900 cm^{-1}, ν_{det}=2900 cm^{-1} a broad bleaching signal is observed. We assign this bleaching signal to the excitation of an O–H vibration of the hydronium H_3O^+ core of an Eigen proton hydration structure [37, 38, 48, 116]. The Eigen structures are dynamically distorted, thus leading to a very broad response around 2600 cm^{-1}. The 2D-spectra also show clear cross-peak signals: the excitation of the proton vibration with ν_{exc}=2900 cm^{-1} leads to a signal at ν_{det}>3250 cm^{-1}. By taking a cut of the 2D-spectrum at a particular excitation frequency we obtain a transient spectrum. The right panel of Fig. 5.1 shows transient spectra at five different delay times for ν_{exc}=2900 cm^{-1}. The transient spectra show a bleaching signal for ν_{det} between 2500 and 3100 cm^{-1}, and induced absorption signals at ν_{det}=3270 cm^{-1} and ν_{det}=3520 cm^{-1}. These latter signals constitute the cross-peak signal in the 2D-IR spectra shown in the left panel of Fig. 5.1.

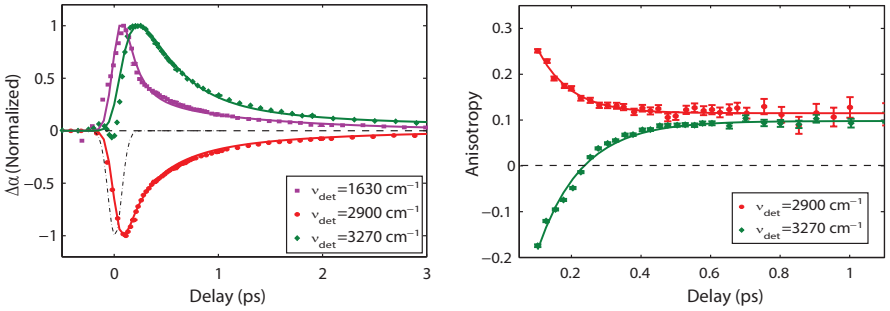

FIGURE 5.2. Left panel: normalized isotropic absorption changes as a function of delay at three different detection frequencies after excitation with ν_{exc}=2900 cm^{-1}. A positive signal implies an induced absorption, a negative signal a bleaching signal. The solid lines result from a fit to a four-level kinetic model (described in the Section 5.4.3). Right panel: anisotropy measured at two detection frequencies after excitation with ν_{exc}=2900 cm^{-1}.

For a complex molecular system like hydrated Nafion the observation of cross-peaks can have different origins. One of these origins is vibrational coupling, implying that the excitation of a vibration of the system induces a change in frequency of other, nearby vibrations. In this case the cross-peak signal should have the same dynamics as the excited vibration [117]. However, in the left panel of Fig. 5.2 it is seen that the induced absorption signal at ν_{det}=3270 cm^{-1} rises with a delay of ∼200 fs with respect to the excitation, thus ruling

out vibrational coupling as its origin.

Another potential origin of the cross-peak signal is a heating effect. The energy of the excited proton vibration is eventually converted to heat which can lead to a breaking of hydrogen bonds and a blueshift of the proton vibration to frequencies >3000 cm^{-1}. To test this explanation we measured the anisotropy of the vibrational signals following excitation of the proton vibration (right panel of Fig. 5.2). The anisotropy at ν_{det}=2900 cm^{-1} is initially positive (∼0.3), while the anisotropy at ν_{det}=3270 cm^{-1} is initially negative (∼-0.1). The induced absorption band at ν_{det}=3520 cm^{-1} shows the same initial negative anisotropy (not shown). The initial negative anisotropy of the bands at 3270 cm^{-1} and 3520 cm^{-1} indicates that the associated vibrational transition dipole moments are at a relatively large angle with respect to that of the excited vibration. The observation of an initial negative anisotropy rules out the possibility that the induced absorption bands would be generated by a heating effect, because in this case the induced absorption bands would have zero anisotropy (complete thermalization), or a positive anisotropy (in case the heating would mainly affect the originally excited vibration).

Finally, cross peak signals can be caused by structural relaxation and equilibration processes that lead to a change of the character and frequencies of the excited and non-excited vibrations [118]. We observe that the rise of the cross peaks is accompanied by a strong red shift of the bleaching signal of the excited proton vibration (Fig. 5.3). This red shift points at a shortening and strengthening of the hydrogen bond donated by the excited O–H stretch vibration [119], implying a strong structural relaxation. We find that the bleaching shifts much further than to the center frequency of 2600 cm^{-1} of the absorption spectrum of the Eigen proton vibration [37, 38, 48]. The strong red-shift of the bleaching indicates that the excited v=1 state of the Eigen vibration evolves into an excited v=1 state of an O···H···O Zundel vibration. This vibration has a frequency of ∼1100 cm^{-1}, much lower than the Eigen vibration [37, 38, 48].

The rise of the cross peaks at ν_{det}=3270 cm^{-1} and ν_{det}=3520 cm^{-1} can be well explained from the excitation-induced structural relaxation from Eigen to Zundel. When the excited O–H vibration in hydronium core of Eigen complex evolves to a Zundel proton vibration, the two other not excited O–H modes of the Eigen complex will turn into higher-frequency O–H stretch vibrations of water molecules flanking the Zundel proton. The frequencies of the O–H stretch vibrations of water molecules flanking a proton in an $H_5O_2^+$ Zundel hydration structure indeed correspond well to the frequencies of 3270 cm^{-1} and 3520 cm^{-1} of the cross peaks [37, 48]. Furthermore, the delay time at which the induced absorption bands of the Zundel proton-hydration structure reach their maximum (Fig. 5.2) is similar to the delay time at which the bleaching below 2200 cm^{-1} reaches its maximum (Fig. 5.3). Finally, these vibrations are at a quite large angle with respect to the proton vibration, which agrees with the initial negative value of the anisotropy of the cross-peak signals.

In the top panel of Fig. 5.4 we present a schematic picture of the evolution from Eigen to Zundel and the corresponding changes in vibrational frequencies. These structures are based on the results of quantum molecular dynamics

simulations of Nafion [112–114].

Quantum molecular dynamics simulations showed that proton transfer in liquid water involves a special pair dance in which the central hydronium ion of the Eigen can form a special pair with one of the three surrounding water molecules [5]. For this special pair the hydrogen bond is shorter than for the other two O–H groups of the hydronium ion. Our observations indicate that the excitation of an O–H stretch vibration of the H_3O^+ core of an Eigen-like cation leads to a contraction of the hydrogen bond at this excited O–H group. As a result, the excited O–H group and the water molecule to which this group is hydrogen bonded, become the special pair. The driving force for contraction of the hydrogen bond is the lowering of the energy of the excited state of the proton vibration. Upon contraction of the hydrogen bond, the vibrational potential changes from a strongly asymmetric and deep potential to a symmetric and broad potential, as illustrated in the lower panel of Fig. 5.4. The energy of the first excited vibrational state is much lower in the symmetric potential than in the original asymmetric potential. The change of the vibrational potential is accompanied by a transfer of proton charge from the non-excited O–H groups of the original H_3O^+ ion to the vibrationally excited Zundel proton. This scenario agrees with the mechanism of infrared activated adiabatic proton transfer proposed by Hynes and others [108, 109]. After relaxation of the v=1 state in the Zundel potential, the system will evolve back to an Eigen hydration structure that can be the same as the one before the excitation, or that can be translated by one water molecule, thus completing a successful proton-transfer reaction.

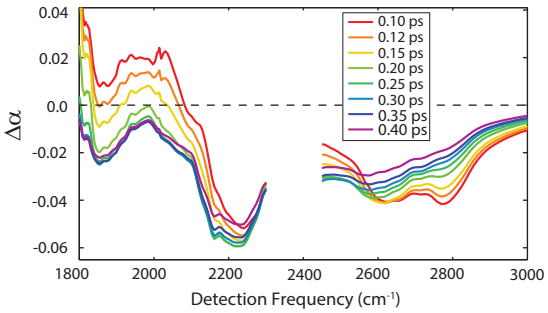

Figure 5.3. Isotropic transient absorption spectra of a proton-terminated Nafion membrane at different delay times at detection frequencies ν_{det} ranging from 1800 to 3000 cm^{-1}. The hydration level of membrane is ∼3 water molecules per sulfonate group. The Nafion membrane is excited with ν_{exc}=2900 cm^{-1}. The spectral region between 2300 and 2450 cm^{-1} is missing because of the strong absorption of Nafion in this frequency region.

To determine the time constants of the transient spectral changes we fitted the data shown in the left panel of Fig. 5.2 to a kinetic model (see Section 5.4.3). The fit results are represented by the solid curves in Fig. 5.2. The bleaching signal at ν_{det}=2900 cm^{-1} and the induced absorption at ν_{det}=1630 cm^{-1} show a pulse-width limited rise (Fig. 5.2), which indicates that these signals are both

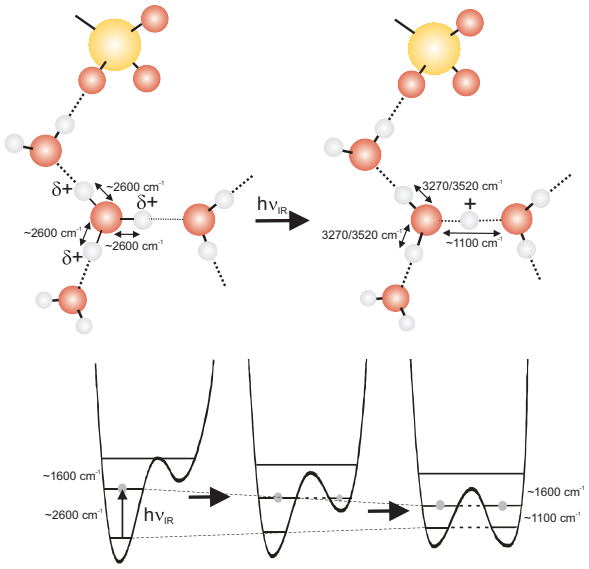

Figure 5.4. Top panel: schematic picture of the evolution from an Eigen proton hydration structure to a Zundel hydration structure following excitation of one of the proton vibrations of the Eigen structure. The vibrational frequencies of the different modes of the hydration structures are indicated. Lower panel: the corresponding adiabatic change in the shape of the vibrational potential of the proton.

due to the direct excitation of the Eigen proton vibration. The excitation of the $v = 1$ state of the Eigen vibration not only leads to a bleaching of the fundamental $v = 0 \rightarrow 1$ transition but also to a new absorption band starting from the $v = 1$ state corresponding to the $v = 1 \rightarrow 2$ transition. This latter transition is very broad and at a much lower frequency than the fundamental transition as a result of the anharmonicity of the proton vibration. We thus assign the broad-band absorption at early delays at frequencies ν_{det}<1850 cm^{-1} (Fig. 5.3) to the v=1→2 excited state absorption of the Eigen proton vibration, which implies that this proton vibration possesses a very large anharmonicity. This assignment agrees with previous calculations of the vibrational levels of the hydrogen-bonded O–H$\cdots$O system based on the Lippincott-Schröder potential [120, 121].

From the fit we find that the Eigen-Zundel transfer and the vibrational relaxation have time constants of 170±20 fs and 350±30 fs, respectively. The Eigen-Zundel transfer leads to a decay of the stimulated emission contribution to the bleaching signal at 2900 cm^{-1} (∼50% of the total bleaching signal), a decay of the v=1→2 excited state absorption of the Eigen proton vibration at 1630 cm^{-1}, and a rise of the induced absorption signals at 3270 and 3520 cm^{-1}. The vibrational relaxation leads to a decay of the induced absorptions at 3270 and 3520 cm^{-1}, and to a further decay of the bleaching signal of the Eigen proton vibration (repletion of the ground state). The vibrational relaxation eventually

results in a local heating effect that is associated with a small residual change in absorption. This absorption change decays by transfer of thermal energy to the Nafion backbone. We model this final equilibration process as a decay with a time constant of 1.3±0.2 ps.

The anisotropy of the excited proton vibration at ν_{det}=2900 cm^{-1} and the induced absorption at ν_{det}=3270 cm^{-1} both relax to a value of ∼0.1 with a time constant of 120±30 fs (right panel of Fig. 5.2). This final value of the anisotropy indicates that the excitation has randomized in the plane of the central H_3O^+ ion of the Eigen hydration structure [122], meaning that the vibrational excitation is delocalized over the three O–H groups of the central H_3O^+ ion. The hydrogen bonds between the central hydronium ion and the three neighboring water molecules are constantly fluctuating in length and strength. These fluctuations modulate the frequencies of the three O–H vibrations of the central hydronium ion, thereby enabling rapid energy transfer between these vibrations. After the vibrational excitation has become delocalized over the three O–H vibrations, the excitation-induced formation of the special pair can occur at each of the three O–H groups. As a result, the anisotropy of both the bleaching and the induced absorption signals become equal to 0.1. Only directly after the excitation there is a preference for Eigen-Zundel transfer along the O–H group that was initially excited, leading to the initial negative anisotropy of the induced absorption at ν_{det}=3270 cm^{-1} and ν_{det}=3520 cm^{-1}.

For bulk liquid water, the excitation of the proton vibration of the Eigen structure does not lead to proton transfer, probably because the vibrational lifetime T_1 of the proton vibration in bulk water is only 110±20 fs [21]. In the Nafion nanochannels, proton transfer can occur within the lifetime because the proton vibration has a relatively long T_1 of 350±30 fs. This favorable comparison of the time scales of proton transfer and vibrational relaxation finds its origin in the molecular structure of the hydrated Nafion nanochannel. Recent quantum molecular dynamics simulations showed that in Nafion nanochannels the proton diffusion via Grotthuss conduction is anti-correlated to the diffusion via thermal motions of the proton hydration structures (vehicular diffusion) [112–114], as a result of the strong association of the hydrated protons with the sulfonate counter-ions and the reduced dimensionality of the water network in which the diffusion takes place. The strong association with sulfonate can be the origin of the relatively slow vibrational relaxation of the excited proton vibration. A similar slowing down has been observed for the hydroxyl vibrations of water molecules bound to sulfonate [123]. The limited extension of the water network in the Nafion nanochannel may also play a role. This network can show a strong intermolecular coupling in one direction, thereby enabling excitation induced proton transfer, while showing little intermolecular coupling in other directions, thus making the vibrational relaxation relatively slow.

5.4 Appendix

5.4.1 Linear Spectra

Fig. 5.5 shows the linear absorption spectrum of a Nafion membrane containing only Na^+ ions and the absorption spectrum of a Nafion membrane for which 10% of the Na^+ has been exchanged by protons. The introduction of protons leads to an additional broad-band absorption ranging from 1500 to 3100 cm^{-1}. At frequencies <1500 cm^{-1} the Nafion membranes are not transparent due to the strong absorption of the C-F vibrations.

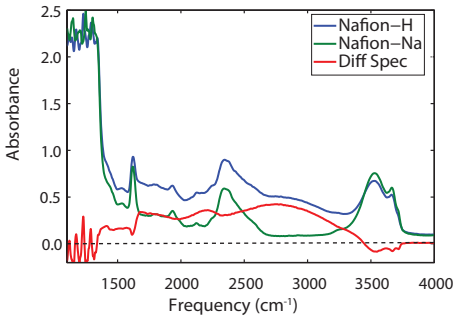

Figure 5.5. Linear infrared absorption spectra of sodium-terminated and partially proton-terminated (10%) Nafion membranes at a hydration level of 3 water molecules per Nafion sulfonate group. Also shown is the difference spectrum highlighting the vibrational spectrum of the hydrated protons.

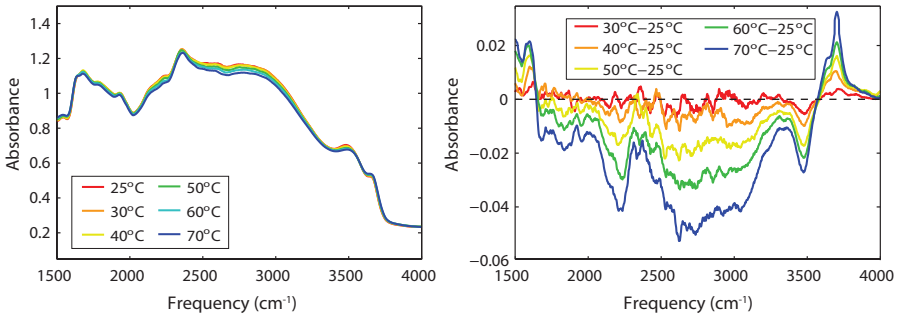

Figure 5.6. Left panel: linear absorption spectra of sodium-terminated and partially proton-terminated (10%) Nafion membranes at a hydration level of 3 water molecules per Nafion sulfonate group at six different temperatures; right panel: difference spectra obtained by subtracting the spectrum at 25° C from the spectra at higher temperatures.

In the left panel of Fig. 5.6 we show linear absorption spectra of the Nafion sample at different temperatures to illustrate the effect of heating on the absorption bands of the hydrated protons and water. In the right panel of Fig. 5.6

difference spectra are shown obtained by subtracting the spectrum at 25°C from the spectra at higher temperatures. Raising the temperature is seen to lead to a broad-band bleaching of the absorption in the frequency region between 1650 and 3550 cm^{-1}. From this result it follows that the observed induced absorption signals at 3270 and 3520 cm^{-1} in the transient spectra cannot be due to a thermal effect. It is also seen that the spectrum of the O-H stretch vibrations of water molecules hydrating the sulfonate groups at ∼3500 cm^{-1} shifts to the blue when the temperature is increased.

The protons become dissociated from the sulfonate groups of the nafion already at a hydration level of 2-3 water molecules per sulfonate group. This is illustrated by the rise of the absorption peak at 1720 cm^{-1} for a 100% protonated nafion sample (Fig. 5.7). This peak can be explained from the doubly degenerate asymmetric bending vibration of the central H_3O^+ ion of the Eigen proton hydration structure or from the bending vibration of water molecules flanking the Zundel proton. In either case the rise of this peak evidences that the proton gets dissociated from the sulfonate group. This finding agrees with the results of previous studies [116, 124].

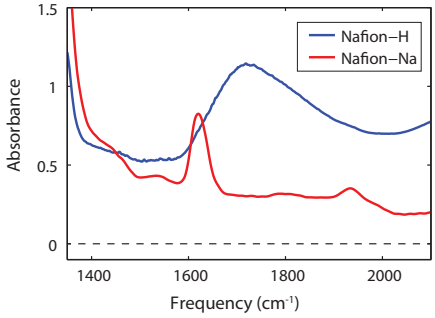

FIGURE 5.7. Linear absorption spectra of sodium-terminated and (100%) proton-terminated Nafion membranes at a hydration level of 3 water molecules per Nafion sulfonate group. The sodium-terminated Nafion membrane shows an absorption peak at 1620 cm^{-1} associated with the bending vibration of H_2O. For proton-terminated Nafion an additional strong band at 1720 cm^{-1} is observed, associated with the doubly degenerate asymmetric bending vibration of H_3O^+.

5.4.2 TRANSIENT ABSORPTION SPECTRA

In Fig. 5.8 we show transient spectra at different delay times measured for a Nafion membrane only containing Na^+ ions and a Nafion membrane for which 10% of the Na^+ ions has been exchanged for H^+. The transient spectra observed for the Nafion membrane only containing Na^+ are all close to the baseline, showing that excitation with ν_{exc}=2900^{-1} leads to a negligible signal if there are no protons present.

In Fig. 5.9 we show transient spectra at different delay times measured with ν_{exc}=2900 cm^{-1} and the detection frequency ν_{det} varied over a broad

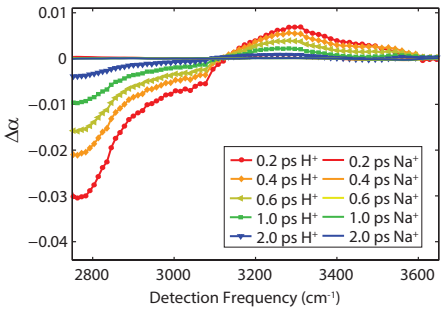

Figure 5.8. Isotropic transient absorption spectra at different delay times of a Nafion membrane containing 100% sodium ions (solid lines close to zero), and a Nafion membrane for which 10% of the sodium ions is replaced by protons (solid lines containing symbols). The Nafion membranes are excited with ν_{exc}=2900 cm^{-1}=2900 cm^{-1}.

frequency range from 1600 to 3700 cm^{-1}. The spectra clearly show the broad bleaching signal of the excited proton vibration between 1850 and 3100 cm^{-1}, the induced absorption cross peaks at 3270 and 3520 cm^{-1}, and an induced absorption signal at frequencies below 1850 cm^{-1}. We assign the latter signal to the 1→2 transition of the excited proton vibration. The large frequency difference between the 1→2 transition and the fundamental 0→1 transition can be explained from the extremely strong anharmonicity of the vibrational potential of the proton vibration.

In Fig. 5.10 we show transient absorption signals as a function of delay following excitation of the Eigen proton vibration with ν_{exc}=2500 cm^{-1}. We observe that the bleaching signal at ν_{det}=2500 cm^{-1} rises instantaneously. The induced absorption signal at ν_{det}=3270 cm^{-1} shows a delayed rise, similar to the case when the proton vibration was excited with ν_{exc}=2900 cm^{-1}. If this signal would have been the result of vibrational coupling, its dynamics are expected to be equal to the dynamics of the excited vibration, i.e. the signal should have risen with the cross-correlate. Vibrational coupling can only give rise to a delayed cross-peak signal if this coupling would be frequency dependent. For instance, if the vibrational coupling would be stronger at the central frequency of 2600 cm^{-1} of the Eigen proton vibration than at 2900 cm^{-1}, spectral diffusion from the excitation frequency of 2900 cm^{-1} to the center frequency would lead to a delayed rise of the cross-peak signal. However, the induced absorption signal at ν_{det}=3270 cm^{-1} shows a similar delayed rise if we excite the Eigen proton vibration with ν_{exc}=2500 cm^{-1}, thus excluding (frequency-dependent) vibrational coupling as the origin of the induced absorption signal. The induced absorption signal at ν_{det}=3270 cm^{-1} only rises after the excited vibration has shifted further to the red, out of the absorption spectrum of the Eigen proton vibration, as illustrated by the signal at ν_{det}=2200 cm^{-1} shown in Fig. 5.10. This redshift of the excited vibration follows from a structural relaxation process in which the hydrogen bond at the excited O–H stretch vibration becomes

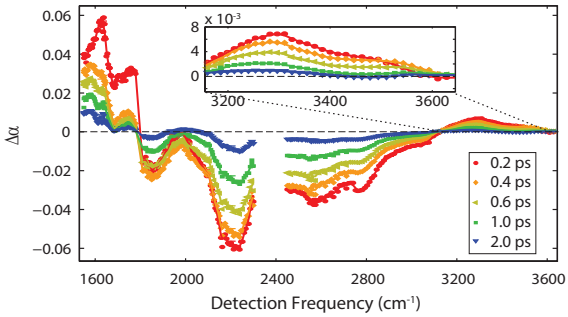

FIGURE 5.9. Isotropic transient absorption spectra at different delay times of a Nafion membrane for which 10% of the sodium ions is replaced by protons (solid lines containing symbols). The spectra are measured with ν_{exc}=2900 cm^{-1} and ν_{det} in the range from 1600 to 3700 cm^{-1}. The spectral region between 2300 and 2450 cm^{-1} is missing because of the strong absorption of Nafion in this frequency region. The induced absorption bands at ν_{det}=3270 and ν_{det}=3520 cm^{-1} are highlighted in the inset.

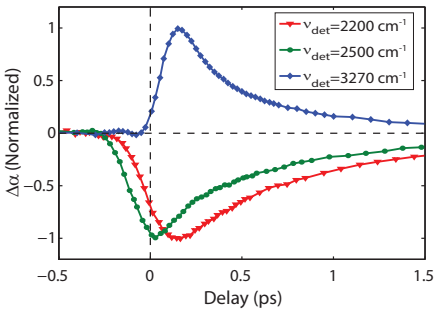

FIGURE 5.10. Normalized isotropic absorption changes as a function of delay at three different detection frequencies after excitation with ν_{exc}=2500 cm^{-1}. A positive signal implies an induced absorption, a negative signal implies a bleaching signal.

shorter, and in which the two other O–H groups of the H_3O^+ become water-like O–H vibrations.

In Fig. 5.11 we show the signal measured for a Nafion membrane that is hydrated with a mixture of 10% H_2O and 90% D_2O, meaning that this membrane will primarily contain D_2O and HDO molecules and Eigen proton/deuteron hydration structures with a central D_3O^+ or HD_2O^+ ion. The signal is much weaker than for a Nafion membrane hydrated with 100% H_2O, because the optical density of the sample in the region of the Eigen proton vibrations is much lower. The signal is quite similar in shape as for the Nafion membrane hydrated with 100% H_2O, indicating that the transfer to a Zundel structure occurs both for protons and for deuterons. The occurrence of deuteron transfer can be explained from the relaxation of the hydrogen-bond structure following

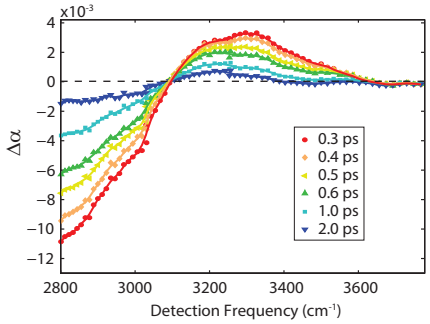

Figure 5.11. Isotropic transient absorption spectra at different delay times of a Nafion membrane that is hydrated with a mixture of 10% H_2O and 90% D_2O, following excitation ν_{exc}=2900 cm^{-1}.

the excitation of the O–H stretch vibration. This relaxation leads to a lowering of the frequency of the O–H stretch vibration and an increase of the frequencies of the non-excited O–D vibrations. When the vibrations get into resonance, the vibrational energy becomes delocalized over the three hydroxyl groups of the HD_2O^+ ion. Subsequently, the system relaxes further by deuteron/proton transfer in one of the three coordinates.

5.4.3 Kinetic Model

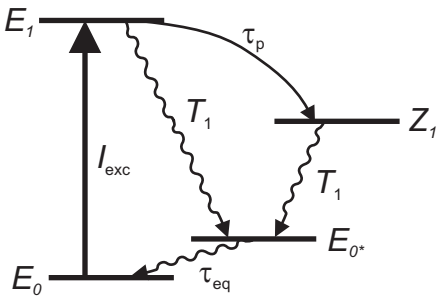

Figure 5.12. Schematic picture of the four-level kinetic model used to describe the transients shown in Fig. 5.3

The transient absorption changes shown in the upper panel of Fig. 5.3 are modeled with a four-level kinetic model that is schematically depicted in Fig. 5.12. The four levels represent the ground state of the Eigen proton hydration structure (level E_0), the first excited vibrational state of this structure (level E_1), the first excited vibrational state of the Zundel proton hydration structure (level Z_1), and a heated ground state of the Eigen hydration structure (level E_{0^*}). The levels are coupled by the excitation laser pulse $I_{\rm exc}(t)$, the proton transfer reaction with time constant $\tau_{\rm p}$, the vibrational relaxation with

time constant T_1, and the final equilibration (cooling) with time constant $\tau_{\rm eq}$. The coupled kinetic equations are:

$$\begin{aligned}
\frac{dn_{E_0}}{dt} &= -\sigma_{E_{01}} I_{\rm exc}(t)(1 - n_{E_1} - n_{E_0}) + n_{E_{0^*}}/\tau_{\rm eq} \qquad (5.1)\\
\frac{dn_{E_1}}{dt} &= \sigma_{E_{01}} I_{\rm exc}(t)(1 - n_{E1} - n_{E_0}) - n_{E_1}/\tau_{\rm p} - n_{E_1}/T_1\\
\frac{dn_{Z_1}}{dt} &= n_{E_1}/\tau_{\rm p} - n_{Z_1}/T_1\\
\frac{dn_{E_{0^*}}}{dt} &= n_{E_1}/T_1 + n_{Z_1}/T_1 - n_{E_{0^*}}/\tau_{\rm eq},
\end{aligned}$$

with n_{E_0}, n_{E_1}, n_{Z_1} and $n_{E_{0^*}}$ the populations of the levels denoted in the subscript, and $\sigma_{E_{01}}$ the absorption cross-section integrated over the frequency spectrum of the excitation pulse. The intensity profile $I_{\rm exc}(t)$ of the excitation pulse is described as a Gaussian pulse with a full-width-at-half maximum of 120 femtoseconds.

The transient absorption change $\Delta\alpha(\nu, t)$ at detection frequency ν is given by:

$$\Delta\alpha(\nu,t) = \sigma_{E_{01}}(\nu)(n_{E_0} - n_{E_1}) + \sigma_{E_{12}}(\nu) n_{E_1} + \sigma_Z(\nu) n_{Z_1} + \sigma_{E_{01^*}}(\nu) n_{E_{0^*}} \quad (5.2)$$

The cross-section $\sigma_{E_{01}}(\nu)$ corresponds to the linear absorption spectrum of the proton vibration of the Eigen hydration structure. This spectrum consists of a broad absorption band centered at 2600 cm^{-1}. As n_{E_0} will be negative (representing ground state depletion) and n_{E_1} will be positive, this contribution to the transient absorption change $\Delta\alpha$ will be a bleaching signal. The cross-section $\sigma_{E_{12}}$ represents the absorption of the proton vibration in the excited $v = 1$ state. This spectrum consists of a broad absorption band at frequencies <1700 cm^{-1}. The cross-section σ_Z represent all absorption changes associated with the excitation of the $v = 1$ state of the proton vibration of a Zundel structure. These spectral changes comprise a broad-band bleaching centered at 1100 cm^{-1} due to $v = 1 \rightarrow 0$ stimulated emission, a broad-band absorption centered at 1600 cm^{-1} due to $v = 1 \rightarrow 2$ excited-state absorption, and absorption peaks at 3270 and 3520 cm^{-1} associated with the O–H vibrations of water molecules flanking the Zundel proton. The cross-section $\sigma_{E_{01^*}}$ represents the absorption of the heated ground state that results after the vibrational relaxation of the excited proton vibration. The effect of heating on the absorption spectrum is illustrated in Fig. 5.6. From this figure it follows that $\sigma_{E_{01^*}}(\nu)$ will show less absorption than $\sigma_{E_{01}}(\nu)$ at frequencies between 1650 and 3530 cm^{-1}, and more absorption than $\sigma_{E_{01}}(\nu)$ at frequencies <1650 cm^{-1}.

The response function $\Delta\alpha(\nu, t)$ is convoluted with the intensity profile of the probe for which we use a Gaussian pulse with a full-width-at-half maximum of 60 femtoseconds. This function is fitted to the delay-time traces measured at detection frequencies of 1630, 2900, and 3270 cm^{-1}. At each of these detection frequencies, the contributions of the different levels to the transient absorption is defined by $\sigma_{E_{01}}(\nu)$, $\sigma_{E_{12}}(\nu)$, $\sigma_Z(\nu)$ and $\sigma_{E_{01^*}}(\nu)$. These cross-sections are

frequency-dependent and fitted to each separate delay time trace. The time constants τ_p, T_1, and τ_{eq} are the global fit parameters. Fitting this model to the experimental data yields τ_p =170±20 fs, T_1 = 350±30 fs, and τ_{eq} = 1.3±0.2 ps.

6

Hydration Dependence of Proton Transfer in Nafion

We study the energy relaxation and structural relaxation dynamics of hydrated protons in Nafion membranes at different hydration levels using femtosecond infrared transient absorption spectroscopy. At low hydration levels we observe that the excitation of the proton vibration of an Eigen-like proton hydration structure leads to a structural relaxation process in which the Eigen-like structure evolves to a Zundel-like proton hydration structure. This reorganization leads to a transfer of the proton charge and closely follows the mechanism of infrared-induced adiabatic proton transfer that has been proposed by S. Hammes-Schiffer, J.T. Hynes and others. At high hydration levels the spectral dynamics are dominated by vibrational energy relaxation and subsequent cooling of the proton hydration structures and the surrounding water molecules. Using a kinetic analysis of the transient spectral data, we determine the rates of proton transfer, vibrational energy relaxation and cooling as a function of hydration level. We find that infrared-induced proton transfer occurs at all hydration levels, but becomes less observable at high hydration levels due to the increasingly dominant influence of the vibrational energy relaxation.

6.1 Introduction

The mobility of protons in liquid water is a factor of 5 higher than that of other cations like Na^+ and K^+ [125]. The high mobility of the proton has been explained from a special transport mechanism that is usually referred to as Grotthuss conduction. In this process the delocalized charge of the proton is transferred to other hydrogen atoms in the hydrogen-bonded network, as a result of a structural reorganization of the water hydrogen-bond network. Ab initio molecular dynamics simulations showed that the proton follows from the structural interconversion between so-called Eigen ($H_9O_4^+$) and Zundel ($H_5O_2^+$) proton hydration structures [5, 83, 126]. The Eigen structure can be viewed as a central H_3O^+ ion with three surrounding hydrogen-bonded H_2O molecules, the Zundel structure is formed by an H^+ ion between two neighboring H_2O molecules.

When water is confined to the nanometer scale the structure and dynamics of the water network will change, and this will in turn affect the rate and mech-

anism of proton conduction. For example, Dellago and co-authors calculated that the proton mobility in water-containing carbon nanotubes is accelerated by a factor of 40 in comparison to bulk water [33]. It was also shown that the proton transfer in water-containing carbon nanotubes involves a Zundel-Zundel conversion mechanism rather than the Eigen-Zundel-Eigen mechanism of bulk liquid water [34]. Experimental studies on proton transfer in nanometer size reverse micelles showed that the rate of proton transfer strongly decreases with decreasing size of the reverse micelle [127–131].

An important nano-confined system for aqueous proton transfer to occur is formed by the nanochannels of Nafion membranes that are widely used as proton exchange membranes (PEM) in hydrogen fuel cells. Nafion is a sulfonated tetrafluoroethylene (Teflon)-based polymer that forms nanometer channels in which the sulfonate ($-SO_3^-$) headgroups bind to water molecules and positive counter ions like Na^+ and protons. It has been found that the proton conductivity of Nafion membranes strongly depends on the hydration level [111, 128, 132, 133]. Only at high hydration levels, i.e. when the nanochannels contain a sufficient amount of water, the Nafion membrane becomes a good conductor of protons. The molecular-scale mechanism of proton conduction in Nafion membranes has been studied with advanced ab initio molecular dynamics simulations [112–114, 134]. It was found that the proton is predominantly hydrated in an Eigen-like hydration structure, except for the first hydration shell of the sulfonate group where the proton-hydration structure is more Zundel-like [112, 134]. It was also shown that proton transfer in hydrated nafion can involve both particle (H_3O^+) diffusion and Grotthuss conduction, the latter process becoming dominant at high hydration levels. An interesting observation is that the two processes are anti-correlated, the particle diffusion takes place dominantly in a direction opposite to the Grotthuss conduction [113, 114].

In Chapter 5, we studied the structural dynamics of proton hydration structures in Nafion membranes at low hydration levels with two-color femtosecond mid-infrared spectroscopy. We observed that the excitation of the proton triggers a structural reorganization that involves a partial transfer of the proton charge [135]. Here we study the structural relaxation for Nafion membranes over a wide range of hydration levels. We find that for high hydration levels the structural relaxation is in strong competition with the vibrational energy relaxation of the excited proton vibration.

6.2 EXPERIMENT

We study the structural relaxation and vibrational energy relaxation of hydrated protons in Nafion membranes with polarization-resolved two-color mid-infrared pump-probe spectroscopy. The infrared generation and two-color pump-probe setup have been explained in Section 3.1 and Section 3.2.1 respectively.

The Nafion membranes were first purified in the steps as described in Section 3.4 and then soaked in 1 M HCl and 1 M NaCl solution for 24 hours, which results in a cation ratio $[H^+]$:$[Na^+]$=1:3 [76]. We also prepared purely

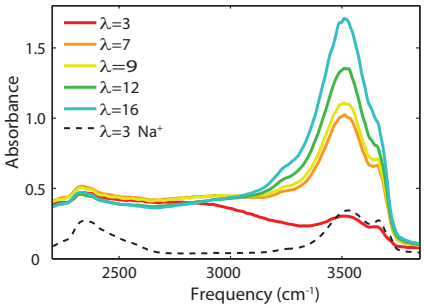

Figure 6.1. Linear absorption spectrum of hydrated H-Nafion membranes measured at different hydration level λ. For comparison also the spectrum of a Nafion membrane only containing Na^+ at λ=3 is shown.

sodiated membranes as reference samples by putting Nafion membranes in a 1 M NaCl solution for 24 hours. The membranes were then rinsed with deionized water. As a final step, the rinsed membranes were move into the sample cell in which the hydration level of the membranes can be controlled, as described also in Section 3.4.

6.3 Results and Discussion

6.3.1 Linear Spectra

Fig. 6.1 shows the linear absorption spectra of protonated Nafion (H-Nafion) membranes at five different hydration levels, λ=3, 7, 9, 12 and 16. These membranes contain 1 cation (H^+ or Na^+, $[H^+]$:$[Na^+]$=1:3) and λ water molecules per sulfonate group. For comparison we also show the linear absorption spectrum of a Nafion membrane containing 1 Na^+ ions and λ=3 water molecules per sulfonate group (Na-Nafion). The peaks at 3520 cm^{-1} and 3660 cm^{-1} in the Na-Nafion membrane can be assigned to the hydrogen-bonded and non-hydrogen-bonded O–H stretch vibrations of H_2O molecules hydrating sulfonate groups.

For the H-Nafion membranes the H_2O bands are broadened and smaller in amplitude. In addition to these water peaks, the H-Nafion samples show a broad absorption that extends over the whole spectral range. This broadband absorption is assigned to proton hydration complexes. The absorption in the frequency range 2200-3000 cm^{-1} is assigned to the O–H stretch vibrations of the central H_3O^+ structure of Eigen proton hydration structures [37, 38, 48, 116]. The absorption at frequencies 3200-3400 cm^{-1} is assigned to the O–H stretch vibrations of H_2O molecules that are hydrogen bonded to the central H_3O^+ ion of the Eigen structure and to the O–H stretch vibrations of H_2O molecules that flank the proton in the Zundel structure. With increasing hydration level, the water bands at 3520 cm^{-1} and 3660 cm^{-1} grow, because the fraction of water

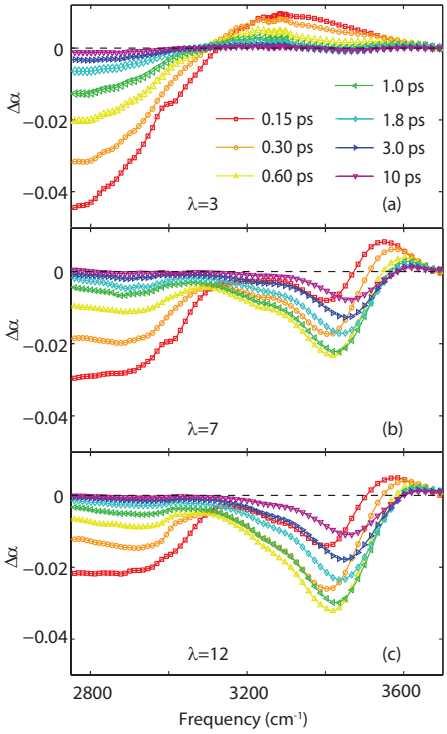

FIGURE 6.2. Isotropic transient absorption spectra of H-Nafion measured at different delays after excitation with an intense pump pulse centered at 2800 cm^{-1}, (a) for λ=3, (b) λ=7 and (c) for λ=12.

molecules that are not involved in proton hydration structures increases.

6.3.2 TRANSIENT ABSORPTION SPECTRA

In Fig. 6.2 transient spectra at different delay times are shown for H-Nafion at three different values of λ. These transient spectra represent the change in isotropic absorption signal $\Delta\alpha$ induced by the excitation of the proton vibrations of an Eigen-like proton hydration structure with a pump pulse centered at 2800 cm^{-1}. The transient spectra thus constitute the difference spectra between the absorption spectra measured at certain pump-probe delays and the room temperature equilibrium spectrum of the sample. The data shown in Fig. 6.2 (a) for λ=3 are similar to the data presented in Fig. 5.8. The data shown here are obtained with an excitation pulse with a different central frequency.

At frequencies <3100 cm^{-1} the transient spectra show a strong bleaching signal (negative $\Delta\alpha$) that rapidly decays with increasing delay time. The bleaching signal decays due to population relaxation of the excited $v = 1$ state and/or structural relaxation. The transient spectrum measured for λ=3 shows an in-

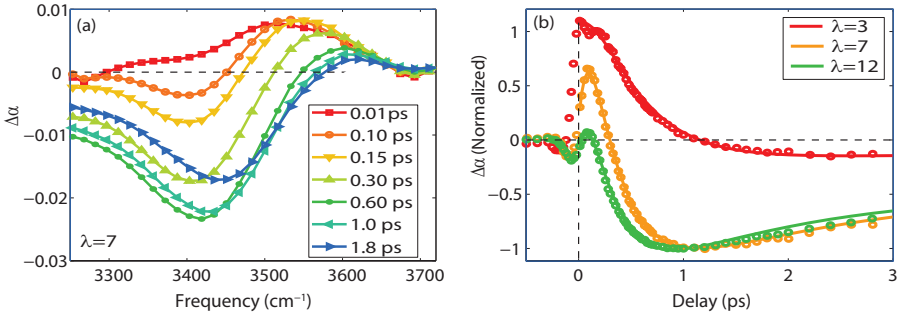

FIGURE 6.3. (a) Zoom in of the high-frequency range of the transient spectra of Fig. 6.2 (b); (b) Normalized isotropic absorption changes of H-Nafion membranes as a function of delay measured at a probe frequency of ν_{det}=3500 cm^{-1} after excitation with ν_{exc}=2800 cm^{-1}. The absorption changes are shown for protonated Nafion membranes at three different hydration levels. Solid lines are guides to the eye.

duced absorption at frequencies >3100 cm^{-1}. This induced absorption decays on a similar time scale as the bleaching at frequencies <3100 cm^{-1}. The transient spectra at λ=7 and 12 show an initial absorption at frequencies >3100 cm^{-1} that rapidly evolves to a strong bleaching signal centered at 3400 cm^{-1} and a weak induced absorption signal at ∼3550 cm^{-1}. With increasing delay, the strong bleaching signal at 3400 cm^{-1} shows a partial decay and a blue shift to a frequency of 3450 cm^{-1}. Simultaneously, the weak absorption at ∼3550 cm^{-1} shows a partial decay and a small blue shift to ∼3600 cm^{-1}.

Measurements for long delay times (not shown) reveal that the amplitude and shape of the transient spectrum observed for delays >10 ps remain constant on a nanosecond time scale. This transient spectral response can be explained from the increase in temperature of the sample that results from the complete relaxation and equilibration of the energy of the excitation of the proton vibration. Heating leads to a decrease and blue shift of the absorption of the water bands. The difference spectrum between the spectrum at an elevated temperature and the spectrum at room temperature thus shows a bleaching at ∼3450 cm^{-1} and a weak induced absorption at ∼3600 cm^{-1}, in agreement with the shape of the transient spectrum observed for delays >10 ps. This transient spectrum remains constant on a nanosecond time scale because heat diffusion out of the focus is a relatively slow process that occurs on a time scale of microseconds.

In Fig. 6.3 (a) we present a zoom-in of the high-frequency part of the transient spectra of H-Nafion at λ=7 at early delay times. This figure also contains transient spectra measured at delays of 10 femtoseconds and 100 femtoseconds. The different transient spectra show that the excitation of the proton vibration at 2800 cm^{-1} leads to a rapid rise of an induced absorption at frequencies >3300 cm^{-1} that subsequently decays to a strong and relatively slowly decaying bleaching signal. The competition between the induced absorption and the bleaching signal is also illustrated in Fig. 6.3 (b). In this figure the normalized

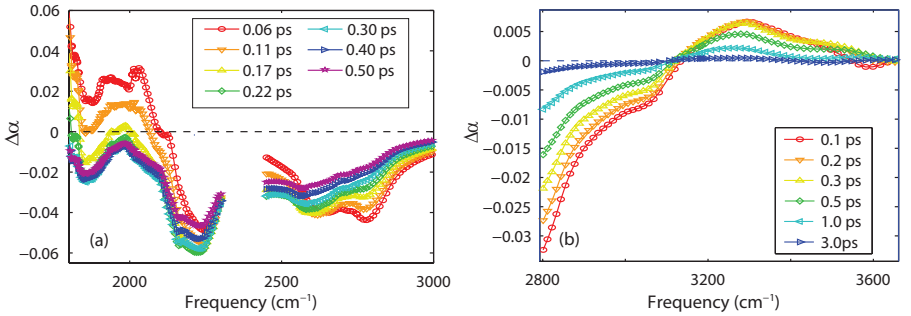

FIGURE 6.4. Isotropic transient absorption spectra of H-Nafion at a hydration level of λ=3 measured at different delays after excitation with an intense pump pulse centered at 2800 cm^{-1}. Compared to Fig. 6.2 (a) the spectrum is measured over a much broader frequency range. The frequency range 2300-2450 cm^{-1} is missing because of the too strong background absorption of the Nafion membrane. Panel (a) shows the Frequency range 1850-3000 cm^{-1} and panel (b) shows the frequency range 2800-3650 cm^{-1}.

absorption change at ν_{det}=3500 cm^{-1} is presented as a function of delay for the three different hydration levels indicated in Fig. 6.2. It is seen that the excitation leads to the rise of an absorption signal that rapidly decays and evolves to a bleaching signal. The amplitude of the bleaching signal strongly increases with increasing λ. At the high hydration level of λ=12 the initial absorption is no longer observable. The bleaching signal shows a partial decay with a time constant of ∼1 ps. This decay becomes slower with increasing hydration level.

In Fig. 6.4 we present transient absorption spectra of H-Nafion with λ=3 over a broad spectral range. Similar data have been presented in Ref. 135. The data shown here are obtained with an excitation pulse with a different central frequency. The transient spectral response of the Nafion membranes can be measured down to a frequency of ∼1500 cm^{-1}. The Nafion membranes are not transparent below this frequency, as a result of their high concentration of C-F vibrations [135]. In Fig. 6.4 (a) we present transient spectra in the frequency range 1850-3000 cm^{-1}. The transient spectra show that the bleaching signal initially peaks at ∼2800 cm^{-1} and undergoes a large shift to lower frequencies in the first few hundred femtoseconds after the excitation. As a result, the bleaching signal at <2000 cm^{-1} reaches its maximum at approximately 300 femtoseconds after the excitation.

In Fig. 6.5 the normalized absorption change is presented as a function of delay for four different detection frequencies. The maximum of the bleaching shifts to later delays with decreasing detection frequency, illustrating that the bleaching signal associated with the excitation of the proton vibration of the Eigen-like hydration structure shows a strong red shift directly after the excitation. It is also seen that the induced absorption at 3300 cm^{-1} shows a delayed rise with respect to the bleaching signal at 2550 cm^{-1}.

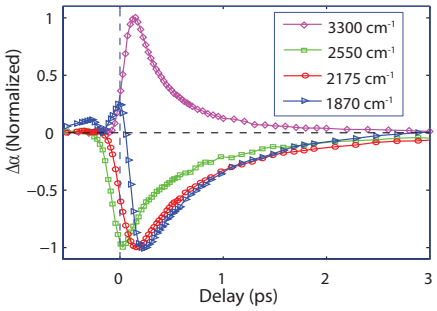

Figure 6.5. Normalized isotropic absorption changes as a function of delay at four different detection frequencies (ν_{det}=3300, 2550, 2175, and 1870 cm^{-1}) after excitation with ν_{exc}=2500 cm^{-1}. The signals are measured for a H-Nafion sample with λ=3. A positive signal implies an induced absorption, a negative signal a bleaching signal.

6.3.3 Interpretation

The large red shift of the bleaching signal of Fig. 6.4 (a) indicates that the excitation of the proton vibration induces a strong structural reorganization of the excited Eigen-like proton hydration structure. As the reorganization leads to a shift of the bleaching signal to frequencies <2000 cm^{-1}, this reorganization likely involves the transfer from the Eigen-like proton hydration structure to a Zundel-like proton hydration structure [37, 38, 48, 88]. In this transfer the excited O–H vibration of the central H_3O^+ ion of the $H_9O_4^+$ Eigen-like structure evolves to the central O···H···O vibration of a $H_5O_2^+$ Zundel-like structure. This reorganization is illustrated in the top panel of Fig. 6.6.

The evolution from an Eigen-like proton hydration structure to a Zundel-like structure also accounts for the rise of an induced absorption signal at frequencies >3200 cm^{-1}. The change from Eigen to Zundel affects the character of the two other, non-excited O–H vibrations of the central H_3O^+ ion of the Eigen-like structure. These vibrations evolve to the O–H vibrations of an H_2O molecule flanking the Zundel proton. This evolution is accompanied by a transfer of positive charge from the H atoms of the two non-excited O–H group of the central H_3O^+ ion to the H atom of the excited O–H group. The decrease in positive charge leads to a weakening of the hydrogen bonds of the non-excited O–H groups to H_2O molecules in the second hydration shell and thus to an increase of the frequency of the O–H stretch vibrations. Hence, the transfer from Eigen to Zundel also leads to the evolution of the (non-excited) Eigen-like proton vibrations that absorb at 2200-3000 cm^{-1} to vibrations that absorb at frequencies >3200 cm^{-1} [37, 38, 48, 116]. This explanation agrees with the fact that the observed induced absorption at 3300 cm^{-1} shows a delayed rise with respect to the bleaching signal at 2550 cm^{-1}.

The excitation induced evolution from Eigen to Zundel can be well explained with the model for vibration-excitation induced proton transfer developed by S. Hammes-Schiffer and J.C. Tully [136], and J.T. Hynes et al. [108, 137]. In this

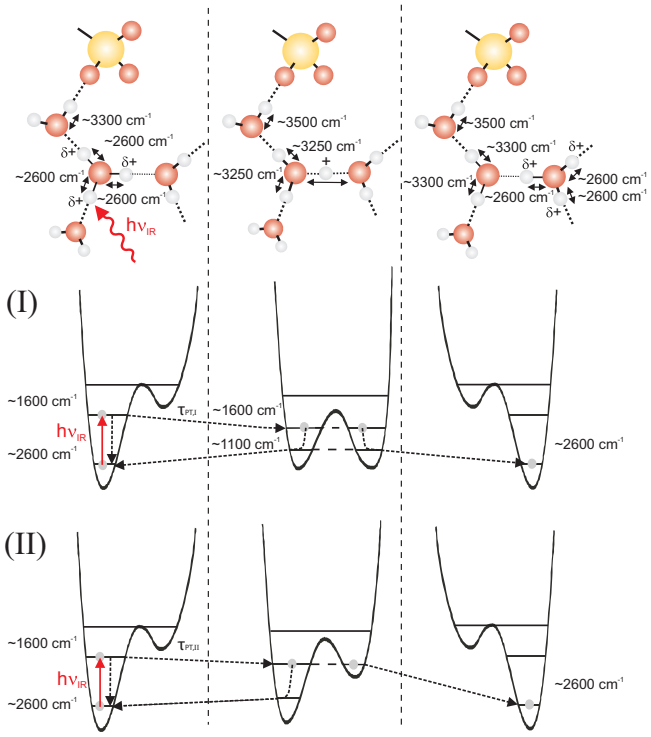

FIGURE 6.6. Upper panel: schematic picture of the evolution from an Eigen proton hydration structure to a Zundel hydration structure and to a final new Eigen proton hydration structure, induced by the excitation of one of the proton vibrations of the Eigen structure. The vibrational frequencies of the different modes of the hydration structures are indicated. Middle and lower panels: two scenarios by which this vibrational excitation induced proton transfer can take place. Scenario (I) is similar to the scenario depicted in Figure 6.1 of Ref 32.

model excitation of the X–H vibration of an X–H$\cdots$Y hydrogen-bonded system induces a reorganization of the surrounding solvent that adiabatically changes the vibrational potential of the X–H$\cdots$Y system to a much more symmetric potential. This reorganization is driven by the energy reduction associated with the adiabatic evolution of the high energy $v = 1$ state in the tight X–H potential to the much lower energy $v = 1$ state in the broad, near-symmetric X$\cdots$H$\cdots$Y potential.

The evolution to the near-symmetric X$\cdots$H$\cdots$Y potential corresponds to a partial transfer of the proton charge. The proton transfer can be completed with two different scenarios, illustrated in the middle and lower panels of Fig. 6.6. In scenario (I) vibrational relaxation of the delocalized $v = 1$ state in the X$\cdots$H$\cdots$Y potential will bring the system to a relatively high energy $v = 0$ state within the broad X$\cdots$H$\cdots$Y potential. This $v = 0$ state rapidly evolves either back to the $v = 0$ state of the original tight X–H$\cdots$Y potential or pro-

ceeds to the $v = 0$ state of a new tight X$\cdots$H–Y potential. The latter case corresponds to a complete proton transfer from X to Y. Such vibrational excitation induced proton transfer has been proposed for the reaction between HF and H_2O [108]. Scenario (I) is similar to the mechanism of vibrational excitation induced proton transfer shown in Figure 6.1 of Ref. 137. In scenario (II), the delocalized $v = 1$ state of the X$\cdots$H$\cdots$Y potential corresponds to the lowest-energy vibrational state in the right well of this potential. This state can adiabatically evolve to the $v = 0$ state of a new tight X$\cdots$H–Y potential, thus completing the proton transfer from X to Y. In scenario (II), the proton transfer is thus directly accompanied by vibrational energy relaxation. Within scenario (II), the delocalized $v = 1$ state of the near-symmetric X$\cdots$H$\cdots$Y potential can also relax back to the $v = 0$ state of this potential, from which the system will evolve back to the $v = 0$ state of the original tight X–H$\cdots$Y potential. The relative importance of the two scenarios will depend on the height of the barrier separating the two wells and the rate at which the vibrational potential changes as a result of the structural evolution of the hydration shell. Scenario II becomes more important if the barrier is low and when the structural evolution is slow.

A prerequisite for both scenarios of excitation-induced proton transfer is that the $v = 1$ state possesses a sufficiently long vibrational lifetime. If the $v = 1$ state would relax very quickly, the system would be back in the vibrational ground state before the adiabatic adaptation of the vibrational potential can take place.

For hydration levels higher than λ =3 we observe that the induced absorption at frequencies >3200 cm^{-1} quickly gives way to a bleaching signal centered at 3400 cm^{-1}. This bleaching signal cannot be due to a transfer of the vibrational excitation from the excited proton vibration to a water O–H vibration, as in this case the resulting signal should not only consist of a $v = 0 \rightarrow 1$ bleaching signal of the water O–H vibrations, but should also contain a clear signature of excited $v = 1 \rightarrow 2$ absorption of these vibrations at a frequency of ∼3200 cm^{-1}. This latter absorption is not observed in the transient absorption spectra of Fig. 6.2. Instead, we observe that the strong bleaching signal at ∼3400 cm^{-1} is accompanied by a weak induced absorption at a higher frequency of ∼3550 cm^{-1}. This spectral signature can be well explained from the effect of heating on the absorption spectrum of the O–H stretch vibrations of water [138]. Therefore, we assign the strong bleaching signal at ∼3400 cm^{-1} and the weak induced absorption at ∼3550 cm^{-1} to a local heating effect that results from the vibrational relaxation of the $v = 1$ state of the excited proton vibration. The vibrational relaxation corresponds to the non-adiabatic transition of the $v = 1$ state of the proton vibration to the $v = 0$ state and is enabled by the strong coupling of the proton vibration to the low-energy degrees of freedom of the hydration shell [139].

The increase in temperature resulting from the vibrational relaxation involves a weakening of the hydrogen bonds between water molecules, and between water molecules and sulfonate groups of Nafion, which in turn leads to a decrease of the absorption cross-section and a blue shift of the O–H stretch

vibrations. This explanation is consistent with the observation that the amplitude of the bleaching increases with increasing hydration level. With increasing level of hydration, the proton will be surrounded (hydrated) by a larger number of water molecules and thus the effect of heating on the direct surroundings of the proton will have a more pronounced effect in the absorption region of the O–H stretch vibrations of water.

The bleaching at $\sim$3400 cm^{-1} and induced absorption at $\sim$3550 cm^{-1} show a partial decay and blue shift on a time scale of $\sim$1 ps. As discussed in the previous subsection, the final transient spectrum corresponds very well to the difference spectrum between the absorption of the Nafion sample at an elevated temperature and the spectrum at room temperature. Therefore, we assign the partial decay and blue shift to the cooling of the local hot surroundings of the proton vibration, leading to a full thermalization of the excess energy. In this cooling process, part of the thermal energy will be transferred to the Nafion membrane, thus explaining the decrease in the amplitudes of the bleaching and the induced absorption signal. In the cooling process the thermal energy will also be transferred to water molecules that are further away from the originally excited hydrated proton vibration. For water molecules that are close to a proton the hydrogen bonds will be stronger than for water molecules that are far away from a proton and for water molecules that are close to Na^+ ions. As a consequence, the absorption spectrum of water molecules close to a proton will be red-shifted compared to that of the other water molecules embedded in the Nafion membrane channels. The transfer of thermal energy from the water molecules close to the originally excited proton to water molecules that are further away will thus lead to a small blue shift of the transient spectrum.

6.3.4 KINETIC MODEL

Following the interpretation of the previous subsection we describe the data of the Nafion membranes with a kinetic model that includes vibration-excitation induced proton transfer, relaxation of the excited proton vibration, and cooling. This model is schematically depicted in Fig. 6.7.

The levels E_1 and Z_1 correspond to the excited vibrational $v = 1$ states of the Eigen-like and Zundel-like proton hydration structures, and E_0 and Z_0 are the $v = 0$ ground states of these structures. The level E_{0^*} corresponds to a locally hot state of the Eigen-like structure, and $E_{0^{**}}$ to the final fully thermalized state of this structure. The excited state E_1 relaxes to Z_1 with a time constant τ_{PT} representing the vibrational-excitation induced proton transfer process. The rate of this transfer is the sum of the proton transfer rates of scenarios (I) and (II), illustrated in Fig. 6.6, meaning that $(\tau_{PT})^{-1} = (\tau_{PT,I})^{-1} + (\tau_{PT,II})^{-1}$. The description of the proton transfer with two discrete excited vibrational levels E_1 and Z_1 forms a simplified description of the gradual evolution of the Eigen-like proton hydration structure to a Zundel-like structure. This approximation is reasonably valid when τ_{PT} is short. The state E_1 not only evolves to Z_1 with τ_{PT} but also relaxes to E_{0^*} with the vibrational relaxation time constant T_1.

The excited proton state Z_1 relaxes with time constant τ_1 to E_{0^*}. In sce-

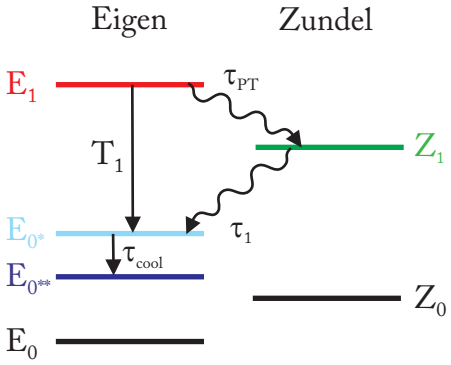

FIGURE 6.7. Schematic picture of the kinetic model for excitation-induced proton transfer and vibrational relaxation used to fit the data of Fig. 6.2.

nario (I) and in the case of backward proton transfer within scenario (II), the τ_1 relaxation process consists of vibrational relaxation within the Zundel-like vibrational potential, followed by a structural relaxation as a result of which the potential evolves (back) to an Eigen-like vibrational potential. In the case of forward proton transfer within scenario (II), the τ_1 relaxation process consists of the evolution of the $v = 1$ state of the Zundel-like potential to the $v = 0$ state of a new Eigen-like potential. In all cases the τ_1 relaxation process involves the transfer of the vibrational energy of the excited Zundel-like proton vibration to low-energy (solvent) degrees of freedom. E_{0^*} cools with τ_{cool} to the final state $E_{0^{**}}$. The levels E_1, Z_1, E_{0^*}, and $E_{0^{**}}$ are thus coupled by four time constants τ_{PT}, T_1, τ_1 and τ_{cool}. The coupled kinetic equations are:

$$\begin{aligned}
\frac{d}{dt}(n_{E_1}) &= -\frac{n_{E_1}}{\tau_{\text{PT}}} - \frac{n_{E_1}}{T_1} \\
\frac{d}{dt}(n_{Z_1}) &= \frac{n_{E_1}}{\tau_{\text{PT}}} - \frac{n_{Z_1}}{\tau_1} \\
\frac{d}{dt}(n_{E_{0*}}) &= \frac{n_{E_1}}{T_1} + \frac{n_{Z_1}}{\tau_1} - \frac{n_{E_0*}}{\tau_{\text{cool}}} \\
\frac{d}{dt}(n_{E_{0**}}) &= \frac{n_{E_{0*}}}{\tau_{\text{cool}}}
\end{aligned} \tag{6.1}$$

with n_{E_1}, n_{Z_1}, n_{E_0*}, and n_{E_0**} the populations of the levels denoted in the subscript.

The value of τ_{PT} is determined from a fit of the data obtained at λ=3, the lowest studied hydration level. At higher hydration levels, the signature of the state Z_1 becomes less clear due to the increasing contribution of the vibrational relaxation, making it cumbersome to determine τ_{PT} and τ_1. Therefore we use the value of τ_{PT} obtained at λ=3 in fitting the data at higher hydration levels, and we take τ_1 to be the same as T_1. The values of T_1 and τ_{cool} are fitted to the data at each studied hydration level. Each of the levels of the model has an associated transient spectrum. The amplitude and shape of these transient

spectra, form free parameters in fitting the transient spectra of the Nafion sample at each hydration level. The total transient absorption change $\Delta\alpha(\nu, t)$ at detection frequency ν and delay time t is given by:

$$\Delta\alpha(\nu,t) = \sigma_{E_1}(\nu)n_{E_1}(t) + \sigma_{Z_1}(\nu)n_{Z_1}(t) + \sigma_{E_0*}(\nu)n_{E_0*}(t) + \sigma_{E_0**}(\nu)n_{E_0**}(t) \tag{6.2}$$

In Fig. 6.8 we show the results of the fit for H-Nafion at λ=7 and 12. The fitted transient spectra, represented by the solid lines in Fig. 6.8 (a) and (b) provide an excellent description of the data. Fig. 6.8 (c) and (d) show the spectral shapes of σ_{E_1}, σ_{Z_1}, σ_{E_0*}, and σ_{E_0**} and Fig. 6.8 (e) and (f) show the population dynamics of these levels.

The spectrum σ_{E_1} consists of a strong bleaching signal around 2800 cm^{-1}, as a result of the excitation of one of the proton vibrations of the Eigen-like hydration structure. This excitation leads to a depletion of the fundamental $v = 0 \rightarrow 1$ absorption from E_0 to E_1 and stimulated emission $v = 1 \rightarrow 0$ from E_1 to E_0. The spectral response σ_{E_1} shows additional small induced absorption changes between 3250 and 3500 cm^{-1}. This latter response can be explained from cross-anharmonic coupling of the excited Eigen proton vibration and the O–H stretch vibrations of nearby water molecules. The cross-anharmonic coupling between an excited vibration and a non-excited vibration leads to a direct shift in frequency of the non-excited vibration, usually to lower frequencies. Hence, excitation of the Eigen proton vibration can lead to a red shift of the O–H stretch vibrations of nearby H_2O molecules, thus explaining the observation of a weak induced absorption in the red wing of the O–H stretch absorption band (near 3350 cm^{-1}) and a decrease in absorption in the blue wing of the O–H stretch absorption band (near 3500 cm^{-1}).

The state E_1 is transferred to Z_1 with a proton transfer time constant τ_{PT} of 170±20 fs. The spectrum of Z_1 shows a smaller bleaching signal in the frequency region around 2800 cm^{-1} than E_1. This change in amplitude is caused by the vanishing of the $v = 1 \rightarrow 0$ stimulated emission contribution to the bleaching signal of the Eigen proton vibration. The residual bleaching around 2800 cm^{-1} is caused by the remaining depletion of the fundamental $v = 0 \rightarrow 1$ absorption from E_0. The spectrum of Z_1 also contains two broad induced absorption peaks at 3250 and 3500 cm^{-1}. This induced absorption signal is present at all studied hydration levels.

As discussed in the previous subsection, the absorption peak centered at 3250 cm^{-1} can be assigned to the O–H stretch vibrations of H_2O molecules flanking the Zundel proton. The absorption peak at 3500 cm^{-1} is assigned to the absorption of water molecules in the second solvation shell of the Zundel proton. The evolution to the Zundel structure turns the water molecules that are hydrogen bonded to the non-excited Eigen proton vibrations to water molecules in the second hydration shell of the Zundel proton. The increased distance to the proton charge weakens the hydrogen bonds of these water molecules, leading to a shift of their absorption bands to higher frequencies. The resulting absorption will be similar to that of water molecules hydrating a sulfonate group without a nearby (hydrated) proton. These bands absorb at ∼3500 cm^{-1}, as can be

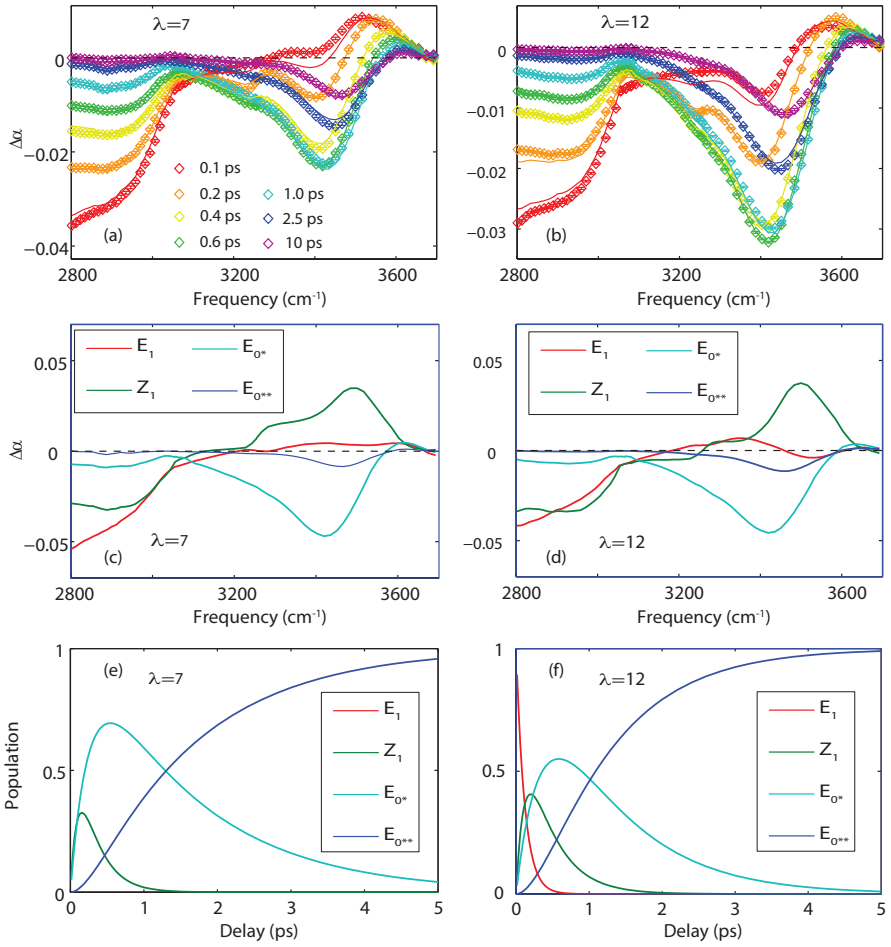

FIGURE 6.8. a) and b): Experimental transient spectra (symbols) and fitted results (solid lines) using the kinetic model of Fig. 6.7 and Eq. 6.2, for hydration level λ=7 (a) and λ=12 (b); c) and d): Spectral components of the different levels, corresponding to the fits of a) and b), respectively; e) and f): Population dynamics of the different levels, corresponding to the fits of a) and b), respectively.

derived from the absorption spectra of Nafion membranes at high hydration levels.

The blue shift of the absorption of the water molecules that are hydrogen bonded to the non-excited Eigen proton vibrations implies that the original absorption of these molecules, at frequencies of ∼3300 cm^{-1}, decreases. This decrease in absorption contributes to the overall amplitude of the σ_{Z_1} spectrum in this frequency region, and thus can explain why the peak at 3250 cm^{-1} of the σ_{Z_1} spectrum is weaker than the absorption peak at 3500 cm^{-1}. This explanation also agrees with the fact that the absorption peak at 3500 cm^{-1}

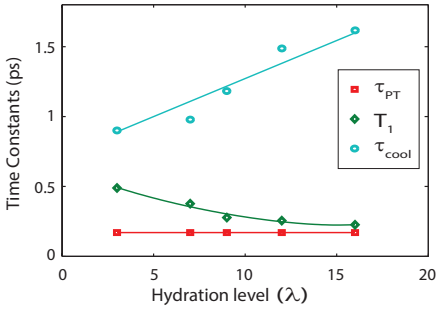

FIGURE 6.9. The time constants τ_{PT}, T_1 (T_1=τ_1), and τ_{cool} as a function of hydration level. The time constants are obtained from fits of the data to the kinetic model of Fig. 6.7 and Eq. 6.1. In the fit the time constants τ_1 and T_1 are assumed to have the same value. The solid lines are guides to the eye.

grows with increasing hydration level, as can be seen from the comparison of the σ_{Z_1} spectra of Nafion membranes with λ=7 and 12 in Fig. 6.8 (c) and (d). At higher hydration levels there will be more water molecules hydrating the central H_3O^+ ion of the Eigen-like proton hydration structure, and the shift in absorption of these water molecules from ~3300 cm^{-1} to ~3500 cm^{-1}, following the transfer from Eigen to Zundel, forms a stronger contribution to the overall σ_{Z_1} spectrum.

The states E_1 and Z_1 both relax to the state E_{0^*}. The spectrum of E_{0^*} consists of a strong bleaching signal centered at 3400 cm^{-1} and a weak absorption around 3550 cm^{-1}. As discussed in the previous subsection, these spectral changes can be well explained from a local heating effect resulting from the relaxation of the proton vibration that changes the absorption spectrum of nearby water molecules. The local hot state E_{0^*} cools to the fully thermalized state $E_{0^{**}}$ that has a spectrum with a similar shape as the spectrum of E_{0^*}, but with a smaller amplitude and shifted to higher frequencies. For the other measured hydration levels (λ=3, 9 and 16) the spectra and population dynamics of the different levels are similar in shape as for the hydration levels shown in Fig. 6.8. In Fig. 6.9 the fitted values of the time constants T_1 and τ_{cool} are presented as a function of hydration level. It is seen that T_1 becomes shorter with increasing hydration level, and that τ_{cool} becomes longer.

6.3.5 DISCUSSION

The results of Fig. 6.4, Fig. 6.5 and Fig. 6.8 demonstrate the occurrence of partial transfer of the proton charge in hydrated Nafion membranes following excitation of a molecular vibration to its first excited state. For most systems, the energy of a single vibrational quantum does not suffice to initiate a chemical reaction. An exception is the cis-trans isomerization of nitrous acid (HONO) that can be induced by excitation of the O–H stretch vibration [106, 107]. Other examples of vibration-induced reactivity all concern systems that are already

in a reactive state, like the bimolecular interactions between radicals and small molecules in the gas phase [104, 105]. For these systems the excitation of a molecular vibration has been observed to increase the rate of particular reaction channels.

It is interesting to compare the presently studied vibration-induced proton transfer in hydrated Nafion with proton transfer by conventional photo-acids. For conventional photo-acids proton transfer is induced by electronic excitation with visible or UV light. This electronic excitation affects the electronic configuration such that a particular O–H or N–H bond of the photo-acid weakens [81, 132, 140–146]. This is a clear difference with vibration-induced proton transfer in Nafion for which the excitation hardly affects the strength of the O–H bond, as excitation of the proton vibration has a minor direct effect on the electronic configuration. The weakening of the O–H or N–H bond of a conventional photo-acid is usually followed by another electronic reorganization that leads to release of the proton and a stabilization of the conjugate photobase. For the widely studied photo-acid HPTS (8-hydroxy-1,3,6-pyrenetrisulfonic acid) it has been shown that this subsequent reorganization involves a transfer of negative charge from the oxygen atom to which the proton was bound to the aromatic ring system [141, 147]. This redistribution of negative charge is essential for the proton to leave, as it turns the excited photobase into a weak base. Vibration-induced proton transfer in Nafion is probably accompanied by a similar transfer of negative charge from the oxygen atom to which the proton was bound to other atoms in the proton hydration structure, as this transfer is an inherent property of the transfer between Eigen to Zundel proton hydration structures [5, 83, 112–114, 126, 134]. As in the excited conjugate photobase of HPTS, this redistribution of negative charge aids in the stabilization of the transferred proton state.

For conventional photo-acids the proton release and stabilization of the conjugate photo-base is accompanied by a repositioning of surrounding solvent molecules that lowers the energy of the excited state [132, 140–143]. The lowering of the energy leads to a very strong red shift (Stokes shift) of the fluorescence and the transient absorption [132, 140–143]. In the case of protons in Nafion, the excited proton vibration of the Eigen structure also undergoes a large Stokes shift when it evolves to the much lower energy state of the excited proton vibration of a Zundel structure.

Vibration-induced proton transfer is in strong competition with vibrational relaxation [137]. Relaxation of the excited proton vibration occurs on a time scale $<$500 fs, and thus the reorganization required for proton transfer has to occur within this short time window. The vibrational relaxation becomes faster with increasing hydration level thus making proton transfer less probable. Nevertheless, the analysis of Fig. 6.8 shows that proton transfer is still possible at higher hydration levels. We find that the state Z_1 which represents the final state of the proton transfer, has a maximum induced absorption of $\sim$0.03 OD in the frequency region $>$3200 cm^{-1}, at all studied hydration levels. The persistence of the amplitude of the absorption of the Z_1 level at $>$3200 cm^{-1} for all studied hydration levels, shows that vibration-excitation induced proton

transfer is still possible at high hydation levels. Nevertheless, the fraction of excited Eigen proton hydration structures that reorganizes to a Zundel structure decreases with increasing hydration level because the competing vibrational relaxation becomes faster. We find that the vibrational relaxation time constant T_1 decreases from 490±40 fs at λ=3 to 230±30 fs at λ=16, which means that an increasing fraction of excited Eigen proton vibrational states E_1 relaxes to the local hot ground state E_{0^*} and thus no longer proceeds to the first excited Zundel vibrational state Z_1. Due to this competition, Z_1 becomes less populated with increasing hydration level, and vibration-excitation proton transfer is no longer as clearly observed as at low hydration levels. An additional effect is that the amplitude of the bleaching signal associated with the relaxed, local hot state E_{0^*} increases with increasing hydration level. This bleaching signal obscures the induced absorption signal in the frequency region >3200 cm^{-1} associated with vibration-induced proton transfer.

The decrease of the vibrational relaxation time constant T_1 with increasing hydration level implies that the density of coupled combination tones that are capable of accepting the energy of the excited proton vibration increases when the number of water molecules close to the proton vibration increases. For pure liquid water the vibrational relaxation time constant T_1 of the Eigen-like proton vibration is observed to be 120±20 femtoseconds [148]. It is to be expected that the value of T_1 of protons in Nafion membranes would approach this value at very high hydration levels. For liquid water, the small value of T_1 of the proton vibration will completely obscure the observation of vibration-excitation induced proton transfer.

We observe that τ_{cool} increases from 0.9±0.05 ps at λ=3 to 1.63±0.05 ps at λ=16, meaning that the cooling of a locally hot cluster of water molecules (surrounding the originally excited proton vibration) becomes slower with increasing hydration level. This increase of the cooling time constant with increasing size of the water cluster is consistent with the results of a study of the cooling of water nanodroplets [149]. In this latter study it was found that the cooling slows down with increasing size of the water nanodroplet. This observation can be explained from the fact that cooling involves the conduction of thermal energy through the surface of the heated volume. As the surface to volume ratio decreases with increasing droplet or water cluster size, the cooling will become slower with increasing level of hydration.

6.4 CONCLUSIONS

We studied the vibrational relaxation and structural reorganization dynamics of hydrated protons in the nanochannels of Nafion membranes. We excited the proton vibration of Eigen-like ($H_9O_4^+$) proton hydration structures with ultrashort mid-infrared light pulses with frequencies in the range 2500-2900 cm^{-1} (3.4 $\sim$ 4.0 μm). The subsequent relaxation and structural dynamics are measured with ultrashort mid-infrared detection pulses that are tunable from 1850-3700 cm^{-1} (2.8-5.6 μm). We find that the excitation of the proton

vibration leads to a reorganization of the Eigen proton hydration structure to a Zundel-like ($H_5O_2^+$) proton hydration structure. This reorganization is driven by the substantial lowering of the energy of the excited $v = 1$ state of the proton vibration when the vibrational potential of the proton adiabatically evolves from the relatively narrow and asymmetric shape associated with the Eigen structure, to the broad and symmetric shape associated with the Zundel structure. The reorganization leads to a transfer of the proton charge from the three hydrogen atoms of the central H_3O^+ ion of the Eigen structure to the central hydrogen atom of the $H_5O_2^+$ Zundel-like structure. The time constant τ_{PT} of this transfer is 170±20 fs.

Vibration-excitation induced proton transfer becomes less prominent with increasing hydration level because the vibrational energy relaxation of the proton becomes faster. We observe that the vibrational relaxation time constant T_1 decreases from 490±40 fs at λ=3 to 230±30 fs at λ=16. Vibrational relaxation is observed to lead to a strong local heating effect of nearby water molecules. These hot water molecules cool by transferring their excess energy to the Nafion membrane and to other water molecules that are further away from the initially excited proton vibration. The cooling time constant τ_{cool} increases from 0.90±0.05 ps at λ=3 to 1.63±0.05 ps at λ=16.

7

Dynamics of the Bending Mode of Hydrated Protons

We study the vibrational dynamics of the bending mode at 1730 cm^{-1} of proton hydration structures in Nafion membranes with polarization-resolved infrared (IR) pump-probe spectroscopy. The main fraction of the excited bending mode vibrations is found to relax to an intermediate state with a time constant T_1 of ∼175 fs, and subsequently to a thermally equilibrated state with a time constant T_{eq} of 1.5±0.2 ps. For a small fraction of the excitations the vibrational relaxation leads to ultrafast predissociation of one of the hydrogen bonds donated by the excited proton hydration structure. The predissociation leads to a long-living bleaching of the absorption band of the bending vibration. Due to the ultrafast character of the predissociation process, this bleaching signal has a high associated anisotropy that decays with a time constant of 38±4 ps, probably as a result of structural relaxation of the water clusters in the Nafion nano-channels.

7.1 Introduction

Proton transfer is one of the most fundamental processes in molecular dynamics and is a key step in many chemical and biochemical processes, such as in hydrogen fuel cells and in light-to-energy conversion during plant photo synthesis. A detailed understanding of the proton transfer mechanism is important for the optimization of technical applications such as hydrogen fuel cells. Over the last decades there has been extensive theoretical and experimental research on the nature of the proton in liquid water [37, 48, 50, 150], and on the molecular-scale mechanism by which the protons is transferred in aqueous systems.

It has been found that the proton is strongly interacting with water molecules thus forming $H^+(H_2O)_n$ proton hydration clusters [5, 39, 151]. The two limiting forms of these clusters are the Eigen hydration structure ($H_9O_4{}^+$), that is formed by a central hydronium (H_3O^+) ion surrounded by three water molecules accepting hydrogen bonds from the O–H groups of the hydronium ion, and the Zundel hydration structure ($H_5O_2{}^+$), in which the proton is flanked by two water molecules [1, 48, 152]. The O-H stretch vibrations of the hydronium core of the Eigen structure exhibit a strong absorption band around ∼2800 cm^{-1}. The O-H stretch vibration of the water molecules flanking the proton in the Zun-

del structure have an absorption band at a frequency of ∼3300 cm^{-1}, whereas the central Zundel proton ($O\cdots H^+\cdots O$) vibration absorbs at ∼1200 cm^{-1}. Additionally, an absorption band at ∼1730 cm^{-1} was assigned to the degenerate symmetric and antisymmetric bending modes of the hydronium core of the Eigen structure [40, 48] However, this band at ∼1730 cm^{-1} might also be caused by the bending vibrations of the water molecules flanking the Zundel proton, coupled to the central Zundel proton ($O\cdots H^+\cdots O$) vibration [58, 59].

In this chapter we study the vibrational dynamics of the ∼1730 cm^{-1} bending vibration using polarization-resolved mid-infrared pump-probe spectroscopy. We measure the rate of vibrational relaxation, and we observe that for a small fraction of the excitations the vibrational relaxation involves the predissociation of a hydrogen bond of the proton hydration structure.

7.2 Experiment

The infrared pump-probe experiments were performed with the one-color pump-probe setup described in section 3.2.2. The generated infrared pulses have a central frequency of 1730 cm^{-1}, a pulse energy of ∼20 μJ, a duration of ∼100 fs, and a bandwidth of ∼300 cm^{-1}. To minimize direct excitation of the H_2O bending mode in the sample, a water (H_2O) filter with an optical density of 1.5 OD at 1630 cm^{-1} was placed in the pump beam path. The details of the Nafion membrane preparation can be found in section 3.4.

7.3 Results and Discussion

7.3.1 Linear Spectra

Fig. 7.1 shows the linear infrared absorption spectra of 50 μm thick proton-terminated ($[H^+] : [Na^+] = 1 : 0$) and sodium-terminated ($[H^+] : [Na^+] = 0 : 1$) Nafion membranes. The absorption spectrum of the sodium-terminated Nafion membrane shows a narrow absorption band with a resonance frequency of ∼1630 cm^{-1}. This band originates from the bending mode of water molecules that are hydrogen bonded to other water molecules. The absorption band is red shifted by ∼10 cm^{-1} relative to the H_2O bending mode in bulk water because of the weaker hydrogen bonding interactions between water molecules in Nafion membranes compared to bulk water. The infrared absorption spectrum of proton-terminated Nafion membranes exhibits a broad and intense absorption band centered at 1730 cm^{-1}. The red side of the 1730 cm^{-1} band exhibits a small, but significant shoulder at ∼1630 cm^{-1}, which can be assigned to the bending mode of water molecules that are not strongly involved in the hydration of the proton, e.g. to water molecules that are located in the outer hydration shells of the proton and water molecules that are embedded in the hydrophobic pockets of the Nafion membrane.

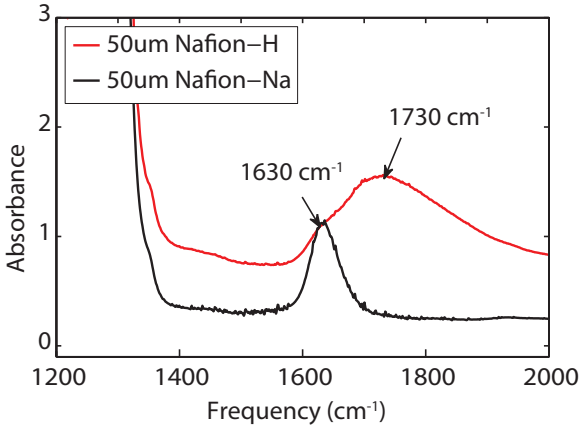

FIGURE 7.1. Linear spectra of proton-terminated (red line) and sodium-terminated (black line) Nafion membranes of 50 μm thickness. The hydration level of both samples corresponds to $\sim$4 water molecules per sulfonate group ($\lambda = 4$). The spectrum of sodium-terminated Nafion membrane has been scaled for clarity.

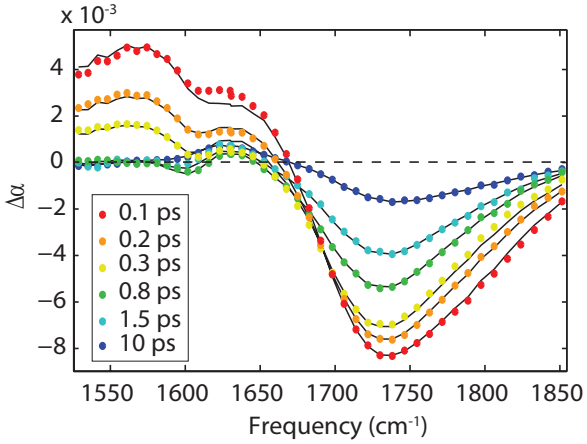

FIGURE 7.2. Transient absorption spectra of proton-terminated Nafion membranes (thickness 50 μm), hydrated with H_2O ($[H^+] : [Na^+] = 1 : 0$) at different delays after excitation of the bending mode at $\sim$1730 cm^{-1}.

7.3.2 VIBRATIONAL RELAXATION

Fig. 7.2 presents isotropic transient absorption changes following excitation of the 1730 cm^{-1} mode in proton-terminated Nafion membranes ($[H^+] : [Na^+] = 1 : 0$) at different delay times. At short delay times, the transient absorption spectra show a negative (bleaching) signal centered at 1730 cm^{-1} and a positive, induced absorption signal at frequencies below 1680 cm^{-1}. The bleaching signal is observed at the fundamental frequency of the bending mode from 1670 cm^{-1} to 1850 cm^{-1} and results from the depletion of the ground state ($\upsilon = 0 \rightarrow 1$ transition) and the stimulated emission from the first excited state ($\upsilon = 1 \rightarrow 0$). The induced absorption at lower frequencies (1530 cm^{-1} to 1650 cm^{-1}) is due to the $\upsilon = 1 \rightarrow 2$ absorption transition of the excited molecules. The absorption changes decay due to vibrational relaxation of the excited $\upsilon = 1$ state. For delay times larger than 15 ps, the transient absorption spectrum shows no further change. The transient spectrum at late delay times reflects the temperature increase of the sample that results from the thermalization of the vibrational excitation. The increase in temperature weakens the hydrogen bonds and leads to a shift of the absorption spectrum of the 1730 cm^{-1} mode to lower frequencies. This shift leads to an increased absorption (positive $\Delta\alpha$) in the lower frequency region $<$1670 cm^{-1} and a bleaching signal (negative $\Delta\alpha$) in the higher frequency region $>$1670 cm^{-1} [153, 154]. At early delay times, an additional weak bleaching signal at a frequency of $\sim$1610 cm^{-1} is seen in Fig. 7.2. This signal is superimposed on the induced absorption, and its frequency matches very well the bending mode frequency ($\sim$1630 cm^{-1}) of water [153, 155, 156]. This weak feature in the transient spectra is thus likely the result of direct excitation of the bending mode of water molecules that are not directly associated with the proton hydration structures.

In Fig. 7.3 we present isotropic transient absorption changes at two different probe frequencies as a function of the delay time between pump and probe. The blue circles represent the bleaching signal at 1730 cm^{-1}, and the red diamonds represent the induced absorption signal at 1550 cm^{-1}. The induced absorption ($\upsilon = 1 \rightarrow 2$) exhibits a vary rapid decay that is complete within the first 500 fs. In contrast, the dynamics of the bleaching signal are much slower than the induced absorption signal and are still not complete at a delay time of 4 ps. This striking difference in the dynamics of the bleaching and induced absorption signals suggests that the excited 1730 cm^{-1} mode does not directly relax to a thermally equilibrated state, but instead relaxes to an intermediate state with a time scale of a few hundred femtoseconds. Subsequently, this intermediate state relaxes to a thermally equilibrated signal with a time constant of a few picoseconds.

We describe the isotropic transient absorption changes with a kinetic model that is schematically depicted in the inset of Fig. 7.4. The states designated as S_0 and S_1 correspond to the vibrational ground state ($\upsilon = 0$) and the first excited state ($\upsilon = 1$) of the 1730 cm^{-1} mode, respectively, and $S_1^{'}$ and S_0^{*} represent the intermediate state and the thermally equilibrated state, respectively. The vibrationally excited state S_1 relaxes to the intermediate state $S_1^{'}$ with

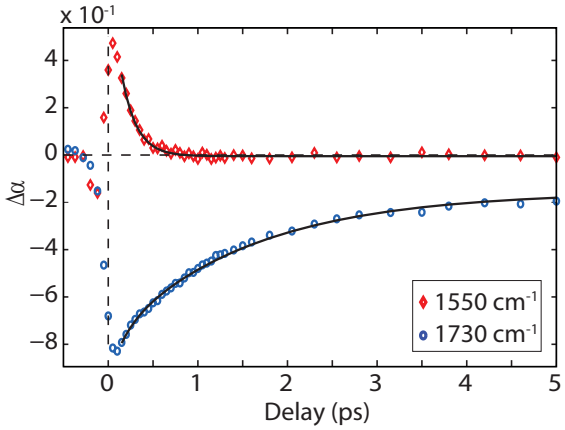

FIGURE 7.3. Transient absorption changes of a proton-terminated Nafion membrane of 50 μm-thickness as a function of pump-probe delay time. The blue circles represent the absorption change at the central frequency of the bleaching signal at 1730 cm^{-1}. The red diamonds show the absorption change in the spectral region of the induced absorption at 1550 cm^{-1}. The black curves represent fits to the kinetic model described in the text.

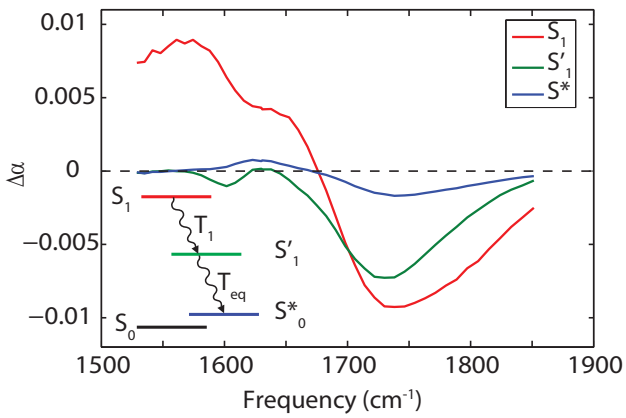

FIGURE 7.4. Spectral components obtained from fitting the kinetic model described in the text to the transient absorption ($\Delta\alpha_{iso}$) data. The kinetic model is schematically depicted in the inset. The red curve indicates the spectrum of the transient absorption change associated with the excitation of the υ=1 state of the 1730 cm^{-1} bending mode. The green and blue curves represent the transient absorption spectra of the intermediate and the final equilibrated thermal states, respectively.

a time constant T_1, and the intermediate state relaxes to the final, thermally equilibrated state with a time constant T_{eq}. The coupled rate equations of this kinetic model are

$$\begin{aligned} \frac{d}{dt}(n_{S_1}) &= -\frac{n_{S_1}}{T_1} \\ \frac{d}{dt}(n_{S_1'}) &= \frac{n_{S_1}}{T_1} - \frac{n_{S_1'}}{T_{eq}} \\ \frac{d}{dt}(n_{S_0^*}) &= \frac{n_{S_1'}}{T_{eq}} \end{aligned} \tag{7.1}$$

Here, n_{S_1}, $n_{S_1'}$ and $n_{S_0^*}$ denote the populations of the states indicated by the subscript. The total isotropic transient absorption change $\Delta\alpha(\nu)_{iso}$ as a function of delay time t can be written as:

$$\Delta\alpha(\nu,t) = \sigma_{S_1}(\nu)n_{S_1}(t) + \sigma_{S_1'}(\nu)n_{S_1'}(t) + \sigma_{S_{0*}}(\nu)n_{S_0^*}(t), \tag{7.2}$$

where σ_{S_1},$\sigma_{S_{1'}}$ and $\sigma_{S_0^*}$ denote the transient spectra associated with each of the three states indicated by the subscript.

We fit the isotropic transient absorption changes by solving the rate-equations in Eq. (7.1) in a least-square minimization routine, in which the time constant T_{eq} is treated as a free parameter. The time constant associated with the vibrational relaxation process is held at a fixed value of $T_1 = 175$ fs that has been obtained from a mono-exponential fit to the dynamics of the induced absorption shown as the red curve in Fig. 7.3. The T_1 value of ∼175 fs of the 1730 cm^{-1} mode is shorter than the T_1 value of 400 fs of the bending mode of H_2O molecules in a mixture of HDO and D_2O [156], and it is very similar to the vibrational lifetime of 170 fs that has been measured for the bending mode of H_2O molecules in pure liquid H_2O[157]. From the fit we obtain a value of $T_{eq} = 1.5\pm0.2$ ps for the thermalization process. The transient spectra σ_i associated with the states S_1, S_1' and S_0^* obtained from the fit, are shown in Fig. 7.4. The resulting fits are shown as black solid lines in Fig. 7.2 and Fig. 7.3. It is clearly seen that the model provides an excellent description of the experimental data.

7.3.3 ANISOTROPY

In Fig. 7.5 we present the anisotropy decay of the 1730 cm^{-1} mode in proton-terminated Nafion membrane, averaged over the frequency interval between 1700 cm^{-1} and 1750 cm^{-1}. The anisotropy exhibits a very fast initial decay from a starting value of 0.3 at 200 fs to 0.15 at ∼2.5 ps. Interestingly, at later delay times the anisotropy slightly re-rises followed by a slow decay that takes place on a time scale of tens of picoseconds.

The initial decay of the anisotropy could in principle be caused by intra- or intermolecular resonant (Förster) energy transfer between different bending modes within the proton hydration structure. The rate of resonant energy transfer strongly depends on the distance between the donating and accepting

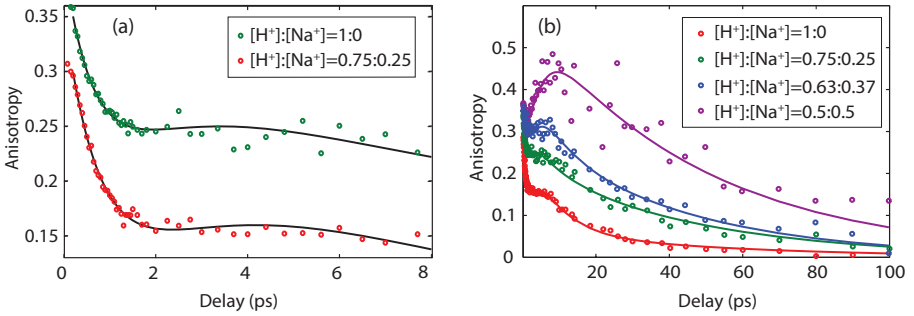

FIGURE 7.5. (a) Anisotropy of the transient absorption signal (averaged from 1700 cm^{-1} to 1750 cm^{-1}) of the 1730 cm^{-1} bending mode as a function of delay time. The cation ratios ($[H^+]$:$[Na^+]$) of the Nafion samples are indicated in the legend. The solid curves are obtained from a bi-exponential fit to the data. (b) Zoom-in of the early component of the anisotropy dynamics shown in panel (a).

vibrations, and thus the presence of such a process can be determined by measuring the effect of a change in average distance of the oscillators on the decay rate of the anisotropy. In order to do so, we systematically varied the cation ration $[H^+]$:$[Na^+]$, i.e. we partially replaced the protons in Nafion membranes by sodium ions, and performed the same polarization-resolved pump-probe experiment. The anisotropy decay of the hydronium bending mode obtained from a Nafion sample with a cation ratio of $[H^+]$:$[Na^+]$=0.75:0.25 is plotted as green circles in Fig. 7.5 (a). In Fig. 7.5 (b), we show a zoom-in of the early dynamics (delay times < 8 ps) of the anisotropy curve. For $[H^+]$:$[Na^+]$=1:0 (pure proton-terminated Nafion), the anisotropy initially decays with a time constant of $\sim$340$\pm$20 fs, while for $[H^+]$:$[Na^+]$=0.75:0.25 the time constant of the initial anisotropy decay is $\sim$360$\pm$30 fs. These time constants are indistinguishable within the experimental uncertainty, which indicates that the contribution of *intermolecular* (Förster-type) energy transfer to the initial anisotropy decay of the bending mode plays a minor role.

The time constant ($\sim$350 fs) of the initial anisotropy decay is longer than the vibrational relaxation time (T_1 =$\sim$175 fs) of the excited bending mode vibration, which implies that the vibrational excitation has relaxed to a large extent before it becomes isotropically distributed. The local intermediate state (designated as S_1' in the preceding section) thus corresponds to a state for which the hydrogen bonds of the excited proton hydration structure are weakened by the local dissipation of the vibrational excitation energy. The dissipation of energy will initially mainly affect the absorption of the originally excited bending mode vibration. Hence, directly after the relaxation the created local hot S_1' state will have a high anisotropy value. The subsequent redistribution of heat over the proton hydration cluster will also affect other bending modes for which the transition dipole moment is oriented differently from the originally excited bending mode. The equilibration of the thermal energy over the proton hydration complex will thus lead to a decay of the anisotropy of the S_1' state.

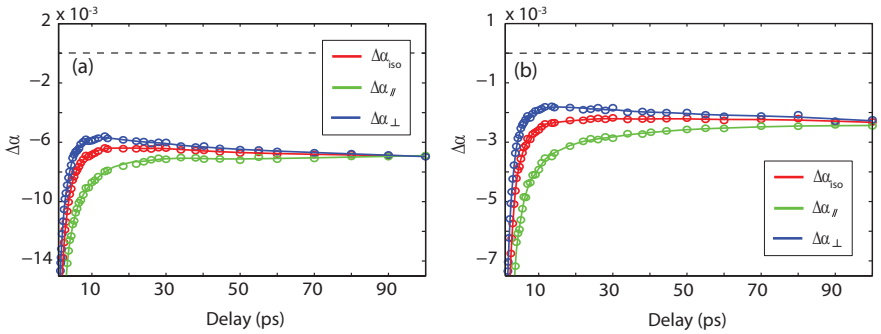

FIGURE 7.6. Isotropic transient absorption changes (red) and transient absorption changes obtained under parallel (green) and perpendicular (blue) polarization configurations of the pump and probe pulses, as a function of delay time. The absorption changes are shown for Nafion membranes with (a) $[H^+]$:$[Na^+]$=1:0 and (b) $[H^+]$:$[Na^+]$=0.75:0.25.

This equilibration process over the proton hydration cluster does not lead to a complete decay of the anisotropy, because the proton hydration clusters will be quite small, containing on average 4 water molecules. Hence, the number of bending modes that will be affected by the spreading of heat over the cluster will be limited, which implies that even after the equilibration over the cluster is complete, there will be a preferential orientation of the affected bending mode absorption spectra in the direction of the polarization of the pump pulse. The anisotropy will decay completely in the transition from the local hot S_1' state to the fully thermally equilibrated S_0^* state. In this relaxation process the local hot cluster cools by transferring its excess thermal energy to the Nafion membrane and to proton-hydration clusters that were not excited.

A striking feature of the anisotropy curves of Fig. 7.5 is that the partial decay within the first ∼2 ps is followed by a re-rise of the anisotropy, which reaches a maximum at a delay time of ∼8-10 ps. After this maximum the anisotropy decays slowly. Interestingly, the anisotropy exhibits a substantial amplitude at delay times for which the vibrational relaxation and subsequent thermalization have long been completed. This is clearly illustrated in Fig. 7.6, where we plot the transient absorption changes obtained under parallel and perpendicular polarization of pump and probe pulses together with the isotropic transient absorption changes. For delay times >10 ps, the isotropic signal (red curve) has reached its end level and remains constant up to a delay time of 100 ps. The bleaching signal that remains at these delay times, results from the temperature increase following the vibrational relaxation, as explained in the previous section. In contrast, the parallel (green curve) and perpendicular (blue curve) transient absorption changes, which are related to the anisotropy by Eq. (2.44), keep evolving over much longer time scales.

A re-rise of the anisotropy as observed in Fig. 7.5 is indicative of the presence of multiple species with different lifetimes and different associated anisotropy

dynamics. In particular, a re-rise in the anisotropy will occur if the transient absorption signal becomes increasingly dominated by a species that exhibits a much slower anisotropy decay than the species that dominated the transient absorption signal at short delay times (and that thus have a short T_1-time).

The re-rise of the anisotropy occurs with a time constant that is similar to T_{eq}, the time constant of the transition from the local hot state S_1' to the fully thermally equilibrated state S_0^*. The latter state corresponds to a complete thermalization of the energy over the focus in the Nafion membranes meaning that this state has zero anisotropy. However, already at delays of ∼1 ps, the anisotropy of the local heating effect will be low as at this time the hot state S_1' has redistributed its high thermal energy content over the proton hydration structure. Hence, the relaxation to the fully thermally equilibrated state S_0^* with time constant T_{eq} corresponds to the decay of a contribution to the total transient absorption that has a very low anisotropy value. As a result, the relative contribution of another long-living (much slower decaying) signal component with a high anisotropy will increase with the same time constant T_{eq}. This interpretation is supported by the observation that the amplitude of the delayed rise in the anisotropy increases as the amplitude of the isotropic thermal bleaching signal decreases, as shown in Fig. 7.5. In panel (b) of this figure, it is clearly seen that the amplitude of the intermediate rise of the anisotropy of the hydronium bending mode changes with hydronium concentrations (corresponding to different cation ratios $[H^+]$:$[Na^+]$ as indicated in the legend). For the case of $[H^+]$:$[Na^+]$=1:0, the anisotropy reaches a maximum intermediate value of ∼0.2 at around ∼10 ps (red circles). In contrast, for the lowest cation ration of $[H^+]$:$[Na^+]$=0.5:0.5, the anisotropy exhibits an intermediate rise up to ∼0.4. This is because for a lower cation ratio, the amplitude of the thermal state is smaller and thus the total amplitude of the delayed rise of the anisotropy is larger.

Obviously, the above explanation for the re-rise of the anisotropy not only requires the decay of an isotropic signal component but also the presence of a long-living bleaching signal component with a high anisotropy. Such a long-living component in the transient absorption could be due to the predissociation of a hydrogen bond directly following the vibrational excitation. The predissociation of a hydrogen bond of the proton hydration structure would lead to the release of a water molecule. The dissociated water molecule can diffuse away from the residual cluster, and it can take a relatively long time before the water molecule comes back and the hydrogen bond is reformed. Hence, vibrational predissociation could potentially account for absorption changes that are long-living on the time scale of our experiment of ∼100 picoseconds. The dissociated water molecules will have a bending mode absorption near 1620 cm^{-1}, outside the spectral region that is monitored in our experiment. The number of oscillators contributing to the broad absorption band around 1730 cm^{-1} is therefore reduced by the predissociation process, leading to a transient absorption change that has a bleaching-like signature in this frequency region.

Hydrogen-bond predissociation processes following vibrational excitation

have been observed before for hydrogen-bonded systems such as ethanol clusters in CCl_4 [158]. However, in this previous work the predissociation followed the excitation of an O–H stretch vibration with a frequency of $\sim$3300 cm^{-1}. One may wonder whether the excitation energy of the bending mode of 1730 cm^{-1} suffices to break a hydrogen bond of the proton hydration cluster. A difference with the previous work on vibrational predissociation is that in the present case the proton hydration clusters will be small, containing an average number of 4 water molecules, and that these clusters are relatively isolated. For small aqueous clusters the hydrogen bonds are weaker than for bulk aqueous solutions, due to the fact that in the bulk the hydrogen bonds become stronger due to cooperative conjugation effects. The strength of the hydrogen bonds of water clusters have been studied both experimentally and theoretically, and it was found that the dissociation energy of a protonated water cluster can vary between 1500 and 5000 cm^{-1}, depending on the size and geometry of the cluster[159, 160]. Hence, the excitation energy of the bending mode could indeed be sufficient to break a hydrogen bond, at least for a small fraction of the excited clusters.

To explain the observations of Fig. 7.5, there should not only be a long-living bleaching signal, but this signal should also have a high anisotropy. The anisotropy of the bleaching signal will depend on the orientation of the transition dipole moments of the bending mode vibrations that disappear as a result of the predissociation. The anisotropy of the bleaching signal will be high if the predissociation leads to the disappearance of the originally excited 1730 cm^{-1} bending mode. This will be the case if the excited 1730 cm^{-1} mode corresponds to the bending mode of an H_2O molecule flanking a Zundel proton, and if the excitation of this bending mode leads to predissociation of one of the hydrogen bonds of the water molecules to the Zundel proton. In this case the absorption spectrum of the originally excited bending mode will shift to that of an isolated H_2O molecule at $\sim$1600 cm^{-1}. As a result, the absorption or the originally excited bending mode vibration at 1730 cm^{-1} will be decreased, and this bleaching will have a high anisotropy value. The Zundel proton will shift towards the other H_2O molecule and the hydrogen bond between the proton and this H_2O molecule will become an O–H chemical bond of an H_3O^+-like structure. The positive charge of the Zundel proton will thus be largely transferred to the hydrogen atoms of the H_2O molecule. If the 1730 cm^{-1} mode corresponds to the bending mode of an H_3O^+ ion, the excitation of one of the bending modes may lead to predissociation of one of the hydrogen bonds donated by the H_3O^+ ion, and this will affect the absorption of several bending modes at 1730 cm^{-1} with different orientations of their transition dipole moment. However, breaking of one of the hydrogen bonds will lead to redistribution of the positive charge of the proton over the proton hydration structure. In particular, the positive charge is expected to leak away from the O–H group at which the hydrogen bond breaks and that most likely was involved in the excited bending mode. Hence, also in case the 1730 cm^{-1} mode represents a bending vibration of H_3O^+, the predissociation is expected to affect mainly the originally excited bending mode, which means that also in this case the anisotropy of the bleaching will be high.

The slow decay of the anisotropy for delay times >8 ps is likely the result

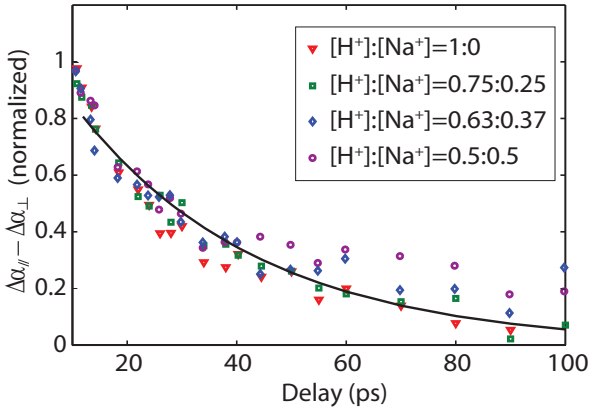

Figure 7.7. Normalized difference between the transient absorption changes obtained under parallel and perpendicular polarization configurations of the pump and probe pulses ($\Delta\alpha_{\parallel} - \Delta\alpha_{\perp}$), as a function of delay time, for delay times >10 ps.

of a slow structural reorganization of the whole proton hydration structure. In Fig. 7.7 the normalized difference absorption between parallel and perpendicular components at four different proton concentrations ($[H^+]$:$[Na^+]$ ratios) are shown. By taking the difference between the parallel and perpendicular components we eliminate the contribution to the signal of the isotropic thermal state as for this state the parallel and perpendicular absorption changes are the same. The difference signal thus only represents the anisotropy of the bleaching signal that results from the predissociation. In Fig. 7.7, the data for all concentrations exhibit very similar dynamics and decay with a time constant τ_2=38±4 ps. This decay cannot be caused by heat diffusion through the Nafion membranes, thereby equilibrating the heat effect over excited and non-excited proton hydration clusters, as such a process would be accompanied by a change in the isotropic transient absorption signal, which is not observed in Fig. 7.6. The time constant τ_2 is the same for all proton concentrations, which indicates that the slow decay results from the restructuring of the separate proton hydration clusters in the Nafion membrane and is likely associated with a restructuring of the proton hydration clusters in the Nafion membranes. This restructuring will lead to a reorientation of the transition dipole moments of the bending modes at 1730 cm^{-1}, thereby erasing the dominant bleaching of these modes along the direction of the polarization of the pump pulse.

7.4 Conclusions

We investigated the vibrational dynamics of the bending mode at 1730 cm^{-1} of proton hydration clusters in hydrated Nafion membranes with polarization-resolved mid-infrared pump-probe spectroscopy. We find that a large fraction of the excited bending modes first relaxes to an intermediate state with a time

constant of T_1 ≈175 fs. This intermediate state represents a strong local heating effect of the excited proton hydration cluster. The initial decay of anisotropy with a time constant of ∼350 fs, which is slower than the vibrational relaxation time T_1 of 175 fs, indicates that the local heat is redistributed over the cluster. Subsequently the heated proton hydration cluster cools by transferring its excess thermal energy to the Nafion membrane and to proton hydration clusters that were not excited. This thermalization process has a time constant T_{eq} of 1.5±0.2 ps, and results in a fully thermally equilibrated state.

The anisotropy of the bleaching signal shows a re-rise with a time constant that is similar to T_{eq}. This observation indicates that for a small fraction of the excited bending modes the relaxation results in predissociation of one of the hydrogen bonds of the proton hydration cluster, and thus to the release of a water molecule. The predissociation creates a long-living bleaching signal with a high associated anisotropy. The anisotropy of this signal slowly decays with a time constant τ_2=38±4 ps. The time constant τ_2 does not depend on the concentration of protons, which indicates that the slow decay results from the restructuring of the separate proton hydration clusters in the Nafion membrane.

8

Dynamics of Aqueous Protons in Acetonitrile

We study the ultrafast O–H stretch vibrational relaxation dynamics of protonated water clusters embedded in a matrix of deuterated acetonitrile, using polarization-resolved mid-IR fs spectroscopy. The clusters are produced by mixing triflic (trifluoro-methanesulfonic) acid and H_2O in molar ratios of 1:1, 1:2 and 1:3, thus varying the degree of hydration of the proton. At all hydration levels the excited O–H stretch vibration shows an ultrafast vibrational relaxation with a time constant T_1<100 fs, leading to an ultrafast local heating of the protonated water cluster. This excess thermal energy, initially highly localized to the region of the initially excited proton, first redistributes over the aqueous cluster and then dissipates into the acetonitrile matrix. For clusters with a triflic acid to H_2O ratio of 1:3 these processes occur with time-constants of 320±20 fs and 1.4±0.1 ps, respectively. The cooling of the clusters reveals a long-living, underlying transient absorption change with high anisotropy. We argue that this feature stems from the vibrational predissociation of a small fraction of the proton hydration structures, directly following the ultrafast infrared excitation.

8.1 Introduction

Understanding the structural dynamics of the aqueous proton, H^+_{aq}, represents a challenging field of research [17]. The transport properties of the proton in water are unique, finding equivalence in no other ion in aqueous solution. The mechanistic base thereof lies in the near-barrier free and ultrafast interconversion of hydrogen and covalent bonds through a continuum of proton hydration structures, of which the Eigen (H_3O^+) and Zundel ($H_5O_2{}^+$) cations form the limiting cases. This process, commonly referred to as Grothuss conduction, results in an effective transport of the proton structure and charge but not of its mass [9, 21, 83, 161].

While the fundamental principles governing proton transport in pure bulk water have by now been studied in great detail, the arguably most interesting and relevant aqueous proton transport processes occur in complex, strongly perturbed environments and are far less well understood. Such perturbations can be due to co-solutes [162] or geometrical constraints on the nanometer scale of the aqueous component on the system, also known as nano-confinement effects.

As such perturbations have a strong effect on the hydrogen-bond structure and dynamics of the water matrix, they are prone to influence the proton-transport mechanism. The importance of nano-confined aqueous protons for biological systems [163] and technological applications, e.g. hydrogen fuel cells [114, 164], makes this an active area of research.

Several kinds of model systems have been devised where the properties of protons and other ionic solutes can be studied under nano-confinement. It has, for example, been found that the proton release by photo-acids is significantly slower inside cati-onic reverse micelles than in bulk water [127, 165]. This observation can be explained by the rotational slowdown of the surrounding water molecules. The orientation mobility of water molecules is also thought to determine the rate of the Grotthuss conduction mechanism. In bulk water this is known to be the case and the process relies on the cooperative reorientation of a large number of water molecules [13, 26].

In this work we follow a different route to study the effect of confinement of the protonic charge; namely in mixtures of water and a polar but aprotic solvent, acetonitrile (CH_3CN or ACN). It has since long been known that the viscosities, densities, and dielectric constants of water-ACN mixtures show a considerable degree of non-ideality [166]. This was interpreted as reflecting inhomogeneous mixing on the molecular level, further evidenced by the quasi-lattice quasi-chemical and inverse Kirkwood-Buff integral treatments by Marcus and Migron, using thermodynamic data [167]. The inhomogeneous character of water-ACN mixtures has been put on solid experimental ground through NMR spectroscopy [168], linear IR spectroscopy and X-ray diffraction [169], as well as ultrafast mid-IR pump-probe spectroscopy experiments [170]. In the latter work, Cringus et al. showed that the vibrational lifetime of O–H stretch vibrations of water molecules is a sensitive reporter of the degree of water-water hydrogen bonding. All these experiments have demonstrated that the local water structure strongly varies with the water molar faction X_{H_2O}. From $X_{H_2O} = 0$ to $X_{H_2O} = 0.05{\sim}0.1$ water molecules go from existing as monomers to primarily forming dimers and trimers. In the range $0.2{<}X_{H_2O}{<}0.7$, the so-called microheterogenous region, the clustering of water molecules becomes significant. Thus, dilute water/ACN mixtures potentially form an excellent basis for studying the behavior of solutes in nanometer-sized water volumes. A second advantage of studying protonated water clusters in ACN is that the aprotic character of ACN ensures that the protonic charge stays localized, and thus confined, in the aqueous domains of the heterogeneous solution. Pines and co-workers have extensively studied the behavior of strong acids in water/ACN-mixtures [58, 171]. While hydrochloric acid, HCl, was found to only partially dissociate in these mixtures, stronger mineral acids such as perchloric acid ($HClO_4$), hydroiodic acid (HI) and the superacid trifluoromethanesulfonic acid (HCF_3SO_3, usually referred to as triflic acid or TfOH) undergo complete dissociation in the aqueous phase.

We use polarization-resolved pump-probe spectroscopy to study the vibrational dynamics of the O–H groups of hydrated protons in aqueous clusters inside a matrix of deuterated acetonitrile (CD_3CN). The acetonitrile was deuterated in order to shift the intense C-H absorption features of ordinary acetonitrile

out of the O–H stretch band that is probed in the femtosecond pump-probe experiment. As a result we have access to a broad spectral range (2700-3700 cm^{-1}), providing detailed information on the structural dynamics of aqueous protons under varying degrees of nano-confinement.

8.2 Experiment

The experiments were performed with a two-color mid-IR pump-probe setup that is very similar to the setup described in Section 3.2.1. This system is based on a Ti:sapphire laser system (Coherent, Legend Duo) delivering 35 fs pulses and a total pulse energy of 7.5 mJ at a repetition rate of 1 kHz. The excitation pulse was generated by pumping a commercial OPA (TOPAS, LightConversion) with the majority of the 800 nm power (∼6.5 W). The excitation pulse has a central frequency of 2800 cm^{-1} and a pulse energy of 20 μJ. The probe pulse was generated in a home-built OPA pumped by the rest of the 800 nm beam. The home-built OPA is described in Section 3.1. The frequency of the probe pulse is tunable from 2800 cm^{-1} to 3700 cm^{-1}. The probe pulse energy is ∼3 μJ.

The samples were prepared directly before the experiments from premade stock solutions of diluted trifluoromethanesulfonic acid solutions of fixed [TfOH]:[H_2O] molar ratios, mixed together with and pure deuterated acetonitrile (CD_3CN or d-ACN, 99.8%, Sigma-Aldrich). The [d-ACN]:[H_2O] ratio was kept at 25:1 to ensure that the water phase is not percolating (thus ensuring confined water volumes). Linear absorption spectra in the mid-IR region were recorded using a commercial Fourier transform spectrometer (Biorad FTS 175 FTIR) directly before and after each pump-probe experiment. This procedure ensured reproducibility in the sample preparation and that sample degradation was not influencing the recorded data.

8.3 Results and Discussion

8.3.1 Linear Spectra

Fig. 8.1 shows linear spectra of TfOH/H_2O mixtures in d-ACN in the spectral range of 2400–3700 cm^{-1} (the d-ACN background has been subtracted). The broad and intense features are associated with the O–H stretch absorption of the protonated water clusters. The [d-ACN]:[H_2O] molar ratio of 25:1 implies that the partial volume of the acidic aqueous phase is small and varies relatively little across the series (∼3.5–7.5%). As a result, the confinement effects on the proton hydration are expected to be large, as has indeed been shown in previous studies [58, 171]. We vary the [TfOH]:[H_2O] ratio from 1:1 to 1:3, implying that the number of water molecules available to hydrate the dissociating acid varies, which will strongly influence the hydration structure of the proton. In fact, this is directly evident in the spectra in Fig. 8.1: for [d-ACN]:[H_2O] = 1:1, the center frequency of the O–H stretch band is as low as ∼2620 cm^{-1}, which is

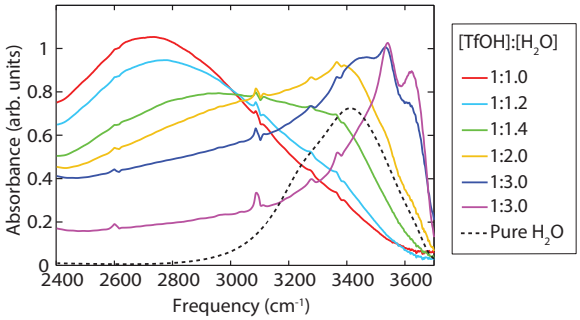

FIGURE 8.1. Linear spectra of various mixtures of water and triflic acid in deuterated acetonitrile (acetonitrile background has been subtracted) in the frequency region of the OH stretch vibrations. The acetonitrile to water molar ratio is 25:1, while the triflic acid to water ratio is varied from 1:1 to 1:10. The black dotted line represents the spectrum of pure H_2O.

strongly red-shifted compared to that of pure water (which is centered at ∼3400 cm^{-1} and represented by the solid black line in Fig. 8.1). This red shift is in good agreement with previous experimental and theoretical determinations of the frequencies of the intra-molecular O–H stretch vibrations of the hydronium cation, H_3O^+, which is expected to be the dominant species at these low hydration levels [37, 48]. At higher hydration levels the spectral center of mass quickly blue-shifts, reflecting the increasing response of water molecules flanking the hydrated proton, and possibly an increased population in Zundel-like hydration structures ($H_5O_2^+$).

8.3.2 NONLINEAR SPECTRA

The three panels in Fig. 8.2 show examples of isotropic pump-probe spectra for three representative triflic acid to water ratios; [TfOH]:[H_2O] = 1:1, 1:2 and 1:3, plotted at various pump-probe delay times. In all cases the samples were pumped by pulses centered at 2800 cm^{-1}, leading primarily to v= 0→1 excitations of intramolecular O–H stretch vibrations of the hydronium (H_3O^+) cation. As a result, a large bleaching signal (negative values of the absorption change $\Delta\alpha_{iso}$) instantaneously appears at frequencies <3000 cm^{-1}. For the [TfOH]:[H_2O] = 1:1 system this bleaching band remains centered at ∼2750 cm^{-1}, whilst the spectrum decays to the (heated) global end level – compare the early red (225 fs) and late purple (100 ps) spectra in Fig. 8.2 (a). For [TfOH]:[H_2O] = 1:2 (Fig. 8.2 (b)) the maximum bleach at 225 fs pump-probe delay is centered at ∼2950 cm^{-1} while a rapid spectral diffusion causes the maximum bleach to shift to ∼3300 cm^{-1} within 350 fs. A similar behavior is observed for [TfOH]:[H_2O] = 1:3 in Fig. 8.2 (c): the initial bleaching at ∼3000 cm^{-1} rapidly blue-shifts towards ∼3375 cm^{-1}.

All spectra furthermore show a pronounced positive $\Delta\alpha_{iso}$ (induced absorp-

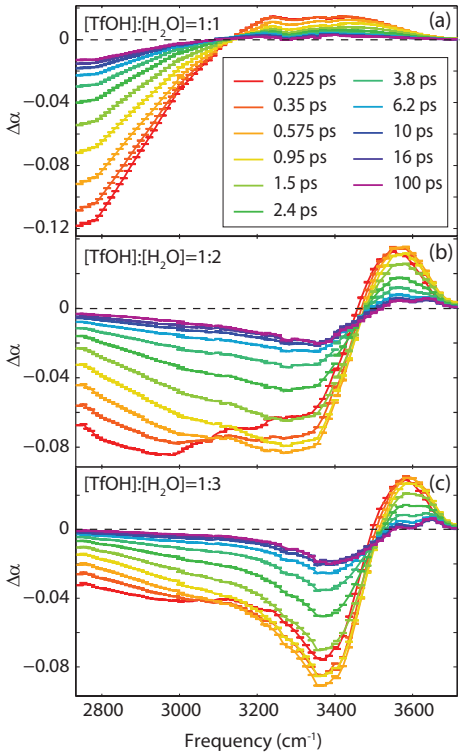

Figure 8.2. Isotropic transient spectra of samples with different triflic acid to water ratios; a) [TfOH]:[H_2O] = 1:1, b) [TfOH]:[H_2O] = 1:2, and c) [TfOH]:[H_2O] = 1:3. In all cases the [d-ACN]:[H_2O] molar ratio is 25:1.

tion) at higher frequencies. For the [TfOH]:[H_2O] = 1:1 case this feature is exceptionally broad and covers the region between ∼3150-3600 cm^{-1}. For the higher hydration levels, the crossing between bleaching and induced absorption is much more blue shifted; a behavior that is correlated with the blue-shift in the linear spectrum.

8.3.3 Vibrational Relaxation and Cluster Cooling Dynamics

In Fig. 8.3 the isotropic absorption change and the anisotropy of the [TfOH]:[H_2O] = 1:1 system are shown as a function of delay time for frequencies of 2900 and 3600 cm^{-1}. The isotropic bleaching signal at 2900 cm^{-1} shows a relatively slow single exponential decay with a time constant of 1.2±0.1 ps (Fig. 8.3 (a)). The induced absorption signal at 3600 cm^{-1} shows more complex dynamics. The signal increases on a time scale of a few hundred femtoseconds and then decays with the same time constant as the bleaching

signal at 2900 cm^{-1} (Fig. 8.3 (b)). The anisotropy at 2900 cm^{-1} shows a rapid decay on a time scale of ∼100 fs to a final level of 0.14. The anisotropy at 3600 cm^{-1} has an initial negative value and rises to a positive value of 0.04. The time constant of this rise is similar as observed for the isotropic absorption change.

We interpret these data in the following way. The pump pulse at 2800 cm^{-1} excites one of the O–H stretch vibrations of a hydronium (H_3O^+) ion, which results in a bleaching of the excited vibration, corresponding to a decrease in absorption around 2800 cm^{-1} with a high anisotropy value (Fig. 8.3 (c)). A striking observation is the initial negative anisotropy value of the induced absorption signal at 3600 cm^{-1}. A similar signal was observed in a recent study of proton hydration structures in Nafion nano-channels. This signal was explained as follows. The excitation of the O–H stretch vibration of H_3O^+ to the υ=1 state leads to a strengthening of the hydrogen bond donated by this O–H bond and a weakening of the hydrogen bonds donated by the other two O–H groups of the H_3O^+ ion [135, 172]. These changes in hydrogen bond strengths are accompanied by a shift of positive charge towards the H atom of the excited O–H group. The weakening of the hydrogen bonds of the two non-excited O–H groups leads to a blue-shift of the absorption bands of the stretch vibrations of these O–H groups and thus to an induced absorption at high frequencies. As these O–H groups are oriented at a large angle with respect to the excited O–H group, the induced absorption signal has a negative anisotropy value. The initial negative anisotropy value of the signal at 3600 cm^{-1} (Fig. 8.3 (c)) can thus be explained from vibration-excitation induced changes in the strengths of the local hydrogen bonds of the hydronium (H_3O^+) ions formed in [TfOH]:[H_2O]:[d-ACN] = 1:1:25 mixtures.

The vibrational excitation rapidly relaxes, leading to a strong local heating effect. The heating causes a weakening of all hydrogen bonds in the proton hydration structures and thus to a blue-shift of all O–H stretch absorption bands within the cluster, including those of the H_3O^+ ion and H_2O molecules that are hydrogen bonded to the H_3O^+ ion. The bleaching associated with the local heating of the proton hydration structure has a lower anisotropy value than the signal associated with the excitation of an O–H stretch vibration. Hence, the vibrational relaxation is accompanied by a decay of the anisotropy of the bleaching signal, as seen in Fig. 8.3 (c). The time constant of the vibrational relaxation is 100±20 fs. The value of the anisotropy at different frequencies depends on the contributions of the different O–H vibrations of the proton hydration structure to the absorption at that particular frequency. At a frequency of 2900 cm^{-1}, the signal is dominated by the O–H vibration that was originally excited, thus yielding a relatively high final anisotropy value of 0.14.

The fact that the local heating effect causes a blue-shift of all O–H vibrations within the proton hydration structure leads to an induced absorption signal at frequencies >3100 cm^{-1}. This induced absorption has a positive anisotropy value at all frequencies. Hence, at 3600 cm^{-1} the vibrational relaxation leads to a rise of the initially negative anisotropy value to a positive value. Interestingly, the time scale of this rise is 180±20 fs and significantly longer than that of the

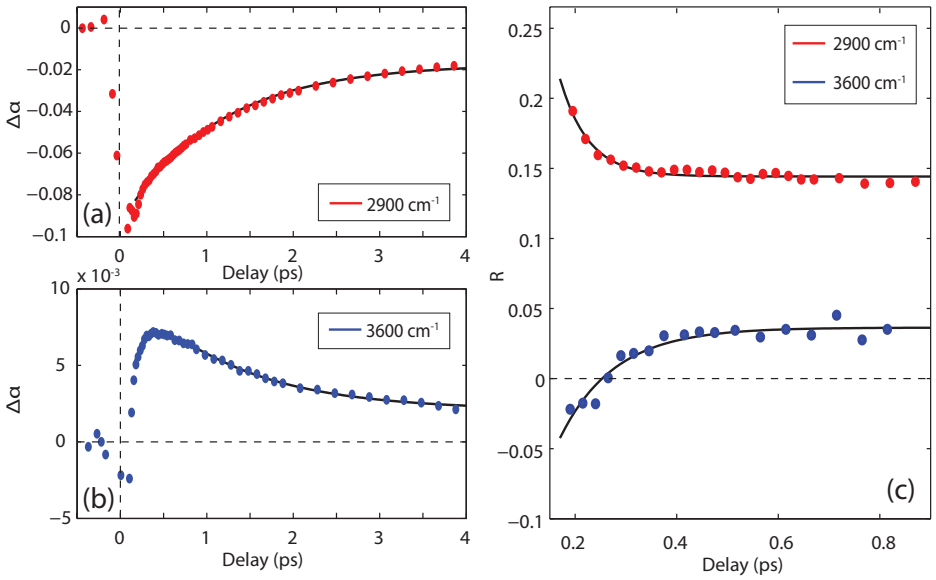

FIGURE 8.3. The isotropic absorption and anisotropy as a function of delay time measured for the [TfOH]:[H_2O] = 1:1 system. Panels a) and b) present delay traces of the isotropic absorption change at υ_{probe} = 2900 cm^{-1} (bleaching region) and υ_{probe} = 3600 cm^{-1} (induced absorption region), respectively. The data are fit with a 3-state cascade model with time constants τ_1 = 180±20 fs and τ_2 = 1.2±0.1 ps; the fit results are given by the solid lines. Panel c) presents the anisotropy dynamics at the same frequencies within the first 800 fs, showing ultrafast mono-exponential relaxation behavior with a time constant of 100±20 fs and 180±20 fs, at υ_{probe} = 2900 cm^{-1} and 3600 cm^{-1}, respectively.

decay of the anisotropy at 2900 cm^{-1}. This slower time scale is also seen in the rise of the isotropic absorption change at higher frequencies (Fig. 8.3 (b)). There are two possible explanations for this relatively slow rise of the isotropic absorption change and its anisotropy at high frequencies. The first explanation is that this rise corresponds to the equilibration of the heat over the whole proton hydration structure, thereby blue shifting O–H absorption bands that are further away from the center of positive charge, and that have higher central frequencies. The other explanation is that the hydrogen bonds of the proton hydration cluster show a further (slower) adaptation (lengthening, bending) to the ultrafast heat dissipation (resulting from the vibrational relaxation). Both explanations account for a relatively slow increase of the absorption signal at 3600 cm^{-1} and a change in the anisotropy of this signal, i.e. a change of the contributions of the different O–H modes of the hydrated proton cluster to the signal.

The subsequent slower decay of the isotropic absorption changes with a time constant of 1.2±0.1 ps can be assigned to the cooling of the hot proton hydration

cluster. In this cooling process thermal energy is transferred to the surrounding d-ACN matrix leading to a decrease of the isotropic absorption changes at all frequencies.

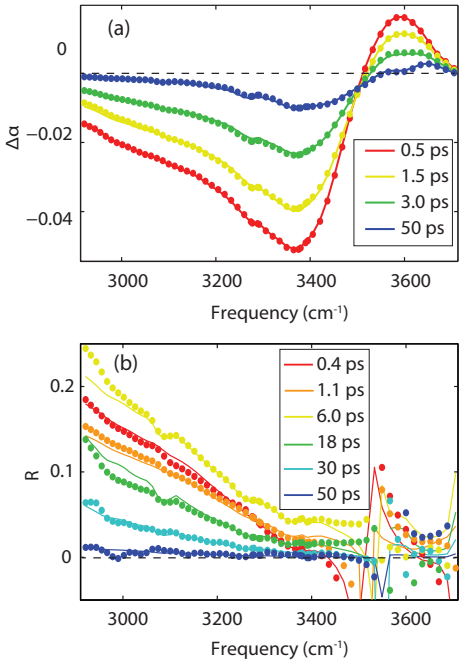

FIGURE 8.4. a) isotropic and b) anisotropic signals as a function of frequency measured for the [TfOH]:[H_2O] = 1:3 system at different delay times. The filled markers correspond to the measured data while the solid lines are the result of the kinetic model that is discussed in the text and that is illustrated in Fig. 8.7.

For the [TfOH]:[H_2O] = 1:2 and 1:3 systems, the transient spectrum shows a strong overall blue-shift occurring within a few hundred femtoseconds. At delay times shorter than the pump-probe cross-correlation time (200 fs) the maximum of the bleach is centered near the pump frequency υ_{pump} = 2800 cm^{-1}. The vibrational relaxation of the O–H stretch vibration is very rapid (<100 fs) and for [TfOH]:[H_2O] = 1:3 the spectrum has already obtained the overall shape of a local thermal spectrum already within the pump-probe cross-correlation time.

The data provide quite detailed information on the heat-relaxation dynamics following vibrational relaxation. Fig. 8.4 (a) presents transient spectra measured for the [TfOH]:[H_2O] = 1:3 system at a few specific delay times. The bleaching feature shows an ultrafast blue-shift with a time constant of a few hundred femtoseconds. Following this blue-shift, the transient spectrum shows a frequency-independent single exponential decay with a time constant of 1.4±0.2 ps. We assign this latter decay to the cooling of the heated proton-hydration clusters to the surrounding d-ACN matrix.

Fig. 8.4 (b) shows the presence of a bleaching signal at frequencies around 3450 cm^{-1} with a negative anisotropy value at early delay times. This negative anisotropy points at a competition between an induced absorption signal with a high anisotropy and a bleaching signal with a low anisotropy. The induced absorption signal contribution with high anisotropy is the local heated response that results directly after the vibrational relaxation. This induced absorption is more red-shifted than that of the thermalized proton hydration cluster, because the initial heating following vibrational relaxation mainly affects O–H vibrations close to the proton charge for which the absorption bands are centered at lower frequencies. The initial heat response thus corresponds to a large positive $\Delta\alpha_{\parallel}$ and a small positive $\Delta\alpha_{\perp}$ near 3450 cm^{-1}. Substraction of these induced absorption signals from the near-isotropic (nearly equal) negative $\Delta\alpha_{\parallel}$ and negative $\Delta\alpha_{\perp}$ (bleaching) signals of the fully thermalized response, yields a net negative $\Delta\alpha_{\parallel}$ (bleaching) signal that is smaller than the net negative $\Delta\alpha_{\perp}$ (bleaching), which implies a negative anisotropy value. This negative anisotropy value only arises at delay times where the two signals are more or less comparable in size, i.e. directly following the vibrational relaxation and before the thermalization of the cluster is complete. After ∼1 ps the contribution of the locally heated state has become negligibly small, meaning that the signal is fully determined by the thermalized response which corresponds to a bleaching signal with a small positive anisotropy value at frequency of 3450 cm^{-1} .

8.3.4 Vibrational Predissociation

Beyond the above mentioned spectral dynamics related to vibrational relaxation and heat flow, we observed two interesting features in the data for the [TfOH]:[H_2O] = 1:3 system that suggest the existence of an additional process induced by the excitation of the O–H stretch vibration of the hydrated proton cluster. The first clue comes from the rather unusual anisotropy dynamics in the bleaching region. Panel (b) in Fig. 8.4 displays the total frequency-resolved anisotropy at various pump-probe delay times. Interestingly, there is a strong and nearly linear frequency dependence in the bleaching region, i.e. ∼2800–3450 cm^{-1}, with higher anisotropy values towards lower frequencies. This feature has complicated associated dynamics, as is evident in Fig. 8.5 (b), showing delay traces of R for a number of frequencies. While the high initial anisotropy at all frequencies rapidly decays within the first picosecond, this is followed by a relatively slow re-rise of the anisotropy until a maximum is reached at ∼6 ps. Thereafter follows an even slower decay that reaches completion only at delays >50 ps.

In a system with only one species contributing to the pump-probe signal it is not possible for the anisotropy to increase over time. However, in systems in which several species contribute to the pump-probe spectrum, as is the case here, the total anisotropy $R(\omega, t)$ is a weighted sum scaled by the relative (time-varying) populations and (frequency-dependent) spectra, see Eq. (2.47). Eq. (2.47) can have peculiar effects: if a slowly decaying state A with an initially small population but high anisotropy value spectrally overlaps with a

more highly populated but rapidly decaying state B with low anisotropy, a re-rise in the total anisotropy can occur. This kind of competitive behavior has previously been observed for water in strongly heterogeneous systems, e.g. in anionic reverse micelles, where the competition between the signal of the slowly orienting but long-living surface water molecules, and the signal of the more fast decaying and reorienting molecules in the bulk of the micelles, caused a re-rise of the total anisotropy in the water O–H region [173, 174].

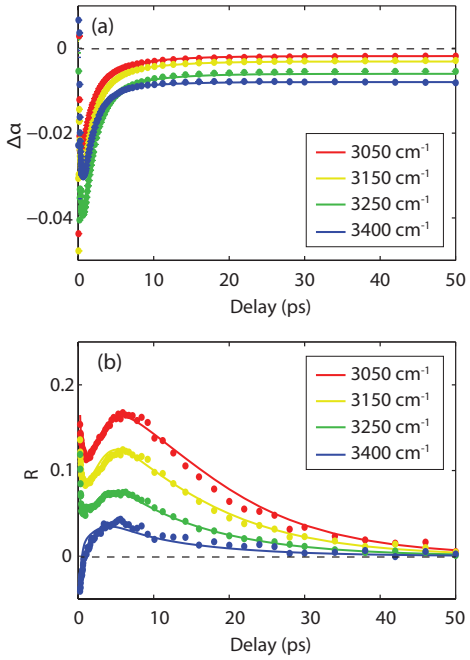

FIGURE 8.5. (a) isotropic absorption change and (b) corresponding anisotropy as a function of delay time measured for the [TfOH]:[H_2O] = 1:3 system at different frequencies. The filled markers correspond to the measured data while the solid lines are the result of the kinetic model that is discussed in the text and that is illustrated in Fig. 8.7.

The observation that the re-rise of the anisotropy closely follows the overall decay of the isotropic signal (compare Fig. 8.5 (a) and (b)), which is dominated by the (isotropic) heat flow from the cluster to the acetonitrile matrix, strongly suggests that there exists a weak, underlying bleaching state with a high and slowly decaying anisotropy. The contribution of this state to the total anisotropy becomes more important over time to the point at which the cooling is complete. An essential clue to the nature of this state is provided by another striking feature of the isotropic spectra in the induced absorption region, as given in Fig. 8.6 for the [d-ACN]:[H_2O] = 1:3 system. At early times there is just one band, initially centered at $\sim$3580 cm^{-1}, which quickly blue-shifts to

$\sim$3590 cm^{-1} during the first 500 fs. The relaxation of this feature, however, reveals an underlying doublet structure (peak maxima at $\sim$3560 and 3650 cm^{-1}), becoming apparent only after $\sim$2 ps. This structure remains at late times, and shows no tendencies of relaxing over several hundreds of picoseconds. The similarity between these transient features and the linear spectra of dilute H_2O in acetonitrile, as given by the black line in bottom of Fig. 8.5, is striking. The linear spectra was recorded at [d-ACN]:[H_2O] = 100:1, i.e. when water clustering is weak and monomeric H_2O is the dominant species [169, 170]. It thus seems that the vibrational excitation of an O–H vibration of a hydrated proton structure leads to the creation of isolated H_2O molecules in acetonitrile.

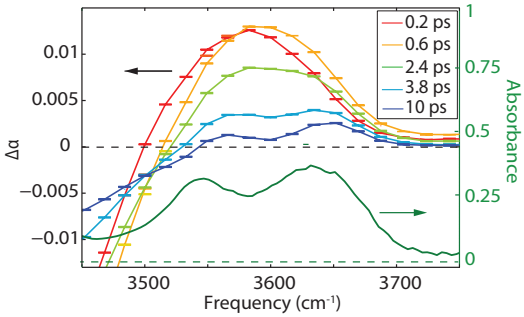

Figure 8.6. High-frequency part of the isotropic transient spectra of the [TfOH]:[H_2O] = 1:3 system. At later delay times (>3 ps) the induced absorption band splits into a doublet structure, that strongly resembles the absorption spectrum of water monomers in acetonitril. The green line at the bottom of the figure presents the linear absorption spectrum of dilute H_2O in d-ACN (for a [d-ACN]:[H_2O] ratio of 100:1).

The above observations lead us to the conclusion that part of the clusters undergo IR-induced predissociation, i.e. the energy absorbed by the proton O–H stretch vibration is for part of the vibrations not dissipated as heat but instead causes a very fast cleavage of the hydrogen bond to one of its water partners. A water molecule – most likely that being hydrogen-bonded to the excited proton O–H group – is thus ejected from the cluster and carries the excess energy as kinetic energy, which will dissipate into the acetonitrile matrix. This hypothesis accounts for all the peculiar features discussed above: 1) As the predissociation preferentially occurs in cases where the proton O–H transition dipole moment was initially parallel to the pump-polarization, the bleaching state will show a large positive anisotropy and 2) as this bleaching feature is associated with cluster dissociation rather than vibrational excitation it can live for long times. As a result its anisotropy also decays slowly, which is indeed what the data show. The final decay of the anisotropy as seen in Fig. 8.5 (b), with a time constant of 12$\pm$0.5 ps, reflects the anisotropy dynamics of the residual cluster that results from the predissociation. 3) The spectral dependence of the anisotropy re-rise can be readily understood by noting that the maximum of the bleach from the

dissociated clusters is probably close to 2800 cm^{-1} while the maximum of the heated state is close to 3400 cm^{-1}, the high-anisotropy contribution from the dissociated clusters is thus stronger to the red, as seen in the data in Fig. 8.5 (b). And finally, 4) the creation of water fragments, ejected into the acetonitrile matrix, is directly observable in the high-frequency induced absorption features shown in Fig. 8.6.

8.3.5 KINETIC MODEL

Based on the reasoning above we have devised a kinetic model to fit the complete isotropic signals and anisotropy for the [TfOH]:[H_2O] = 1:3 data set. The kinetic model describes the population transfer between states with time-independent associated spectra and time-dependent (but frequency-independent) anisotropies. The model is presented in Fig. 8.7. Panel (a) outlines the structure of the kinetic model while (b) gives the respective spectra associated with each of the states obtained from the fit. For each delay point the model produces values of $\Delta\alpha_{\parallel}(\omega, t)$ and $\Delta\alpha_{\perp}(\omega, t)$ from which a total residual sum of squared errors is calculated. By singular value decomposition (SVD) and least square fitting we obtain the population relaxation times, the state spectra and the anisotropy parameters that provide the best fit to the measured data. The time- and frequency-dependent results of the model are shown together with the experimental data in Fig. 8.4 and Fig. 8.5 as solid lines. As is immediately clear, the model captures all essential features of the data, both in the isotropic and anisotropic components.

As argued above there are two types of relaxation pathways available in which the energy of the vibrational excitation can dissipate; heating of the aqueous cluster, with subsequent cooling to the surroundings, or fragmentation of the cluster. The former process is governed by molecular-scale heat transport and generally results in complex non-exponential time-dependent dynamics [149]. The state S_1 represents the initial excitation of the O–H stretch vibration. This state has largely relaxed within the pump-probe cross-correlation time and thus does not contribute to the here considered data. As a result, a simpler approximation of using only two states S_2 and S_3 (see Fig. 8.7), the former describing a locally hot (red-shifted) state and the latter one where the heat has delocalized over the aqueous cluster, well describes the present data. The state S_3 is, as expected, found to be isotropic ($R = 0$). This is due to the random orientation of the hot O–H groups over the aqueous cluster. S_2 however has a non-zero anisotropy due to the highly local nature of the heating directly following the vibrational relaxation. As shown in Fig. 8.6 (a), both S_2 and S_3 are initially populated (approximating the fast part of the non-exponential heat transport), while the remaining part of S_2 mono-exponentially relaxes to S_3. From the fit we find a relaxation time constant of $\tau_{2,3} = 320\pm20$ fs. At frequencies near 3450 cm^{-1} the S_2 spectrum constitutes an induced absorption signal with a high anisotropy while the S_3 spectrum represents a bleaching with a low anisotropy. As discussed in the previous section, the competition between these spectra explains the negative sign of the anisotropy of the net bleaching

signal at delay times before the thermalization. i.e. before the relaxation to S_3 is complete. The relaxation of S_3 to S_5, representing the cooling of the hot cluster to the d-ACN matrix, is significantly slower, $\tau_{3,5} = 1.4 \pm 0.1$ ps, and causes the large relaxation of the overall signal at later delay times.

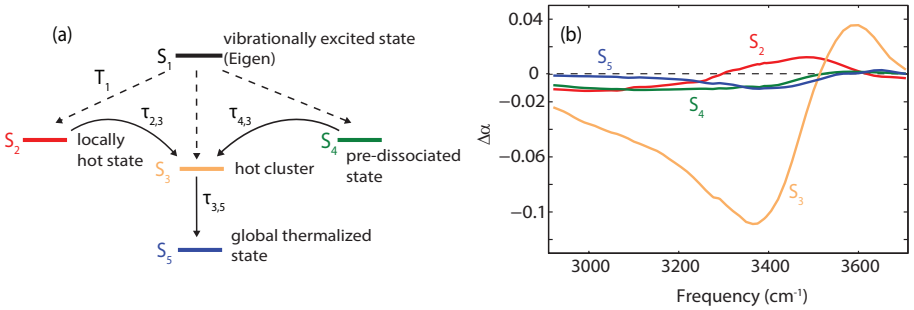

FIGURE 8.7. Panel a) schematically illustrates the kinetic model used to describe the dynamics of the [TfOH]:[H_2O] = 1:3 system upon excitation with $\upsilon_{pump} = 2800$ cm^{-1}. The transient spectra that correspond to the different states of the model are presented in panel b). The fit of the model to the experimental data is represented by the solid lines in Fig. 8.4 and Fig. 8.5.

The competing relaxation mechanism with heat-dissipation from S_1 is IR-induced predissociation of the cluster, most likely causing the ejection of a H_2O monomer into the surrounding d-ACN. The predissociation results in the population of state S_4. The corresponding transient spectrum shows a broad bleach in the proton absorption region (see Fig. 8.7) and a weak induced absorption feature in the blue wing pertaining to the IR-induced monomeric water. In fitting the data it has become apparent that while most of the S_4 population (∼60%) stays constant during the measured time window (100 ps), a smaller fraction (∼40%) relaxes to the S_3 state with a time-constant of $\tau_{4,3} = 5.7 \pm 0.2$ ps. A probable interpretation of this process is that some of the ejected water molecules are re-associating with the parent cluster, potentially after elastic collisions within the first molecular layer(s) of the acetonitrile matrix. A similar behavior was observed for pre-dissociating and partly re-associating ethanol clusters in CCl_4 upon IR-excitation of the ethanol O–H stretch vibration [175, 176].

Despite the complex spectral dynamics described by our model the anisotropy relaxation dynamics of S_2 and S_4 are well constrained, given that S_3 and S_5 are isotropic (R=0). This is because both S_2 and S_4 show high initial anisotropy values (∼0.4), but dramatically different population dynamics. As discussed above, the contribution of S_4 to the total anisotropy in the bleaching region is initially negligible due to the small fraction of S_1 (20%) decaying to this state. Instead, the rapid anisotropy dynamics within the first picosecond is almost exclusively due to the S_2 state and governed by the short lifetime of the state. The anisotropy behavior of S_4 is however more

complex, showing clear non-exponential behavior that can be modeled with a bi-exponential decay function with time constants of 2.3±0.1 ps and 12±0.5 ps. Several origins of such a behavior can be thought of. The simplest hypothesis is that the short time scale is related to a structural relaxation of the residual cluster upon the ejection of the water fragment leading to a partial decay of the anisotropy, while the long time constant reflects the rotation of the whole residual cluster leading to a complete decay of the anisotropy.

8.3.6 DISCUSSION

It is of interest to compare the vibrational relaxation dynamics of the aqueous proton in clusters inside acetonitrile with that of other systems. In previous studies of the Nafion membrane a vibrational-excitation-induced change of the proton-hydration structure was observed that was found to involve the transfer of the proton charge [135, 172]. The relatively long proton transfer time, τ_{PT} = 170±20 fs, allowed the real-time observation of the IR-activated interconversion from Eigen to Zundel-like proton hydration structures. An essential condition for this to be possible is a relatively long vibrational relaxation time compared to the proton transfer time; in the dry Nafion membrane the T_1 of proton O–H vibration was found to be 350±30 fs, i.e. about two times of τ_{PT} [135]. In bulk liquid water, on the other hand, the proton vibrational lifetime is significantly shorter (T_1 = 110±20 fs) and no IR-induced proton transfer is observed [21]. The reason for the large T_1 of the proton O–H stretch vibration in the dry Nafion membrane is most likely the association of the H_3O^+ with the sulfonate-terminated side-chains (forming the counter ion of the proton in Nafion) and the relatively poor coordination to other water molecules in the Nafion nano-channels [112, 114]. The nano-confinement thus causes a strong reduction of the intermolecular couplings required for efficient relaxation of the vibrational excitation. The Nafion and bulk water systems can thus be thought of as limiting cases; an aqueous proton in bulk water is completely non-confined whereas the proton in a dry Nafion channel is strongly confined in two of the three spatial dimensions, strongly affecting the available pathways for vibrational relaxation and thus the efficiency for IR-induced proton transfer. Apparently, the H_2O/TfOH/d-ACN systems studied here are in this respect more similar to the bulk water case as we cannot clearly distinguish any IR-induced proton transfer process. Though the existence of such a process is not unexpected, and some indications of the occurrence of such a process were found for the [TfOH]:[H_2O] = 1:1 system (i.e. the initial negative anisotropy value of the induced absorption at 3600 cm^{-1} of Fig. 8.4 (c)), the short T_1 (< 100 fs) of the proton O–H stretch vibration in the H_2O/TfOH/d-ACN systems makes it an insignificant channel. Finally, it is worth reflecting on the surprisingly high efficiency for predissociation of the aqueous clusters in acetonitrile upon excitation of the proton O–H stretch vibration. As a comparison it is interesting to note that Cringus et al. observed no signs of fragmentation of pure water clusters in acetonitrile upon selective excitation of the O–H stretch vibration of hydrogen bonded water molecules [170]. This is somewhat surprising given that

the $H_2O\cdots H_2O$ hydrogen bonds could be expected to be weaker than those of $H_3O^+\cdots H_2O$, thus more easily disrupted. Furthermore, the vibrational quantum energy required to excite the hydrogen bonded water molecule (3400 cm^{-1}) is larger than that of the proton (2800 cm^{-1}), thus providing more excess energy for the fragmentation of the cluster. One possible explanation is the highly heterogeneous character of the proton hydration structures in the aqueous clusters. As mentioned earlier, the aqueous proton tends to strongly associate with the triflate counterion [112]. In configurations where this association becomes exceptionally strong there will be a significant charge redistribution over the H_3O^+ ion towards the triflate ion, thus weakening the remaining $H_3O^+\cdots H_2O$ hydrogen bonds. Such an effect most likely contributes to the broad blue wing of the linear spectrum that is already observed at moderate hydration levels; see Fig. 8.1. It is thus likely that the vibrational predissociation preferentially occurs in clusters with such weakened $H_3O^+\cdots H_2O$ hydrogen bonds, lacking a counterpart in the case of pure water clusters in acetonitrile.

8.4 Conclusions

We studied the vibrational relaxation and thermal relaxation dynamics of hydrated proton clusters in acetonitrile at different hydration levels following the ultrafast excitation of one of the O–H stretch vibrations of the hydrated proton. We found that the O–H stretch vibration relaxes very rapidly with a time constant <100 fs. We observed that there are two relaxation pathways; for most excited vibrations the vibrational energy dissipated in the relaxation is taken up as heat by the aqueous cluster. Subsequently, the hot cluster cools by transferring its thermal energy to the acetonitrile surroundings. For a small fraction of the clusters the excitation results in predissociation of one of the hydrogen bonds of the hydrated proton cluster. This predissociation results in the ejection of water monomer fragments, of which a minority fraction (∼40%) recombines with the parent cluster. As a result, a long-living anisotropy is observed in the proton O–H absorption region; the bi-exponential decay of which can be assigned to a structural re-organization and rotation of the residual predissociated cluster.

9

Isotope Effect of Hydrophobic Anions Hydration Shell

We study the properties of water molecules at the surface of salt solutions containing hydrophobic anions like triflate ($CF_3SO_3^-$), ethanesulfonate ($C_2H_5SO_3^-$), and butanesulfonate ($C_4H_9SO_3^-$) using vibrational surface sum-frequency generation (VSFG). The VSFG spectra reveal a surprisingly strong isotope effect in the intra- and intermolecular mixing of the water molecules contained in the hydration shells of the hydrophobic anions. The O–H stretch vibrations of H_2O molecules in the hydration shell are strongly mixed whereas the O–D stretch vibrations of hydrating D_2O molecules are decoupled. This isotope effect is not observed for other ions like perchlorate (ClO_4^-), and can be explained from the enhanced tetrahedral structure organization of the hydration shells of the hydrophobic ions.

9.1 Introduction

The addition of inorganic salts leads to an increase of the surface tension of water, which implies that the ions avoid the surface. However, this notion only concerns the average concentration of cations and anions, it does not imply that the concentrations of cations and anions would show a gradual decrease towards the interface. Molecular dynamics simulations showed that the concentrations of halogenic anions show large irregularities close to the interface [177, 178]. According to these simulations, weakly hydrated anions like Br^- and I^- show an excess concentration at the water-air interface, whereas strongly interacting ions like F^- ion are excluded from this interface. These predictions were confirmed in several experiments, including studies using surface second harmonic generation (SHG), vibrational surface sum-frequency generation (VSFG) spectroscopy, soft X-ray photoelectron spectroscopy, and even atmospheric chemical reactions [179–184].

The technique of VSFG has also been used to study the surface propensity of more complex inorganic ions like ammonium (NH_4^+), nitrate(NO_3^-), sulfate (SO_4^-), thiocyanate (SCN^-) and perchlorate ClO_4^- [185–187]. In all these studies the surface propensity was found to depend strongly on the strength of the interaction between the ion and water. Ions that show a weak interaction

with water like perchlorate have the highest surface propensity. The surface propensity of inorganic ions thus closely follows the Hofmeister series.

The surface propensity of ions can be strongly enhanced by introducing hydrophobic groups to the ions [188]. Ions containing large hydrophobic groups, like stearate and palmitate, have such a high surface propensity that they lower the surface tension of liquid water, meaning that these ions are surfactants. In this chapter, we study the vibrational response of the water molecules contained in the hydration shells of the hydrophobic anions triflate ($CF_3SO_3^-$), ethanesulfonate ($C_2H_5SO_3^-$) and butanesulfonate ($C_4H_9SO_3^-$) using conventional vibrational sum frequency generation (VSFG) spectroscopy and phase sensitive vibrational sum frequency generation (PS-VSFG) spectroscopy. The measurements reveal a surprisingly strong isotope effect in the intra- and intermolecular interaction of the hydroxyl stretch vibrations of the water molecules in the hydrations shell of these ions.

9.2 Experiment

We study the vibrational response of the hydration shells of ions at water-air interfaces with vibrational sum-frequency generation (VSFG) spectroscopy, as described in Section 3.3. Besides, we performed also phase-sensitive SFG experiments.

VSFG is only capable of measuring the squared amplitude of the complex second-order nonlinear susceptibility $\chi^{(2)}(\omega_3 = \omega_1 + \omega_2)$. Information on the phase and sign of $\chi^{(2)}$ can be obtained by interfering the sum-frequency light coming from the sample with sum-frequency light coming from a local oscillator. We perform such a phase-sensitive VSFG (PS-VSFG) experiment by sending the infrared and 800 nm beams first on a gold mirror to generate broadband light at the sum frequency (local oscillator). Subsequently, the three beams (infrared, 800 nm and sum-frequency light) are sent together onto the salt solution to generate the sample sum-frequency light. The sum-frequency light beam that is generated at the gold mirror is delayed by $\Delta\tau$ by sending this beam through a tilted fused silica plate. The sum-frequency light generated at the gold mirror and the sum-frequency light generated at the sample co-propagate to the spectrograph and are detected by the CCD camera. The detected intensity is given by:

$$\begin{aligned} I_{\mathrm{PS-VSFG}}(\omega_3) \propto & |E_{sample}(\omega_3)|^2 + |E_{LO}(\omega_3)|^2 \\ & + E^*_{sample}(\omega_3) E_{LO}(\omega_3) e^{i\omega_3 \Delta\tau} \\ & + E_{sample}(\omega_3) E^*_{LO}(\omega_3) e^{-i\omega_3 \Delta\tau} \end{aligned} \tag{9.1}$$

The cross-term $E_{sample}E^*_{LO}e^{-i\omega_3\Delta\tau}$ contains the electric field of the sum-frequency light originating from the sample and is directly proportional to the complex $\chi^{(2)}$.

The studied salts sodium triflate, sodium ethanesulfonate, sodium butanesulfonate and sodium perchlorate are all purchased from Sigma-Aldrich and

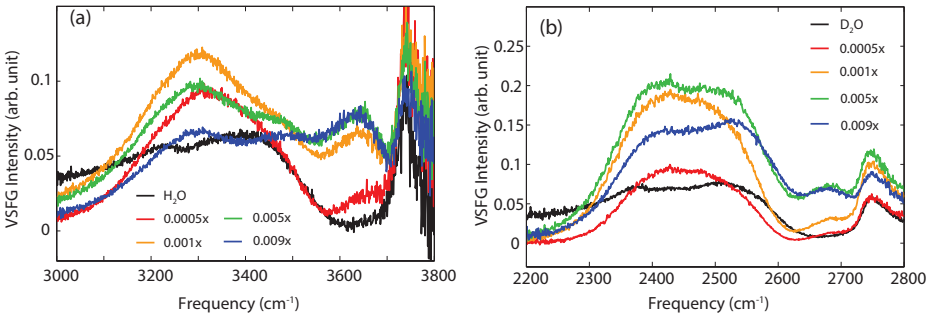

Figure 9.1. Vibrational sum frequency generation (VSFG) spectra of solutions of sodium triflate ($NaCF_3SO_3$) at different molar fractions x. (a) in H_2O and (b) in D_2O

are used without further purification. The salts are dissolved in H_2O and D_2O in a series of concentrations that are indicated with molar fractions x =[salt]/([salt]+[water]).

9.3 Results and Discussion

Fig. 9.1 shows VSFG spectra of sodium triflate solutions at different molar fractions. The spectrum of pure H_2O shows a broad double band structure with maxima at 3200 and 3400 cm^{-1}, and an additional peak at 3750 cm^{-1}. The double band has been assigned to O–H stretch vibrations forming hydrogen bonds to other water molecules. The structure of this band has been explained from the near-resonant intra- and intermolecular coupling of the O–H stretch vibrations, and the coupling of the O–H stretch vibrations with the overtone of the bending mode [189]. The band at 3750 cm^{-1} has been assigned to the stretch vibrations of non-hydrogen-bonded O–H groups that are sticking out of the surface. The VSFG spectrum of pure D_2O has a very similar shape. The hydrogen-bonded O–D stretch vibrations give rise to a broad-band feature with maxima at 2360 and 2500 cm^{-1} and the dangling O–D groups give rise to the narrow band at 2730 cm^{-1}.

The addition of sodium triflate leads to an additional band in the VSFG spectrum at 3660 cm^{-1}/2670 cm^{-1} for solutions in H_2O/D_2O. The amplitude of this band increases with increasing mole fraction of sodium triflate. We assign this band to a hydroxyl group forming a hydrogen bond to the sulfonate group of the $CF_3SO_3^-$ anion. This hydrogen bond is weak, which explains the relatively high frequency of the hydroxyl stretch vibration. The additional band at 3660 cm^{-1}/2670 cm^{-1} is already observed at mole fractions of $x = 0.0002$, corresponding to a bulk concentration of 10 mM, which implies that the triflate anion shows a high surface propensity, which is a direct consequence of its hydrophobic nature. The addition of sodium triflate also changes the shape

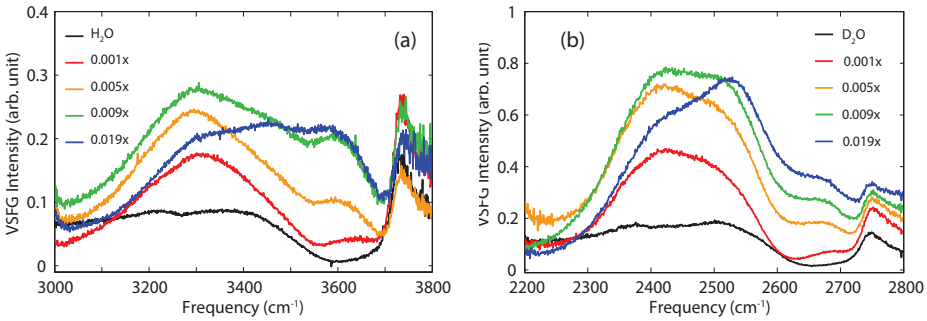

FIGURE 9.2. Vibrational sum frequency generation (VSFG) spectra of solutions of sodium butanesulfonate ($NaC_4H_9SO_3$) at different molar fractions x. (a) for solutions in H_2O and (b) in D_2O

and amplitude of the double band structure associated with the O–H/O–D groups forming hydrogen bonds to H_2O/D_2O molecules. Interestingly, these changes strongly depend on whether the salt is dissolved in H_2O or D_2O. In the case of H_2O the addition of sodium triflate leads to a blue shift of the double band and little change in amplitude, whereas for D_2O the addition of sodium triflate hardly changes the frequency position of the double band but leads to a significant increase of its amplitude.

In Fig. 9.2 we present VSFG spectra of solutions of sodium butanesulfonate ($NaC_4H_9SO_3$) in H_2O and D_2O. The butanesulfonate anion has the same sulfonate anionic group as triflate and only differs from the triflate anion in the character of the hydrophobic group. The addition of sodium butanesulfonate leads to very similar changes of the VSFG spectrum as the addition of sodium triflate (Fig. 9.1). As in the case of sodium triflate, these changes occur already at low molar fractions of sodium butylsulfonate, which shows that butanesulfonate anions have a high surface propensity. The spectral changes in the frequency region of the O–H/O–D groups forming hydrogen bonds to H_2O/D_2O show again a strong isotope effect. Similar effects are observed for solutions of sodium ethanesulfonate ($NaC_2H_5SO_3$) (see Fig. 9.3).

In Fig. 9.3 we show vibrational sum-frequency generation (VSFG) spectra of solutions of sodium ethanesulfonate ($NaC_4H_9SO_3$) at molar fractions ranging from x=0 to x=0.019. The addition of sodium ethanesulfonate leads to an additional band in the VSFG spectrum at 3620 cm^{-1}/2670 cm^{-1} for solutions in H_2O/D_2O. The amplitude of this band increases with increasing mole fraction of sodium ethanesulfonate. This band is assigned to OH/OD groups of H_2O/D_2O molecules that donate a hydrogen bond to the sulfonate group of the ethanesulfonate ion. The two bands at lower frequencies are assigned to OH/OD groups of H_2O/D_2O molecules that donate hydrogen bonds to H_2O/D_2O molecules. The concentration dependence of the VSFG spectra of sodium ethanesulfonate ($NaC_2H_5SO_3$) in H_2O and D_2O is very similar to that of solutions of sodium

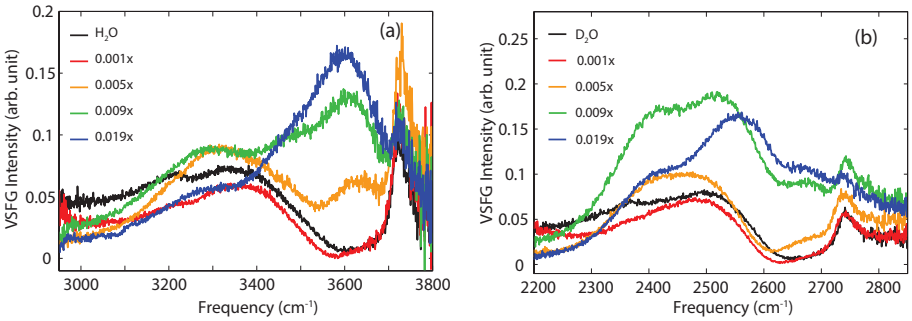

Figure 9.3. Vibrational sum frequency generation (VSFG) spectra of solutions of sodium ethanesulfonate ($NaC_2H_5SO_3$) at different molar fractions x, ranging from $x = 0$ to $x = 19 \times 10^{-3}$. a) for solutions in H_2O; b) for solutions in D_2O

butanesulfonate and sodium triflate, and shows a strong isotope effect. For solutions in H_2O the addition of ethanesulfonate results in a blue shift of the two low-frequency peaks and little change in amplitude, whereas for solutions in D_2O the addition of ethanesulfonate mainly results in an increase in amplitude of the two bands. The physical origin of this isotope effect are explained in details in this chapter.

We performed PS-VSFG experiments to study the effect of hydrophobic anions on the O–H and O–D stretch vibrations in more detail. In Fig. 9.4 we present the measured $\mathrm{Im}(\chi^{(2)})$ as a function of frequency for sodium triflate solutions of different concentration in H_2O and D_2O. For comparison we also present $\mathrm{Im}(\chi^{(2)})$ of the water-air interfaces of pure H_2O and D_2O. The sign of the imaginary part of the second-order susceptibility $\mathrm{Im}(\chi^{(2)})$ directly reflects the orientation of the transition dipole moments of the interfacial O–D/O–H vibrations [72, 190–192]. A positive imaginary $\chi^{(2)}$ corresponds to O–H/O–D groups pointing towards air. For pure H_2O/D_2O $\mathrm{Im}(\chi^{(2)})$ has a small positive value at hydroxyl stretch vibrational frequencies <3100/2300 cm^{-1}. These hydroxyl stretch vibrations correspond to strongly hydrogen-bonded O–H/O–D groups. The main part of $\mathrm{Im}(\chi^{(2)})$ between 3100 and 3600 cm^{-1} for H_2O and between 2300 and 2650 cm^{-1} for D_2O, has a negative sign, indicative of a net orientation towards the water phase. Finally, $\mathrm{Im}(\chi^{(2)})$ of the dangling O–H/O–D groups is positive, in line with the fact that these groups are sticking out of the H_2O/D_2O surface.

The addition of sodium triflate leads to a large change in the amplitude and sign of $\mathrm{Im}(\chi^{(2)})$. The dominant negative part of pure H_2O/D_2O completely disappears and gives way to a strong positive $\mathrm{Im}(\chi^{(2)})$. This change in sign of $\mathrm{Im}(\chi^{(2)})$ reflects a change in the net orientation of the hydroxyl groups. This change in net orientation can be explained from the difference in surface propensity between the negative triflate anions and the positive sodium cations. The hydrophobic triflate anions have a strong tendency to accumulate at the

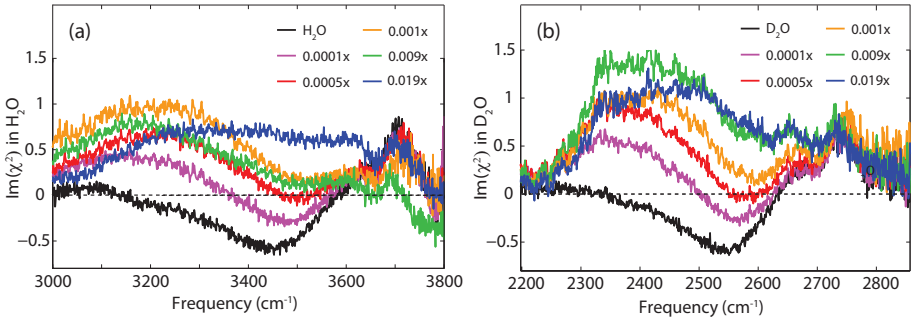

FIGURE 9.4. Imaginary part of the second-order susceptibility $\chi^{(2)}$ of sodium triflate ($NaCF_3SO_3$) solutions at different molar fractions x. (a) in H_2O and (b) in D_2O. The imaginary $\chi^{(2)}$ is determined with PS-VSFG spectroscopy.

water-air interface, whereas the sodium cations remain further away from this interface. This separation of positive and negative charge near the water-air interface yields a strong local electric field that orients the O–H/O–D groups towards the interface, thus resulting in a positive $\mathrm{Im}(\chi^{(2)})$. The mole fraction of sodium triflate at which $\mathrm{Im}(\chi^{(2)})$ becomes positive at all frequencies is approximately $x = 0.0005$ (≈25 mM), both for H_2O and for D_2O. This similarity in concentration indicates that the triflate anions show a similar surface propensity in H_2O and D_2O. Hence, there appears to be no isotope effect in the surface propensity of triflate. Nevertheless, at higher triflate concentrations the frequency position and amplitude of $\mathrm{Im}(\chi^{(2)})$ strongly differ for H_2O and D_2O. For H_2O $\mathrm{Im}(\chi^{(2)})$ is much more strongly blue shifted than for D_2O, whereas for D_2O the amplitude of the positive $\mathrm{Im}(\chi^{(2)})$ is more enhanced than for H_2O. These observations agree with the results of the intensity VSFG spectra of Fig. 9.1. It is clearly show in Figs. 9.1, 9.2 and 9.4 that the addition of triflate and butanesulfonate has a quite different effect on the VSFG spectrum for solutions in H_2O than for solutions in D_2O.

This strong isotope effect can be explained from the difference in strength of the intramolecular and intermolecular (Förster) dipole-dipole interactions of the hydroxyl vibrations of H_2O and D_2O. For pure H_2O and pure D_2O the near-resonant intramolecular and intermolecular interactions lead to a strong mixing of the local hydroxyl vibrations and a delocalization of the hydroxyl stretch vibrations. As a result, the first excited state of the O–H/O–D vibration is a delocalized exciton state that comprises several local O–H/O–D excitations [92, 193, 194].

For solutions of triflate, ethanesulfonate and butanesulfonate in H_2O, the intra- and intermolecular couplings lead to the formation of delocalized vibratonial exciton states that include both O–H groups forming hydrogen bonds to H_2O molecules and O–H groups that form weak hydrogen bonds to the sul-

fonate group. These exciton states will be blue shifted in comparison to the exciton states of pure H_2O. The absence of such a blue shift for solutions of these hydrophobic anions in D_2O indicates that the O–D stretch vibrations are far less mixed than the O–H stretch vibrations.

The amount of mixing of O–H/O–D vibrations depends both on the interaction energy and the difference in site energy. Substantial mixing occurs when the interaction energy exceeds the differences in site energies. Going from H_2O to D_2O the intra- and intermolecular interaction energies and the differences in site energies will decrease. The intramolecular and intermolecular interaction energies are both proportional to the product of the transition dipole moments of the coupled hydroxyl stretch vibrations. The transition dipole moment of the O–H stretch vibration is $\sim\sqrt{2}$ larger than that of the O–D stretch vibration, and thus the interaction energy will be $\sim$2 times larger for H_2O than for D_2O. The smaller interaction energy of D_2O corresponds to a lower rate of near-resonant energy transfer between local O–D stretch vibrations. Indeed this rate was measured to be >2 times smaller for D_2O than for H_2O [92, 193, 194]. Going from H_2O to D_2O the differences in site energies, i.e. the differences in local hydroxyl vibrational frequencies, are expected to decrease by a factor $\sim\sqrt{2}$. The isotope effect of the site energy differences is thus smaller than the isotope effect of the intra- and intermolecular interactions. This difference in isotope effect explains why the water-bound and anion-bound hydroxyl vibrations are well mixed in solutions of triflate, ethanesulfonate and butanesulfonate in H_2O and poorly mixed in solutions of these anions in D_2O.

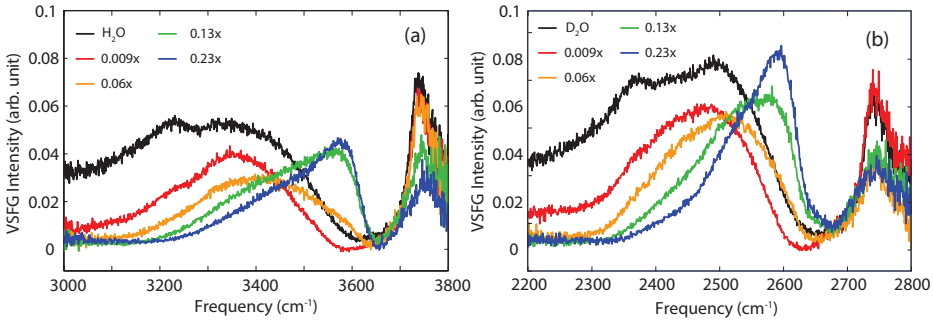

Figure 9.5. Vibrational sum frequency generation (VSFG) spectra of solutions of sodium perchlorate ($NaClO_4$) at different molar fractions x.(a) in H_2O and (b) in D_2O.

From the above it is clear that the amount of mixing of water-bound and anion-bound hydroxyl vibrations is a subtle effect that depends on the distribution of the local site energies of the hydroxyl vibrations. To study this effect in more detail we measured VSFG spectra of solutions of other salts in H_2O and D_2O. In Fig. 9.5 we show VSFG spectra of solutions of sodium perchlorate in H_2O and D_2O. The addition of sodium perchlorate is also seen to lead to

an additional band in the spectrum at a relatively high frequency, as was the case for the triflate (Fig. 9.1), butanesulfonate (Fig. 9.2) and ethanesulfonate (Fig. 9.3) solutions. Following the work of the group of Allen we assign this band at 3600 cm^{-1}/2620 cm^{-1} to O–H/O–D groups forming hydrogen bonds to the perchlorate (ClO_4^-) anions [185]. These hydrogen bonds are weak and probably directed towards the middle of the O-O ridges of the tetrahedral perchlorate anion [195]. The changes of the VSFG spectrum induced by perchlorate are quite similar for H_2O and D_2O. For both solvents the VSFG spectrum of the broad double band shows a blue shift and a decrease in amplitude. Hence, the isotope effect on the shape of the VSFG spectra of perchlorate solutions is small, in strong contrast to the VSFG spectra of solutions of triflate (Fig. 9.1), ethanesulfonate (Fig. 9.3) , and butanesulfonate (Fig. 9.2).

The results of Fig. 9.5b show that for solutions of sodium perchlorate in D_2O the stretch vibrations of O–D groups donating hydrogen bond to D_2O are quite well mixed with the stretch vibrations of O–D groups donating hydrogen to ClO_4^-. This finding implies that for ClO_4^- the intra- and intermolecular interaction energy is sufficiently large to overcome the differences in local frequencies of the O–D stretch vibrations. As the transition dipole moments are not very different, it thus appears that for ClO_4^- the stretch vibration of the O–D group donating a hydrogen bond to the anion is closer in frequency to the stretch vibrations of other nearby O–D groups than for triflate, ethanesulfonate and butanesulfonate. This can be due to two effects. The first effect is that the frequency of O–D group donating a hydrogen bond to the anion is somewhat less blue shifted for perchlorate than for the studied hydrophobic anions. A second effect is that the stretch frequencies of other nearby O–D groups that form hydrogen bonds to D_2O would be lower in the case of the studied hydrophobic anions than in the case of perchlorate. It has been found that water molecules hydrating hydrophobic groups have an enhanced tetrahedral hydrogen-bonded structure which implies that their vibrational spectrum will be redshifted and narrower compared to that of water molecules in bulk liquid water [196]. Hence the O–H/O–D groups that donate a hydrogen bond to an H_2O/D_2O molecule in the hydrophobic hydration shell of triflate, ethanesulfonate and butanesulfonate can have frequencies that are quite strongly redshifted with respect to the O–H/O–D groups that donate a hydrogen bond to the sulfonate group of these hydrophobic anions. In the case of D_2O, this large frequency difference in combination with the weaker interaction energy, precludes the mixing of the O–D stretch vibrations in the hydration shell of the hydrophobic anion. For H_2O, the interaction energy still suffices to mix the O–H stretch vibrations of the H_2O molecules hydrating the hydrophobic part with the O–H stretch vibrations of the hydroxyl groups donating a weak hydrogen bond to the sulfonate group.

We also measured bulk IR absorption spectra of solutions of sodium triflate and sodium perchlorate in H_2O and D_2O to investigate whether the differences in vibrational response are specific for the water surface. The results are shown in Fig. 9.6. It is seen that the IR spectra show very similar trends as the VSFG spectra. The addition of sodium triflate leads to a much stronger blue shift

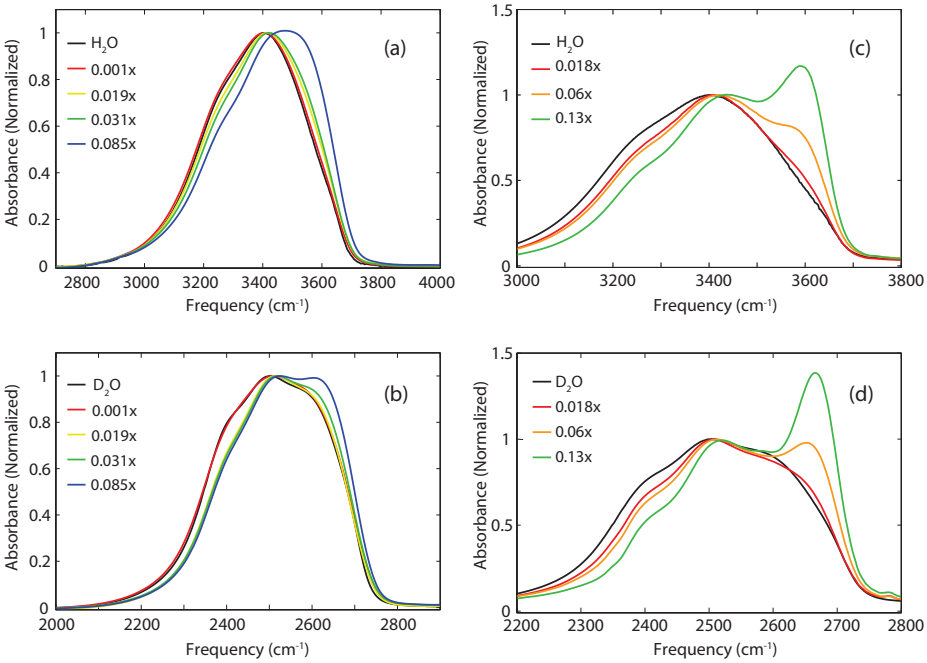

Figure 9.6. Infrared absorption spectra of solutions of sodium triflate ($NaCF_3SO_3$) in H_2O (a), in D_2O (b) and sodium perchlorate ($NaClO_4$) in H_2O (c), in D_2O (d).

of the main hydrogen-bonded band for solutions in H_2O than for solutions in D_2O. This shows again that the stretch vibrations of the anion-bound and water-bound hydroxyl groups are much more strongly mixed for solutions in H_2O than for solutions in D_2O. The poor mixing of anion-bound and D_2O-bound O–D vibration in the hydration shells of triflate and butanesulfonate thus persists in the bulk. For the perchlorate solutions the blue shift of the main band of the IR spectrum is similar for H_2O and D_2O, showing that the perchlorate-bound and water-bound hydroxyl stretch vibrations show a similar strong mixing in H_2O and D_2O.

Solutions of triflate, ethanesulfonate and butanesulfonate do not only show a strong isotope effect in the frequency position of the bands but also in the amplitude. The addition of these anions to D_2O leads to a rather strong increase in amplitude of the main band of the VSFG spectrum, whereas for H_2O the amplitude of this band hardly changes. This isotope effect can also be explained from the difference in mixing of the anion- and water-bound hydroxyl vibrations for H_2O and D_2O. The addition of triflate, ethanesulfonate and butanesulfonate or butanesulfonate to H_2O and D_2O affects the amplitude in different ways. In the first place, the electric field resulting from the accumulation of anions at the surface increases the orientation of O–H/O–D groups towards the inter-

face, thus enhancing the VSFG signal. This orientation effect is clearly seen in the increase of $\mathrm{Im}(\chi^{(2)})$ shown in Fig. 9.4. Second, the accumulation of the hydrophobic anions at the interface will lead to a decrease of the density of H_2O/D_2O molecules which decreases the VSFG signal. These two effects will be similar for H_2O and D_2O. For H_2O a third effect is formed by the mixing of the O–H groups forming hydrogen bonds to H_2O with O–H groups bonded to the anion. This mixing leads to the formation of new delocalized states with a large frequency spread and a weaker average hydrogen-bond strength which decreases the associated VSFG signal. This latter effect will be small for D_2O as the O–D groups forming hydrogen bonds to D_2O poorly mix with O–D groups forming hydrogen bonds to the anion. As a result, the average hydrogen bond strength and thus the cross-section of the O–D vibrations in the main VSFG band remains large. Hence, for D_2O the main band of the VSFG spectrum increases in amplitude because of the orienting electric field created by the anions at the interface, whereas for H_2O the main band hardly changes in amplitude because the orientation effect is counteracted by the deteriorating effects of mixing on the cross-section.

9.4 Conclusions

We studied the vibrational response of water molecules at the surface of solutions containing hydrophobic anions using vibrational surface sum-frequency generation (VSFG) spectroscopy. The addition of ions like triflate ($CF_3SO_3^-$), ethanesulfonate ($C_2H_5SO_3^-$), butanesulfonate ($C_4H_9SO_3^-$) is observed to lead to the rise of a high-frequency resonance at 3660/2670 cm^{-1} that is assigned to the stretch vibration of an O–H/O–D group forming a weak hydrogen bond to the anion. This additional band is already observed at a low mole fraction of $x = 0.0002$ (corresponding to a concentration of 10 mM), which shows that these ions have a very high surface propensity.

The addition of triflate, ethanesulfonate, and butanesulfonate strongly affects the frequency position and amplitude of the main band of the VSFG spectrum of H_2O/D_2O. For solutions in H_2O, the addition of these hydrophobic anions is observed to lead to a strong blue shift of the main band of the VSFG spectrum and little change in amplitude, whereas for solutions in D_2O the addition of these anions hardly changes the frequency position of the main band but leads to a strong increase in amplitude.

This strong isotope effect can be explained from the difference in intra- and intermolecular coupling of O–H and O–D vibrations in the hydration shells of the hydrophobic anions. The intra- and intermolecular coupling of water hydroxyl vibrations scales with the product of the transition dipole moments of the coupled stretch vibrations, which means that this interaction is $\sim$2 times larger in H_2O than in D_2O. As a result, O–H groups forming hydrogen bonds to H_2O show significant mixing with O–H groups forming weak hydrogen bonds to the sulfonate group of triflate, ethanesulfonate or butanesulfonate, whereas for the O–D groups in D_2O this mixing is poor. This isotope effect is not ob-

served for other ions like perchlorate, which can be explained from the enhanced tetrahedral structure of water hydrating hydrophobic groups. As a result of the enhanced structure, the stretch vibrations of the hydroxyl groups hydrating the hydrophobic part of the ion have low and well-defined vibrational frequencies, which in the case of D_2O precludes their mixing with the high-frequency stretch vibrations of the hydroxyl group hydrating the sulfonate group of the ion. For H_2O, the interaction energy still suffices to mix the O–H stretch vibrations of the H_2O molecules hydrating the hydrophobic part with the O–H stretch vibrations of the hydroxyl groups donating a weak hydrogen bond to the sulfonate group.

Bibliography

1. M. Eigen. Proton transfer, acid-base catalysis, and enzymatic hydrolysis. part I: Elementary processes. *Angew. Chem. Int. Edit.*, 3(1):1–19, 1964.

2. G. A. Voth. Computer simulation of proton solvation and transport in aqueous and biomolecular systems. *Accounts. Chem. Res.*, 39(2):143–150, 2006.

3. A. Botti, F. Bruni, M. A. Ricci, and A. K. Soper. Eigen versus Zundel complexes in HCl-water mixtures. *J. Chem. Phys.*, 125(1):014508, 2006.

4. T. J. F. Day, A. V. Soudackov, M. Čuma, U. W. Schmitt, and G. A. Voth. A second generation multistate empirical valence bond model for proton transport in aqueous systems. *J. Chem. Phys.*, 117(12):5839–5849, 2002.

5. O. Markovitch, H. Chen, S. Izvekov, F. Paesani, G. A. Voth, and N. Agmon. Special pair dance and partner selection: Elementary steps in proton transport in liquid water. *J. Phys. Chem. B*, 112(31):9456–9466, 2008.

6. M. Park, I. Shin, N. J. Singh, and K. S. Kim. Eigen and Zundel forms of small protonated water clusters : Structures and infrared spectra. *J. Phys. Chem. A*, 111(42):10692–10702, 2007.

7. Z. Xie, R. Bau, and C. A. Reed. A crystalline $H_9O_4^+$ hydronium ion salt with a weakly coordinating anion. *Inorg. Chem.*, 34(22):5403–5404, 1995.

8. C. J. T. Grotthuss. Sur la décomposition de l'eau et des corps qu'elle tient en dissolution à l'aide de l'électricité galvanique. *Annales, de Chimie*, 58:54, 1806.

9. D. Marx, M. E. Tuckerman, J. Hutter, and M. Parrinello. The nature of the hydrated excess proton in water. *Nature*, 397(6720):601–604, 1999.

10. U. W. Schmitt and G. A. Voth. Multistate empirical valence bond model for proton transport in water. *J. Phys. Chem. B*, 102(29):5547–5551, 1998.

11. U. W. Schmitt and G. A. Voth. The computer simulation of proton transport in water. *J. Chem. Phys.*, 111(20):9361–9381, 1999.

12. T. J. F. Day, U. W. Schmitt, and G. A. Voth. The mechanism of hydrated proton transport in water. *J. Am. Chem. Soc.*, 122(48):12027–12028, 2000.

13. H. Lapid, N. Agmon, M. K. Petersen, and G. A. Voth. A bond-order analysis of the mechanism for hydrated proton mobility in liquid water. *J. Chem. Phys.*, 122(1):014506, 2005.

14. Y. Wu, H. Chen, F. Wang, F. Paesani, and G. A. Voth. An improved multistate empirical valence bond model for aqueous proton solvation and transport. *J. Phys. Chem. B*, 112(2):467–482, 2008.

15. M. E. Tuckerman, A. Chandra, and D. Marx. A statistical mechanical theory of proton transport kinetics in hydrogen-bonded networks based on population correlation functions with applications to acids and bases. *J. Chem. Phys.*, 133(12):124108, 2010.

16. D. Marx, A. Chandra, and M. E. Tuckerman. Aqueous basic solutions: Hydroxide solvation, structural diffusion, and comparison to the hydrated proton. *Chem. Rev.*, 110(4):2174–2216, 2010.

17. D. Marx. Proton transfer 200 years after von Grotthuss: Insights from ab initio simulations. *Chem. Phys. Chem*, 7(9):1848–1870, 2006.

18. M. Tuckerman, K. Laasonen, M.l Sprik, and M. Parrinello. Ab initio molecular dynamics simulation of the solvation and transport of H_3O^+ and OH^- ions in water. *J. Phys. Chem.*, 99(16):5749–5752, 1995.

19. M. Tuckerman, K. Laasonen, M. Sprik, and M. Parrinello. Abinitio molecular dynamics simulation of the solvation and transport of hydronium and hydroxyl ions in water. *J. Chem. Phys.*, 103(1):150–161, 1995.

20. M. E. Tuckerman, D. Marx, M. L. Klein, and M. Parrinello. On the quantum nature of the shared proton in hydrogen bonds. *Science*, 275(5301):817–820, 1997.

21. S. Woutersen and H. J. Bakker. Ultrafast vibrational and structural dynamics of the proton in liquid water. *Phys. Rev. Lett.*, 96(13), 2006.

22. W. Amir, G. Gallot, F. Hache, S. Bratos, J.-C. Leicknam, and R. Vuilleumier. Time-resolved observation of the Eigen cation in liquid water. *J. Chem. Phys.*, 126(3):034511, 2007.

23. B. Winter, M. Faubel, I. V. Hertel, C. Pettenkofer, S. E. Bradforth, B. Jagoda-Cwiklik, L. Cwiklik, and P. Jungwirth. Electron binding energies of hydrated H_3O^+ and OH^-: Photoelectron spectroscopy of aqueous acid and base solutions combined with electronic structure calculations. *J. Am. Chem. Soc.*, 128(12):3864–3865, 2006.

24. B. Kirchner. Eigen or Zundel ion: News from calculated and experimental photoelectron spectroscopy. *Chem. Phys. Chem*, 8(1):41–43, 2007.

25. R. Shevchuk, N. Agmon, and F. Rao. Network analysis of proton transfer in liquid water. *J. Chem. Phys.*, 140(24):244502, 2014.

26. K. J. Tielrooij, R. L. A. Timmer, H. J. Bakker, and M. Bonn. Structure dynamics of the proton in liquid water probed with terahertz time-domain spectroscopy. *Phys. Rev. Lett.*, 102(19):198303, 2009.

27. M. E. Tuckerman, D. Marx, and M. Parrinello. The nature and transport mechanism of hydrated hydroxide ions in aqueous solution. *Nature*, 417(6892):925–929, 2002.

28. A. Chandra, M. E. Tuckerman, and D. Marx. Connecting solvation shell structure to proton transport kinetics in hydrogen-bonded networks via population correlation functions. *Phys. Rev. Lett.*, 99(14), 2007.

29. M. E. Tuckerman, A. Chandra, and D. Marx. Structure and dynamics of OH^-(aq). *Accounts. Chem. Res.*, 39(2):151–158, 2006.

30. E. S. Stoyanov, I. V. Stoyanova, and C. A. Reed. The structure of the hydrogen ion $H_{(aq)}{}^+$ in water. *J. Am. Chem. Soc.*, 132(5):1484–1485, 2010.

31. E.i S. Stoyanov, I. V. Stoyanova, and C. A. Reed. The unique nature of H^+ in water. *Chem. Sci.*, 2(3):462–472, 2011.

32. K.-D. Kreuer, A. Rabenau, and W. Weppner. Vehicle mechanism, a new model for the interpretation of the conductivity of fast proton conductors. *Angew. Chem. Int. Edit.*, 21(3):208–209, 1982.

33. C. Dellago, M. M. Naor, and G. Hummer. Proton transport through water-filled carbon nanotubes. *Phys. Rev. Lett.*, 90(10):105902, 2003.

34. Z. Cao, Y. Peng, T. Yan, S. Li, A. Li, and G. A. Voth. Mechanism of fast proton transport along one-dimensional water chains confined in carbon nanotubes. *J. Am. Chem. Soc.*, 132(33):11395–11397, 2010.

35. O. Vendrell, R. Gelabert, M. Moreno, and J. M. Lluch. Operation of the proton wire in green fluorescent protein. a quantum dynamics simulation. *J. Phys. Chem. B*, 112(17):5500–5511, 2008.

36. K. Schmidt-Rohr and Q. Chen. Parallel cylindrical water nanochannels in Nafion fuel-cell membranes. *Nature Materials*, 7(1):75–83, 2008.

37. J. Kim, U. W. Schmitt, J. A. Gruetzmacher, G. A. Voth, and N. E. Scherer. The vibrational spectrum of the hydrated proton: Comparison of experiment, simulation, and normal mode analysis. *J. Chem. Phys.*, 116(2):737–746, 2002.

38. J. Q. Xu, Y. Zhang, and G. A. Voth. Infrared spectrum of the hydrated proton in water. *J. Phys. Chem. Lett.*, 2(2):81–86, 2011.

39. W. Kulig and N. Agmon. A 'clusters-in-liquid' method for calculating infrared spectra identifies the proton-transfer mode in acidic aqueous solutions. *Nat Chem*, 5(1):29–35, 2013.

40. Paul A. Giguère Michael Falk. Infrared spectrum of the H_3O^+ ion in aqueous solution. *Can. J. Chem.*, 35:1195–1204, 1957.

41. N. B. Librovich, V. P. Sakun, and N. D. Sokolov. H^+ and OH^- ions in aqueous solutions vibrational spectra of hydrates. *Chem. Phys.*, 39(3):351–366, 1979.

42. L. I. Yeh, M. Okumura, J. D. Myers, J. M. Price, and Y. T. Lee. Vibrational spectroscopy of the hydrated hydronium cluster ions $H_3O^+ \cdot (H_2O)_n$ (n=1, 2, 3). *J. Chem. Phys.*, 91(12):7319–7330, 1989.

43. M. Okumura, L. I. Yeh, J. D. Myers, and Yuan T. Lee. Infrared spectra of the solvated hydronium ion: Vibrational predissociation spectroscopy of mass-selected $H_3O^+ \cdot (H_2O)_n \cdot (H_2)_m$. *J. Phys. Chem.*, 94(9):3416–3427, 1990.

44. J.-C. Jiang, Y.-S. Wang, H.-C. Chang, Sheng H. L., Y. T. Lee, G. Niedner-Schatteburg, and H.-C. Chang. Infrared spectra of $H^+(H_2O)_{(5-8)}$ clusters: Evidence for symmetric proton hydration. *J. Am. Chem. Soc.*, 122(7):1398–1410, 2000.

45. K. R. Asmis, N. L. Pivonka, G. Santambrogio, M. Brümmer, C. Kaposta, D. M. Neumark, and L. Wöste. Gas-phase infrared spectrum of the protonated water dimer. *Science*, 299(5611):1375–1377, 2003.

46. T. D. Fridgen, T. B. McMahon, L. MacAleese, J. Lemaire, and P. Maitre. Infrared spectrum of the protonated water dimer in the gas phase. *J. Phys. Chem. A*, 108(42):9008–9010, 2004.

47. E. G. Diken, J. M. Headrick, J. R. Roscioli, J. C. Bopp, M. A. Johnson, and A. B. McCoy. Fundamental excitations of the shared proton in the $H_3O_2^-$ and $H_5O_2^+$ complexes. *J. Phys. Chem. A*, 109(8):1487–1490, 2005.

48. J. M. Headrick, E. G. Diken, R. S. Walters, N. I. Hammer, R. A. Christie, J. Cui, E. M. Myshakin, M. A. Duncan, M. A. Johnson, and K. D. Jordan. Spectral signatures of hydrated proton vibrations in water clusters. *Science*, 308(5729):1765–1769, 2005.

49. G. E. Douberly, R. S. Walters, J. Cui, K. D. Jordan, and M. A. Duncan. Infrared spectroscopy of small protonated water clusters, $H^+(H_2O)_n$ (n=2-5): isomers, argon tagging, and deuteration. *J. Phys. Chem. A*, 114(13):4570–4579, 2010.

50. S. G. Olesen, T. L. Guasco, J. R. Roscioli, and M. A. Johnson. Tuning the intermolecular proton bond in the $H_5O_2^+$ 'Zundel ion' scaffold. *Chem. Phys. Lett.*, 509(4–6):89–95, 2011.

51. A. B. McCoy, T. L. Guasco, C. M. Leavitt, S. G. Olesen, and M. A. Johnson. Vibrational manifestations of strong non-condon effects in the $H_3O^+ \cdot X_3$ (X = Ar, N_2, CH_4, H_2O) complexes: A possible explanation for the intensity in the "association band" in the vibrational spectrum of water. *Phys. Chem. Chem. Phys.*, 14(20):7205–7214, 2012.

52. N. Heine, M. R. Fagiani, M. Rossi, T. Wende, G. Berden, V. Blum, and K. R. Asmis. Isomer-selective detection of hydrogen-bond vibrations in the protonated water hexamer. *J. Am. Chem. Soc.*, 135(22):8266–8273, 2013.

53. Mitsuhiko Miyazaki, Asuka Fujii, Takayuki Ebata, and Naohiko Mikami. Infrared spectroscopic evidence for protonated water clusters forming nanoscale cages. *Science*, 304(5674):1134–1137, 2004.

54. C.-K. Lin, C.-C. Wu, Y.-S. Wang, Y. T. Lee, H.-C. Chang, J.-L. Kuo, and M. L. Klein. Vibrational predissociation spectra and hydrogen-bond topologies of $H^+(H_2O)_{9-11}$. *Phys. Chem. Chem. Phys.*, 7(5):938–944, 2005.

55. H.-C. Chang, C.-C. Wu, and J.-L. Kuo. Recent advances in understanding the structures of medium-sized protonated water clusters. *Int. Rev. Phys. Chem.*, 24(3-4):553–578, 2005.

56. Kenta Mizuse, Asuka Fujii, and Naohiko Mikami. Long range influence of an excess proton on the architecture of the hydrogen bond network in large-sized water clusters. *J. Chem. Phys.*, 126(23):231101, 2007.

57. Chih-Che Wu, Chih-Kai Lin, Huan-Cheng Chang, Jyh-Chiang Jiang, Jer-Lai Kuo, and Michael L. Klein. Protonated clathrate cages enclosing neutral water molecules: $H^+(H_2O)_{21}$ and $H^+(H_2O)_{28}$. *J. Chem. Phys.*, 122(7):074315, 2005.

58. N. B. Kalish, E. Shandalov, V. Kharlanov, D. Pines, and E. Pines. Apparent stoichiometry of water in proton hydration and proton dehydration reactions in CH_3CN/H_2O solutions. *J. Phys. Chem. A*, 115(16):4063–4075, 2011.

59. V. Buch, A. Dubrovskiy, F. Mohamed, M. Parrinello, J. Sadlej, A. D. Hammerich, and J. P. Devlin. HCl hydrates as model systems for protonated water. *J. Phys. Chem. A*, 112(11):2144–2161, 2008.

60. H. Haken and Wolf H. C. *Molecular Physics and Elements of Quantum Chemistry.* Springer, 1995.

61. R. W. Boyd. *Nonlinear Optics.* Academic Press, 2003.

62. Y. R. Shen. *The Principles of Nonlinear Optics.* Wiley-Interscience, 2002.

63. S. Mukamel. *Principles of Nonlinear Optical Spectroscopy.* Oxford University Express, 1995.

64. T. F. Heinz. *Second-Order Nonlinear Optical Effects at Surfaces and Interfaces. In Nonlinear Surface Electromagnetic Phenomena.* Elsevier, 1991.

65. Alex G. Lambert, Paul B. Davies, and David J. Neivandt. Implementing the theory of sum frequency generation vibrational spectroscopy: A tutorial review. *Appl. Spectrosc. Rev.*, 40(2):103–145, 2005.

66. Y. R. Shen. Basic theory of surface sum-frequency generation. *J. Phys. Chem. C*, 116(29):15505–15509, 2012.

67. De-Sheng Zheng, Yuan Wang, An-An Liu, and Hong-Fei Wang. Microscopic molecular optics theory of surface second harmonic generation and sum-frequency generation spectroscopy based on the discrete dipole lattice model. *Int. Rev. Phys. Chem.*, 27(4):629–664, 2008.

68. X. Zhuang, P. B. Miranda, D. Kim, and Y. R. Shen. Mapping molecular orientation and conformation at interfaces by surface nonlinear optics. *Phys. Rev. B*, 59(19):12632–12640, 1999.

69. Wei Gan, Dan Wu, Zhen Zhang, Ran-ran Feng, and Hong-Fei Wang. Polarization and experimental configuration analyses of sum frequency generation vibrational spectra, structure, and orientational motion of the air/water interface. *J. Chem. Phys.*, 124(11):114705, 2006.

70. R. Lu, W. Gan, B. Wu, Z. Zhang, Y. Guo, and H. Wang. C-H stretching vibrations of methyl, methylene and methine groups at the vapor/alcohol (n = 1-8) interfaces. *J. Phys. Chem. B*, 109(29):14118–14129, 2005.

71. Victor Ostroverkhov, Glenn A. Waychunas, and Y. R. Shen. New information on water interfacial structure revealed by phase-sensitive surface spectroscopy. *Phys. Rev. Lett.*, 94(4):046102, 2005.

72. Ruben E. Pool, Jan Versluis, Ellen H. G. Backus, and Mischa Bonn. Comparative study of direct and phase-specific vibrational sum-frequency generation spectroscopy: Advantages and limitations. *J. Phys. Chem. B*, 115(51):15362–15369, 2011.

73. Hamm P. and Zanni M. *Concepts and Methods of 2D Infrared Spectroscopy.* Cambridge University Express, 2011.

74. Simona Strazdaite, Jan Versluis, Ellen H. G. Backus, and Huib J. Bakker. Enhanced ordering of water at hydrophobic surfaces. *J. Chem. Phys.*, 140(5):054711, 2014.

75. Lisa M. Onishi, John M. Prausnitz, and John Newman. Water-Nafion equilibria. Absence of Schroeder's Paradox. *J. Phys. Chem. B*, 111(34):10166–10173, 2007.

76. Tatsuhiro Okada, Steffen Moller-Holst, Oddvar Gorseth, and Signe Kjelstrup. Transport and equilibrium properties of Nafion® membranes with H^+ and Na^+ ions. *J. Electroanal. Chem.*, 442(1–2):137–145, 1998.

77. L. B. Rockland. Saturated salt solutions for static control of relative humidity between 5^{o}C and 40^{o}C. *Anal. Chem.*, 32(10):1375–1376, 1960.

78. N. H. Jalani and R. Datta. The effect of equivalent weight, temperature, cationic forms, sorbates, and nanoinorganic additives on the sorption behavior of Nafion®. *J. Membrane Sci.*, 264(1-2):167–175, 2005.

79. T. A. Zawodzinski, C. Derouin, S. Radzinski, R. J. Sherman, V. T. Smith, T. E. Springer, and S. Gottesfeld. Water-uptake by and transport through Nafion® 117 membranes. *J. Electrochem. Soc.*, 140(4):1041–1047, 1993.

80. S. Ochi, O. Kamishima, J. Mizusaki, and J. Kawamura. Investigation of proton diffusion in Nafion® 117 membrane by electrical conductivity and nmr. *Solid State Ionics*, 180(6-8):580–584, 2009.

81. M. Rini, B.-Z. Magnes, E. Pines, and E. T. J. Nibbering. Real-time observation of bimodal proton transfer in acid-base pairs in water. *Science*, 301(5631):349–352, 2003.

82. S. Woutersen and H. J. Bakker. Ultrafast vibrational and structural dynamics of the proton in liquid water. *Phys. Rev. Lett.*, 96(13):138305, 2006.

83. N. Agmon. The Grotthuss mechanism. *Chem. Phys. Lett.*, 244(5-6):456–462, 1995.

84. O. F. Mohammed, D. Pines, J. Dreyer, E. Pines, and E. T. J. Nibbering. Sequential proton transfer through water bridges in acid-base reactions. *Science*, 310(5745):83–86, 2005.

85. D. Asthagiri, L. R. Pratt, J. D. Kress, and M. A. Gomez. Hydration and mobility of HO^-(aq). *Proc. Natl. Acad. Sci. U.S.A.*, 101(19):7229–7233, 2004.

86. N. Agmon. Mechanism of hydroxide mobility. *Chem. Phys. Lett.*, 319(3-4):247–252, 2000.

87. H. K. Nienhuys, A. J. Lock, R. A. van Santen, and H. J. Bakker. Dynamics of water molecules in an alkaline environment. *J. Chem. Phys.*, 117(17):8021–8029, 2002.

88. S. T. Roberts, P. B. Petersen, K. Ramasesha, A. Tokmakoff, I. S. Ufimtsev, and T. J. Martinez. Observation of a Zundel-like transition state during proton transfer in aqueous hydroxide solutions. *Proc. Natl. Acad. Sci. U.S.A.*, 106(36):15154–15159, 2009.

89. S. T. Roberts, K. Ramasesha, P. B. Petersen, A. Mandal, and A. Tokmakoff. Proton transfer in concentrated aqueous hydroxide visualized using ultrafast infrared spectroscopy. *J. Phys. Chem. A*, 115(1):3957–3972, 2011.

90. Y. L. A. Rezus and H. J. Bakker. On the orientational relaxation of HDO in liquid water. *J. Chem. Phys.*, 123(11):114502, 2005.

91. A. J. Lock and H. J. Bakker. Temperature dependence of vibrational relaxation in liquid H_2O. *J. Chem. Phys.*, 117(4):1708–1713, 2002.

92. M. L. Cowan, B. D. Bruner, N. Huse, J. R. Dwyer, B. Chugh, E. T. J. Nibbering, T. Elsaesser, and R. J. D. Miller. Ultrafast memory loss and energy redistribution in the hydrogen bond network of liquid H_2O. *Nature*, 434(7030):199–202, 2005.

93. Y. L. A. Rezus and H. J. Bakker. Orientational dynamics of isotopically diluted H_2O and D_2O. *J. Chem. Phys.*, 125(14):144512, 2006.

94. G. Seifert, T. Patzlaff, and H. Graener. Size dependent ultrafast cooling of water droplets in microemulsions by picosecond infrared spectroscopy. *Phys. Rev. Lett.*, 88(14):147402, 2002.

95. A. Botti, F. Bruni, S. Imberti, M. A. Ricci, and A. K. Soper. Ions in water: The microscopic structure of concentrated NaOH solutions. *J. Chem. Phys.*, 120(21):10154–10162, 2004.

96. Sylvia E. McLain, Silvia Imberti, Alan K. Soper, Alberto Botti, Fabio Bruni, and Maria Antonietta Ricci. Structure of 2 molar NaOH in aqueous solution from neutron diffraction and empirical potential structure refinement. *Phys. Rev. B*, 74(9):094201, 2006.

97. Lauterbach Verfahrenstechnik GmbH. Properties of sodium hydroxide (naoh). http://www.lv-soft.com/software/fachbereiche/stoff/naoh-e.htm.

98. A. Yamakata, T. Uchida, J. Kubota, and M. Osawa. Laser-induced potential jump at the electrochemical interface probed by picosecond time-resolved surface enhanced infrared absorption spectroscopy. *J. Phys. Chem. B*, 110(13):6423–6427, 2006.

99. M. F. Kropman, H. K. Nienhuys, and H. J. Bakker. Real-time measurement of the orientational dynamics of aqueous solvation shells in bulk liquid water. *Phys. Rev. Lett.*, 88(7):077601, 2002.

100. S. Woutersen and H. J. Bakker. Resonant intermolecular transfer of vibrational energy in liquid water. *Nature*, 402(6761):507–509, 1999.

101. N. F. Scherer and A. H. Zewail. Picosecond photofragment spectroscopy. ii. the overtone initiated unimolecular reaction $H_2O_2(\upsilon_{OH}{=}5){\longrightarrow}2OH$. *J. Chem. Phys.*, 87(1):97–114, 1987.

102. Y. Kim, T. Komeda, and M. Kawai. Single-molecule reaction and characterization by vibrational excitation. *Phys. Rev. Lett.*, 89(12):126104, 2002.

103. J. I. Pascual, N. Lorente, Z. Song, H. Conrad, and H. P. Rust. Selectivity in vibrationally mediated single-molecule chemistry. *Nature*, 423(6939):525–528, 2003.

104. J. P. Camden, H. A. Bechtel, D. J. A. Brown, and R. N. Zare. Effects of C–H stretch excitation on the H+CH_4 reaction. *J. Chem. Phys.*, 123(13):134301, 2005.

105. S. Yoon, R.J. Holiday, and F. F. Crim. Vibrationally controlled chemistry: Mode- and bond- selected reaction of CH_3D with Cl. *J. Phys. Chem. B*, 109(17):8388–8392, 2005.

106. R. T. Hall and G. C. Pimentel. Isomerization of nitrous acid: An infrared photochemical reaction. *J. Chem. Phys.*, 38(8):1889–1897, 1963.

107. R. Schanz, V. Boan, and P. Hamm. A femtosecond study of the infrared-driven cis-trans isomerization of nitrous acid (HONO). *J. Chem. Phys.*, 122(4):044509, 2005.

108. K. Ando and J.T. Hynes. Molecular mechanism of HF acid ionization in water: An electronic structure−monte carlo study. *J. Phys. Chem. A*, 103(49):10398–10408, 1999.

109. T. Joutsuka and K. Ando. Hydration structure in dilute hydrofluoric acid. *J. Phys. Chem. A*, 115(5):671–677, 2011.

110. K. A. Mauritz and R. B. Moore. State of understanding of Nafion. *Chem. Rev.*, 104(10):4535–4585, 2004.

111. A. V. Anantaraman and C. L. Gardner. Studies on ion-exchange membranes. Part 1. Effect of humidity on the conductivity of Nafion®. *J. Elec. Chem.*, 414(2):115–120, 1996.

112. M. K. Petersen and G. A. Voth. Characterization of the solvation and transport of the tydrated proton in the perfluorosulfonic acid membrane Nafion. *J. Phys. Chem. B*, 110(37):18594–18600, 2006.

113. S. Feng and G. A. Voth. Proton solvation and transport in hydrated Nafion. *J. Phys. Chem. B*, 115(19):5903–5912, 2011.

114. Y.-L. S. Tse, A. M. Herring, K. Kim, and G. A. Voth. Molecular dynamics simulations of proton transport in 3m and Nafion perfluorosulfonic acid membranes. *J. Phys. Chem. C*, 117(16):8079–8091, 2013.

115. D. E. Moilanen, I. R. Piletic, and M. D. Fayer. Water dynamics in Nafion fuel cell membranes: The effects of confinement and structural changes on the hydrogen bond network. *J. Phys. Chem. C*, 111:8884–8891, 2007.

116. M. Laporta, M. Pegoraro, and L. Zanderighi. Perfluorosulfonated membrane (Nafion): FT-IR study of the state of water with increasing humidity. *Phys. Chem. Chem. Phys.*, 1(19):4619–4628, 1999.

117. S. Woutersen and P. Hamm. Structure determination of trialanine in water using polarization sensitive two-dimensional vibrational spectroscopy. *J. Phys. Chem. B*, 104(47):11316–11320, 2000.

118. J. Zheng, K. Kwak, J. Asbury, X. Chen, I. R. Piletic, and M. D. Fayer. Ultrafast dynamics of solute-solvent complexation observed at thermal equilibrium in real time. *Science*, 309(5739):1338–1343, 2005.

119. W. Mikenda. Stretching frequency versus bond distance correlation of O-D(H)$\cdots$Y (Y=N,O, S, Se, Cl, Br, I) hydrogen bonds in solid hydrates. *J. Mol. Struct.*, 147(1–2):1–15, 1986.

120. H. J. Bakker, H.-K. Nienhuys, G. Gallot, N. Lascoux, G. M. Gale, J.-C. Leicknam, and S. Bratos. Transient absorption of vibrationally excited water. *J. Chem. Phys.*, 116(6):2592–2598, 2002.

121. F. Perakis, S. Widmer, and P. Hamm. Two-dimensional infrared spectroscopy of isotope-diluted ice Ih. *J. Chem. Phys.*, 134(20):204505, 2011.

122. J. R. Lakowicz. *Principles of Fluorescence Spectroscopy.* Springer, New York, USA, 2006.

123. I. R. Piletic, D. E. Moilanen, D. B. Spry, N. E. Levinger, and M. D. Fayer. Testing the core/shell model of nanoconfined water in reverse micelles using linear and nonlinear IR spectroscopy. *J. Phys. Chem. A*, 110:4985–4999, 2006.

124. V. Glezakou, M. Dupuis, and C.J. Mundy. Acid/base euilibria in custers and their role in proton exchange membranes: Computational insight. *Phys. Chem. Chem. Phys.*, 9(43):5752–5760, 2007.

125. J.M.J. Swanson, C.M. Maupin, H. Chen, M.K. Petersen, J. Xu, Y. Wu, and G.A. Voth. Proton solvation and transport in aqueous and biomolecular systems: Insights from computer simulations. *J. Phys. Chem. B*, 111:4300, 2007.

126. D. Marx, M. E. Tuckerman, J. Hutter, and M. Parrinello. The nature of the hydrated excess proton in water. *Nature*, 397:601, 1999.

127. Klaas Jan Tielrooij, M. Jocelyn Cox, and Huib J. Bakker. Effect of confinement on proton-transfer reactions in water nanopools. *Chem. Phys. Chem.*, 10(1):245–251, 2009.

128. D. B. Spry, A. Goun, K. Glusac, D. E. Moilanen, and M. D. Fayer. Proton transport and the water environment in Nafion fuel cell membranes and AOT reverse micelles. *J. Am. Chem. Soc.*, 129(26):8122–8130, 2007.

129. P. Choi, N. H. Jalani, and R. Datta. Thermodynamics and proton transport in Nafion-II. Proton diffusion mechanisms and conductivity. *J. Elec. Soc.*, 152(3):E123–E130, 2005.

130. Boiko Cohen, Dan Huppert, Kyril M. Solntsev, Yossi Tsfadia, Esther Nachliel, and Menachem Gutman. Excited state proton transfer in reverse micelles. *J. Am. Chem. Soc.*, 124(25):7539–7547, 2002.

131. M. Cappadonia, J. W. Erning, S. M. S. Niaki, and U. Stimming. Conductance of Nafion 117 membranes as a function of temperature and water-content. *Solid State Ionics*, 77:65–69, 1995.

132. D. B. Spry, A. Goun, and M. D. Fayer. Deprotonation dynamics and stokes shift of pyranine (HPTS). *J. Phys. Chem. A*, 111(2):230–237, 2007.

133. D. B. Spry and M. D. Fayer. Proton transfer and proton concentrations in protonated Nafion fuel cell membranes. *J. Phys. Chem. B*, 113(30):10210–10221, 2009.

134. S. L. Feng, J. Savage, and G. A. Voth. Effects of polymer morphology on proton solvation and transport in proton-exchange membranes. *J. Phys. Chem. C*, 116(36):19104–19116, 2012.

135. Liyuan Liu and Huib J. Bakker. Infrared-activated proton transfer in aqueous Nafion proton-exchange-membrane nanochannels. *Phys. Rev. Lett.*, 112(25):258301, 2014.

136. Sharon Hammes-Schiffer and John C. Tully. Vibrationally enhanced proton transfer. *J. Phys. Chem.*, 99(16):5793–5797, 1995.

137. H. J. Kim, A. Staib, and J. T. Hynes. *Femtochemistry and Femtobiology: Ultrafast Reaction Dynamics at Atomic-Scale Resolution.* Nobel Symposium 101;World Scientific: Imperial College Press, London, 1996.

138. Y. L. A. Rezus and H. J. Bakker. Observation of immobilized water molecules around hydrophobic groups. *Phys. Rev. Lett.*, 99(14):4, 2007.

139. Gabriel Hanna and Eitan Geva. Isotope effects on the vibrational relaxation and multidimensional infrared spectra of the hydrogen stretch in a hydrogen-bonded complex dissolved in a polar liquid. *J. Phys. Chem. B*, 112(49):15793–15800, 2008.

140. T. H. Tran-Thi, T. Gustavsson, C. Prayer, S. Pommeret, and James T. Hynes. Primary ultrafast events preceding the photoinduced proton transfer from pyranine to water. *Chem. Phys. Lett.*, 329(5–6):421–430, 2000.

141. James T. Hynes, Thu-Hoa Tran-Thi, and Giovanni Granucci. Intermolecular photochemical proton transfer in solution: New insights and perspectives. *J. Photoch. Photobio. A*, 154(1):3–11, 2002.

142. Pavel Leiderman, Liat Genosar, and Dan Huppert. Excited-state proton transfer: Indication of three steps in the dissociation and recombination process. *J. Phys. Chem. A*, 109(27):5965–5977, 2005.

143. Elizabeth-Ann Gould, Alexander V. Popov, Laren M. Tolbert, Itay Presiado, Yuval Erez, Dan Huppert, and Kyril M. Solntsev. Excited-state proton transfer in n-methyl-6-hydroxyquinolinium salts: Solvent and temperature effects. *Phys. Chem. Chem. Phys.*, 14(25):8964–8973, 2012.

144. Omar F. Mohammed, Jens Dreyer, Ben-Zion Magnes, Ehud Pines, and Erik T. J. Nibbering. Solvent-dependent photoacidity state of pyranine monitored by transient mid-infrared spectroscopy. *ChemPhysChem*, 6(4):625–636, 2005.

145. K. Adamczyk, M. Premont-Schwarz, D. Pines, E. Pines, and E. T. J. Nibbering. Real-time observation of carbonic acid formation in aqueous solution. *Science*, 326(5960):1690–1694, 2009.

146. Mirabelle Premont-Schwarz, Tamar Barak, Dina Pines, Erik T. J. Nibbering, and Ehud Pines. Ultrafast excited-state proton-transfer reaction of 1-naphthol-3,6-disulfonate and several 5-substituted 1-naphthol derivatives. *J. Phys. Chem. B*, 117(16):4594–4603, 2013.

147. Noam Agmon, Wolfgang Rettig, and Christian Groth. Electronic determinants of photoacidity in cyanonaphthols. *J. Am. Chem. Soc.*, 124(6):1089–1096, 2002.

148. S. Woutersen and H.J. Bakker. Ultrafast vibrational and structural dynamics of the proton in liquid water. *Phys. Rev. Lett.*, 96:138305, 2006.

149. G. Seifert, T. Patzlaff, and H. Graener. Size dependent ultrafast cooling of water droplets in microemulsions by picosecond infrared spectroscopy. *Phys. Rev. Lett.*, 88(14):147402, 2002.

150. L. I. Yeh, M. Okumura, J. D. Myers, J. M. Price, and Y. T. Lee. Vibrational spectroscopy of the hydrated hydronium cluster ions $H_3O^+(H_2O)$ n (n=1, 2, 3). *J. Chem. Phys.*, 91(12):7319–7330, 1989.

151. D. Marx, M. E. Tuckerman, and M. Parrinello. Solvated excess protons in water: quantum effects on the hydration structure. *J. Phys-Condens. Mat.*, 12(8A):A153–A159, 2000.

152. Georg Zundel. *Hydrogen Bonds with Large Proton Polarizability and Proton Transfer Processes in Electrochemistry and Biology*, pages 1–217. John Wiley & Sons, Inc., 2007.

153. Michael Falk. Frequencies of H-O-H, H-O-D and D-O-D bending fundamentals in liquid water. *J. Ram. Spec.*, 21(9):563–567, 1990.

154. Y. Maréchal. Infrared spectra of water. i. effect of temperature and of h/d isotopic dilution. *J. Chem. Phys.*, 95(8):5565–5573, 1991.

155. Detlef W. M. Hofmann, Liudmila Kuleshova, Bruno D' Aguanno, Vito Di Noto, Enrico Negro, Fosca Conti, and Michele Vittadello. Investigation of water structure in Nafion membranes by infrared spectroscopy and molecular dynamics simulation. *J. Phys. Chem. B*, 113(3):632–639, 2008.

156. O. F. A. Larsen and S. Woutersen. Vibrational relaxation of the h_2o bending mode in liquid water. *J. Chem. Phys.*, 121(24):12143–12145, 2004.

157. N. Huse, S. Ashihara, E. T. J. Nibbering, and T. Elsaesse. Ultrafast vibrational relaxation of o-h bending and librational excitations in liquid h_2o. *Chem. Phys. Lett.*, 404(4-6):389–393, 2005.

158. S. Woutersen, U. Emmerichs, and H. J. Bakker. A femtosecond midinfrared pump-probe study of hydrogen-bonding in ethanol. *J. Chem. Phys.*, 107(5):1483–1490, 1997.

159. T. Wróblewski, L. Ziemczonek, E. Gazda, and G.P. Karwasz. Dissociation energies of protonated water clusters. *Radiat. Phys. Chem.*, 68:313–318, 2003.

160. T. Wróblewski and G.P. Karwasz. Protonated water clusters. *Eur. Phys. J. Special Topics*, 222:2217–2221, 2013.

161. U. W. Schmitt and G. A. Voth. The computer simulation of proton transport in water. *J. Chem. Phys.*, 111:9361–9381, 1999.

162. N. Ottosson and H. J. Hunger, J.; Bakker. Effect of cations on the hydrated proton. *J. Am. Chem. Soc.*, 136:12808–12811, 2014.

163. K. Takeshita, S. Sakata, E. Yamashita, Y. Fujiwara, A. Kawanabe, T. Kurokawa, Y. Okochi, M. Matsuda, H. Narita, Y. Okamura, and A. Nakagawa. X-ray crystal structure of voltage-gated proton channel. *Nat. Struct. Mol. Biol.*, 21:352–357, 2014.

164. K. Chmidt-Rohr and Q. Chen. Parallel cylindrical water nanochannels in nafion fuel-cell membranes. *Nat. Mater.*, 7:75–83, 2008.

165. M. Sedgwick, R. L. Cole, C. D. Rithner, D. C. Crans, and N. E. Levinger. Correlating proton transfer dynamics to probe location in confined environments. *J. Am. Chem. Soc.*, 134:11904–11907, 2012.

166. G. P. Cunningham, G. A. Vidulich, and R. L. Kay. Several properties of acetonitrile-water, acetonitrile-methanol, and ethylene carbonate-water systems. *J. Chem. Eng. Data*, 12:336–337, 1967.

167. Y. Marcus and Y. Migron. Polarity, hydrogen bonding, and structure of mixtures of water and cyanomethane. *J. Phys. Chem.*, 95:400–406, 1991.

168. H. Kovacs and A. Laaksonen. Molecular dynamics simulation and nmr study of water-acetonitrile mixtures. *J. Am. Chem. Soc.*, 113:5596–5605, 1991.

169. T. Takamuku, M. Tabata, A. Yamaguchi, J. Nishimoto, M. Kumamoto, H. Wakita, and T. Yamaguchi. Liquid structure of acetonitrile-water mixtures by x-ray diffraction and infrared spectroscopy. *J. Phys. Chem. B*, 102:8880–8888, 1998.

170. D. Cringus, S. Yeremenko, M. S. Pshenichnikov, and D. A. Wiersma. Hydrogen bonding and vibrational energy relaxation in water-acetonitrile mixtures. *J. Phys. Chem. B*, 108:10376–10387, 2004.

171. M. V. Sigalov, N. Kalish, B. Carmeli, D. Pines, and E. Pines. Probing small protonated water clusters in acetonitrile solutions by 1 h nmr. *Zeitschr. Phys. Chem.*, 227:983–1007, 2013.

172. Liyuan Liu and Huib J. Bakker. Vibrational excitation induced proton transfer in hydrated nafion membranes. *J. Phys. Chem. B*, 119:2628–2637, 2015.

173. A. M. Dokter, S. Woutersen, and H. J. Bakker. Inhomogeneous dynamics in confined water nanodroplets. *Proc. Natl. Acad. Sci.*, 103:15355–15358, 2006.

174. Moilanen D.E., Fenn E.E., Wong D.B., and Fayer M.D. Water dynamics at the interface in aot reverse micelles. *J. Phys Chem B*, 113:8560–8568, 2009.

175. H. Graener, T. Q. Ye, and A. Laubereau. Ultrafast dynamics of hydrogen bonds directly observed by time-resolved infrared spectroscopy. *J. Chem. Phys.*, 90:3413–3416, 1989.

176. H. Graener, T. Q. Ye, and A. Laubereau. Ultrafast vibrational predissociation of hydrogen bonds: Mode selective infrared photochemistry in liquids. *J. Chem. Phys.*, 91:1043–1046, 1989.

177. Pavel Jungwirth and Douglas J. Tobias. Molecular structure of salt solutions: A new view of the interface with implications for heterogeneous atmospheric chemistry. *J. Phys. Chem. B*, 105(43):10468–10472, 2001.

178. Martin Mucha, Tomaso Frigato, Lori M. Levering, Heather C. Allen, Douglas J. Tobias, Liem X. Dang, and Pavel Jungwirth. Unified molecular picture of the surfaces of aqueous acid, base, and salt solutions. *J. Phys. Chem. B*, 109(16):7617–7623, 2005.

179. Dingfang Liu, Gang Ma, Lori M. Levering, and Heather C. Allen. Vibrational spectroscopy of aqueous sodium halide solutions and air–liquid interfaces: Observation of increased interfacial depth. *J. Phys. Chem. B*, 108(7):2252–2260, 2004.

180. Poul B. Petersen, Richard J. Saykally, Martin Mucha, and Pavel Jungwirth. Enhanced concentration of polarizable anions at the liquid water surface: SHG spectroscopy and MD simulations of sodium thiocyanide. *J. Phys. Chem. B*, 109(21):10915–10921, 2005.

181. Elizabeth A. Raymond and Geraldine L. Richmond. Probing the molecular structure and bonding of the surface of aqueous salt solutions. *J. Phys. Chem. B*, 108(16):5051–5059, 2004.

182. N. Ottosson, L. Cwiklik, J. Söderström, O. Björneholm, G. Öhrwall, and P. Jungwirth. Increased propensity of I^-_{aq} for the water surface in non-neutral solutions: Implications for the interfacial behavior of $H_3O^+_{aq}$ and OH^-_{aq}. *J. Phys. Chem. Lett.*, 2(9):972–976, 2011.

183. J. H. Hu, Q. Shi, P. Davidovits, D. R. Worsnop, M. S. Zahniser, and C. E. Kolb. Reactive uptake of Cl_2(g) and Br_2(g) by aqueous surfaces as a function of Br^- and I^- ion concentration: The effect of chemical reaction at the interface. *J. Phys. Chem.*, 99(21):8768–8776, 1995.

184. Alexander Laskin, Daniel J. Gaspar, Weihong Wang, Sherri W. Hunt, James P. Cowin, Steven D. Colson, and Barbara J. Finlayson-Pitts. Reactions at interfaces as a source of sulfate formation in sea-salt particles. *Science*, 301(5631):340–344, 2003.

185. Wei Hua, Dominique Verreault, and Heather C. Allen. Surface prevalence of perchlorate anions at the air/aqueous interface. *J. Phys. Chem. Lett.*, 4(24):4231–4236, 2013.

186. Chuanshan Tian, Steven J. Byrnes, Hui-Ling Han, and Y. Ron Shen. Surface propensities of atmospherically relevant ions in salt solutions revealed by phase-sensitive sum frequency vibrational spectroscopy. *J. Phys. Chem. Lett.*, 2(15):1946–1949, 2011.

187. Robert M. Onorato, Dale E. Otten, and Richard J. Saykally. Adsorption of thiocyanate ions to the dodecanol/water interface characterized by UV second harmonic generation. *Proc. Natl. Acad. Sci.*, 106(36):15176–15180, 2009.

188. Yi Rao, Mahamud Subir, Eric A. McArthur, Nicholas J. Turro, and Kenneth B. Eisenthal. Organic ions at the air/water interface. *Chem. Phys. Lett.*, 477(4–6):241–244, 2009.

189. Maria Sovago, R. Kramer Campen, George W. H. Wurpel, Michiel Müller, Huib J. Bakker, and Mischa Bonn. Vibrational response of hydrogen-bonded interfacial water is dominated by intramolecular coupling. *Phys. Rev. Lett.*, 100(17):173901, 2008.

190. Na Ji, Victor Ostroverkhov, Chao-Yuan Chen, and Yuen-Ron Shen. Phase-sensitive sum-frequency vibrational spectroscopy and its application to

studies of interfacial alkyl chains. *J. Am. Chem. Soc.*, 129(33):10056–10057, 2007.

191. Ran-Ran Feng, Yuan Guo, Rong Lü, Luis Velarde, and Hong-Fei Wang. Consistency in the sum frequency generation intensity and phase vibrational spectra of the air/neat water interface. *J. Phys. Chem. A*, 115(23):6015–6027, 2011.

192. Igor V. Stiopkin, Champika Weeraman, Piotr A. Pieniazek, Fadel Y. Shalhout, James L. Skinner, and Alexander V. Benderskii. Hydrogen bonding at the water surface revealed by isotopic dilution spectroscopy. *Nature*, 474(7350):192–195, 2011.

193. S. Woutersen and H. J. Bakker. Resonant intermolecular transfer of vibrational energy in liquid water. *Nature*, 402(6761):507–509, 1999.

194. L. Piatkowski and H. J. Bakker. Vibrational relaxation pathways of AI and AII modes in n-methylacetamide clusters. *J. Phys. Chem. A*, 114(43):11462–11470, 2010.

195. G. E. Walrafen. Raman spectral studies of the effects of perchlorate ion on water structure. *J. Chem. Phys.*, 52(8):4176–4198, 1970.

196. Joel G. Davis, Kamil P. Gierszal, Ping Wang, and Dor Ben-Amotz. Water structural transformation at molecular hydrophobic interfaces. *Nature*, 491(7425):582–585, 2012.

Summary

The proton (H^+) exists in water as a hydrated complex instead of a bare ion, because of its extremely high charge density, as a result of which it strongly binds to surrounding water molecules. Hydration of the proton by one water molecule leads to the formation of a hydronium ion (H_3O^+). In liquid water the hydronium ion is further hydrated to form proton hydration complexes like the Eigen complex ${H_9O_5}^+$ and the Zundel complex ${H_5O_2}^+$. In fact there exists a broad distribution of different proton hydration complexes $H{\cdot}(H_2O)_n{}^+$ in water, and the Eigen and the Zundel complexes just form two limiting cases. In liquid water the proton hydration complexes are very dynamic, the hydrogen bonds in the hydration shell continuously break and reform. As a result of these structural dynamics the proton charge can get transferred from one water molecule to another.

Protons in water are transferred by the Grotthuss mechanism which involves an ongoing restructuring of the hydrogen-bond network. Thanks to this mechanism, the proton and the hydroxide ion diffuse several times faster than normal ions, that diffuse via oridinary Stokes diffusion: the conductivity of H^+ in water is about seven times higher than that of Na^+, and the conductivity of OH^- in water is about three times higher than that of Cl^-. Because of its high conductivity and unique transfer mechanism, the proton plays a key role in many chemical and biological processes like atmospheric reactions, photosynthesis, and hydrogen fuel cells. Most of these proton-involved processes take place in confined environments, such as the channels provided by ATP synthetic systems and the nano-channels of Nafion membranes. Understanding the mechanism of proton transfer in confinement is essential for the utilization and control of proton-involved processes.

In order to understand the proton transfer mechanism in confinement on the molecular scale, we investigated the structural and dynamical properties of the O–H vibrations (which strongly absorb light in the infrared region of the spectrum) of the proton hydration complexes, using polarization-resolved femtosecond infrared pump-probe spectroscopy. In this method the O–H vibrational modes of proton hydration complexes are excited by a short and intense infrared pulse. The absorption spectrum of the excited sample is different from

that of the non-excited sample, and this absorption change is monitored by a delayed probe pulse. By varying the delay time of the probe relative to the pump, we obtain the time evolution of the absorption difference spectra, from which we obtain information on several dynamical aspects of the proton hydration complex, like vibrational relaxation, spectral diffusion, molecular reorientation, Förster energy transfer. This information provides us with unprecedented information on the mechanism of proton transfer on the molecular scale.

In Chapter 4, we study the vibrational relaxation and anisotropy dynamics of the hydration shells of OH^- ions. We observe that the excited O–H stretch vibration of water molecules that hydrate the OH^- ion first relax to a local hot state with a concentration independent time constant of 200 fs. The local hot state then decays to a final state in which the energy is thermally distributed over the focus of the exciting laser pulse. The time constant of the equilibration process rises with increasing concentration, from 1.2 ps for a 0.5 M solution to 4.5 ps for a 10 M solution. The local hot state is observed to be anisotropic, showing that the energy of the excited O–H stretch vibrations is first dissipated within the hydration complex. The anisotropy of the local hot state decays both as a result of the reorientation of the OH^- hydration complex and as a result of heat diffusion from the excited complexes to non-excited complexes. Modelling the anisotropy data at different concentrations allows for an accurate determination of the number of water molecules in the hydration shell of the OH^- ion, the reorientation dynamics of the OH^- hydration complex, and the molecular-scale heat diffusivity.

In Chapter 5, we observe a strong reorganization of the proton hydration structure in hydrated Nafion membranes following single-quantum excitation of a proton vibration with $\sim$4 μm light pulses. After excitation by an intense infrared pulse, the O–H vibration in the hydronium core of an Eigen complex evolves to a Zundel proton vibration ($O\cdots H^+\cdots O$), which is observed as a strong red-shift of the transient bleaching spectrum. Accompanied by the evolution of the O–H vibration to a proton vibration, the other two non-excited O–H modes of the Eigen complex turn into higher-frequency O–H stretch vibrations of water molecules that are flanking the Zundel proton. This evolution is observed as a delayed extra absorption at 3270/3520 cm^{-1}. This structural reorganization takes place with a time constant of 170$\pm$20 fs. The higher-frequency O–H stretch vibrations of water molecules flanking the Zundel proton are at a quite large angle with respect to the proton vibration, which agrees with the initial negative value of the anisotropy of the induced water-like O–H stretch absorption bands. The anisotropy values of the excited proton vibration and the induced absorption both relax to a value of $\sim$0.1 with a time constant of 120$\pm$30 fs. This final value of the anisotropy indicates that the excitation has randomized in the plane of the central H_3O^+ ion of the Eigen hydration structure, meaning that the vibrational excitation is delocalized over the three O–H groups of the central H_3O^+ ion.

In Chapter 6, we study the vibrational dynamics of hydrated protons in Nafion membranes at different hydration levels. At low hydration levels we observe that the excitation of the proton vibration of an Eigen-like proton hydra-

tion structure leads to a structural relaxation process in which the Eigen-like structure evolves to a Zundel-like proton hydration structure, as observed in Chapter 5. At high hydration levels the spectral dynamics are dominated by vibrational energy relaxation and subsequent cooling of the proton hydration complex. Using a kinetic analysis of the transient spectral data, we determine the rates of proton transfer, vibrational energy relaxation and cooling as a function of the hydration level. We find that infrared-induced proton transfer occurs at all hydration levels, but becomes less observable at high hydration levels due to the acceleration of the vibrational relaxation and the increasingly dominant influence of the heating effect that results from the vibrational energy relaxation.

In Chapter 8, We studied the vibrational relaxation and thermal relaxation dynamics of proton hydration complexes in acetonitrile at different proton to water ratios ($[H^+]$:$[H_2O]$ varies from 1:1 to 1:3), following the ultrafast excitation of one of the O–H stretch vibrations of the H_3O^+ ion. We found that there are two relaxation pathways: for most excited vibrations the vibrational energy dissipated in the relaxation (with a time constant <100 fs) is taken up as heat by the aqueous cluster (with a time constant of 320±20 fs). Subsequently, the hot complex cools by transferring its thermal energy to the acetonitrile surroundings (with a time constant of 1.4±0.1 ps). For a small fraction of the complexes the excitation leads to ultrafast predissociation of one of the hydrogen bonds of the proton hydration complex,and thus to the ejection of water monomer fragments. As a result, a long living bleaching signal with high anisotropy is created.

A similar pre-dissociation of proton hydration complexes is observed in *Chapter 7*. In this chapter we investigated the dynamics of the bending mode of the hydronium ion in hydrated Nafion. The excited bending mode relaxes via two relaxation channels. The main fraction of the excited hydronium ions is found to relax to an intermediate (local hot) state with a time constant T_1 of 175 fs, and subsequently to an equilibrated thermal state with a time constant T_{eq} of 1.53 ps. A small fraction of the excited bending modes is observed to relax via predissociation of a hydrogen bond. In this process, one of the hydrogen bonds between the hydronium ion and its first hydration shell is broken, leading to a long-living bleaching of the absorption band of the hydronium bend vibration. Due to the ultrafast character of the predissociation process, this bleaching signal has a high associated anisotropy that decays with a long time constant of 38±4 ps, probably as a result of structural relaxation of the proton hydration complex within the Nafion nano-channel.

In Chapter 9 we use vibrational surface sum-frequency generation (VSFG) spectroscopy to study the vibrational response of the hydration shells of hydrophobic anions like triflate ($CF_3SO_3^-$), ethanesulfonate ($C_2H_5SO_3^-$), and butanesulfonate ($C_4H_9SO_3^-$). The addition of triflate, ethanesulfonate, and butanesulfonate strongly affects the frequency and amplitude of the main band of the VSFG spectrum of H_2O/D_2O. For solutions in H_2O, the addition of these hydrophobic anions leads to a strong blue shift of the main band of the VSFG spectrum but little change in amplitude. In contrast, for solutions in D_2O the addition of these anions hardly changes the frequency of the main band but

leads to a strong increase in amplitude. This observation can be explained by a strong isotope effect in the intra- and intermolecular mixing of the hydroxyl stretch vibrations of the water molecules contained in the hydration shells of the hydrophobic anions. The O–H stretch vibrations of H_2O molecules in the hydration shell are strongly mixed whereas the O–D stretch vibrations of the hydrating D_2O molecules are decoupled. This isotope effect is not observed for other ions like perchlorate (ClO_4^-), which can be explained from the stronger mixing of the OH vibrations as a result of the smaller difference between the frequencies of the water hydroxyl groups that are hydrogen bonded to anions and the frequencies of the water hydroxyl groups that are hydrogen bonded to other water molecules.

Samenvatting

Het proton (H^+) bestaat in water als een gehydrateerd complex in plaats van een kaal ion, omdat het proton zich zeer sterk bindt aan omringende watermoleculen. Deze sterke binding is een direct gevolg van de zeer hoge ladingsdichtheid van het proton. Als het proton door een enkel watermolecuul wordt gehydrateerd, vormt zich een zogenaamd hydronium ion (H_3O^+). In vloeibaar water wordt het hydronium verder gehydrateerd tot gehydrateerde protoncomplexen als het Eigen complex ${H_9O_5}^+$ en het Zundel complex ${H_5O_2}^+$. In feite bestaan er in water heel veel verschillende gehydrateerde protoncomplexen $H{\cdot}(H_2O)_n{}^+$, met het Eigen en het Zundel complex als limietgevallen In vloeibaar water zijn gehydrateerde protoncomplexen zeer dynamisch, de waterstofbruggen in de hydratieschil breken en hervormen op zeer korte tijdschaal. Een belangrijke consequentie van deze voortdurende structurele reorganisatie is dat de lading van het proton voortdurend van het ene water molecuul naar het andere wordt overgedragen.

Het proton diffundeert in water voornamelijk via het zogenaamde Grotthuss mechanisme. In dit mechanisme wordt de gehydrateerde protonstructuur locaal afgebroken en ergens anders weer opnieuw opgebouwd. Dankzij het Grotthuss mechanisme, diffunderen protonen en hydroxide ionen vele malen sneller door water dan normale ionen (die zich verplaatsen via normale Stokes diffusie): de geleidbaarheid van H^+ in water is ongeveer zeven keer hoger dan de geleidbaarheid van Na^+ en de geleidbaarheid van OH^- in water is ongeveer drie keer hoger dan de geleidbaarheid van Cl^-. Vanwege de hoge geleidbaarheid en het unieke transportmechanisme speelt het proton een belangrijke rol in vele chemische en biologische processen, zoals in atmosferische reacties, fotosynthese en in waterstof brandstofcellen. Veel van deze processen vinden plaats in een sterk begrensde omgeving, zoals de kanalen van transmembraaneiwitten als ATP synthetase en de kanalen van Nafion protonuitwisselingsmembranen. Een beter begrip van het mechanisme waarmee protonen in dit soort sterk ingeperkte omgevingen worden getransporteerd kan sterk bijdragen aan de optimalisatie van complexe chemische systemen als waterstof brandstofcellen.

In dit proefschrift heb ik onderzoek gedaan naar het mechanisme van protongeleiding in sterk ingeperkt water. Hiertoe heb ik de dynamica van de O–H

vibraties van proton hydratiecomplexen onderzocht met behulp van polarisatie-opgeloste femtoseconde infrarood pomp-probe spectroscopie. In deze techniek worden de O–H strekvibraties van de proton hydratiecomplexen geëxciteerd met een ultrakorte (femtoseconde) intense infrarood puls. Door de excitatie verandert het absorptiespectrum van de proton hydratiecomplexen. Deze absorptieverandering wordt gemeten met een vertraagde ultrakorte infrarood probe puls. Door het tijdsverschil tussen de pomp en de probe puls te variëren, kunnen we de tijdsevolutie van het absorptiespectrumverschil bepalen. Uit deze dynamica verkrijgen we belangrijke informatie over de vibratierelaxatie, spectrale diffusie, moleculaire reorientatie, en de Förster energie overdracht van het proton hydratatiecomplex. Deze parameters geven op hun beurt inzicht in het mechanisme van protonoverdracht op moleculaire schaal.

In hoofdstuk 4, bestuderen we de vibratierelaxatie en anisotropiedyna-mica van de hydratatieschillen van hydroxide (OH^-) ionen. We vinden dat de aangeslagen O–H strekvibraties van water moleculen rondom het OH^- ion relaxeren met een tijdsconstante van 200 fs, onafhankelijk van de OH^- concentratie. Deze relaxatie leidt tot een hele sterke lokale verhitting. Deze lokaal verhitte toestand relaxeert vervolgens naar een toestand waarin de energie thermisch verdeeld is over het focus van de pomp puls. De tijdsconstante van dit tweede equilibratieproces neemt toe met toenemende concentratie, van 1.2 ps voor een 0.5 M oplossing tot 4.5 ps voor een 10 M oplossing. De lokaal verhitte toestand is anisotroop, wat betekent dat de energie van de aangeslagen O–H strekvibraties wordt overgedragen aan een beperkt aantal moleculen binnen het hydratatiecomplex van het OH^- ion. De anisotropie van de lokaal verhitte toestand relaxeert zowel door reorientatie van het OH^- hydratatiecomplex als door diffusie van warmte van de geëxciteerde complexen naar niet- geëxciteerde complexen. Door de anisotropiedata voor verschillende concentraties te modelleren kunnen we een aantal belangrijke parameters bepalen zoals het aantal watermoleculen in de hydratieschil van het OH^- ion, de reorientatietijdsconstante van het OH^- hydratiecomplex en de snelheid van warmtediffusie op moleculaire schaal.

In hoofdstuk 5 beschrijven we de resultaten van metingen aan de vibraties van proton hydratatiestructuren in Nafion membraanen. We ontdekten dat excitatie van een protonvibratie met ∼4um lichtpulsen.leidt tot een in-grijpende structurele reorganisatie van de proton hydratatiestructuur. Door deze reorganisatie verandert de geëxciteerde O–H vibratie van de hydroniumkern (H_3O^+) van een Eigen complex in de protonvibratie van een Zundel complex ($O\cdots H^+\cdots O$) . Tegelijkertijd met deze verandering van de geëxciteerde O–H vibratie van het hydronium ion, veranderen de twee niet-aangeslagen O–H groepen van het hydronium ion in een H_2O molecuul wat direct grenst aan het Zundel proton. Door deze verandering krijgen de niet-geëxciteerde O–H vibraties een hogere frequentie, wat in ons experiment wordt waargenomen als een ingroeiende extra absorptie bij 3270/3520 cm^{-1}. Deze fundamentele structurele reorganisatie vindt plaats met een tijdsconstante van 170±20 fs en vertoont buitengewoon grote verwantschap met de structurele omzetting die ten grondslag ligt aan het protontransport in vloeibaar water via het Grotthuss

gelei-dingsmechanisme. De hoog-frequente O–H strekvibraties van de water moleculen die direct grenzen aan het nieuw gevormde Zundel proton staan onder een vrij grote hoek ten opzichte van de geëxciteerde O–H vibratie. Hierdoor heeft de anisotropie van de extra absorptie bij 3270/3520 cm^{-1} een negatieve waarde. De anisotropie van de extra absorptie en de geëxciteerde O–H vibratie relaxeren allebei naar een waarde van ∼0.1 met een tijdsconstante van 120±30 fs. Deze eindwaarde van de anisotropie wijst erop dat de excitatie wordt herverdeeld over de drie O–H groepen van het centrale H_3O^+ ion.

In hoofdstuk 6 bestuderen we de vibratiedynamica van proton hydratatiestructuren in Nafion membranen voor verschillende hydratatieniveaus. Bij lage hydratatieniveaus leidt excitatie van een protonvibratie van een Eigen proton hydratatiestructuur tot omzetting naar een Zundel proton hydratatiestructuur, precies zoals is waargenomen in hoofdstuk 5. Bij hoge hydratatieniveaus wordt de spectrale dynamica gedomineerd door de vibratierelaxatie en het daaropvolgende afkoelen van het proton hydratatiecomplex. We analyseren de tijdsopgeloste spectrale veranderingen met een kinetisch model. Uit de modellering volgen de snelheidsconstantes van de protonoverdracht, de vibratierelaxatie en het afkoelingsproces als functie van het hydratatieniveau. Uit de analyse volgt dat infrarood-geinduceerde proton overdracht plaatsvindt bij alle hydratatieniveaus. Echter, de protonoverdracht wordt steeds moeilijker waarneembaar met toenemende hydratatiegraad omdat het competitieve vibratierelaxatieproces steeds sneller verloopt en geassocieerde absorptieveranderingen heeft die het signaal in steeds sterkere mate gaan domineren.

In hoofdstuk 8, bestuderen we de vibratierelaxatie en thermische relaxatiedynamica van proton hydratatiecomplexen in acetonitril voor verschillende verhoudingen van het proton en water (($[H^+]$:$[H_2O]$ varieert van 1:1 tot 1:3). We vonden dat de O–H strekvibraties van het H_3O^+ ion relaxeren via twee verschillende paden. Voor de meeste vibraties relaxeert de vibratie met een tijdsconstante <100 fs binnen het hydratatiecomplex, wat leidt tot een zeer sterke lokale verhitting. Vervolgens koelt het verhitte complex af door overdracht van thermische energie naar de acetonitril omgeving (met een tijdsconstante van 1.4±0.1 ps). Voor een kleine fractie van de clusters leidt het exciteren van de O–H strekvibratie tot een dissociatie van één van de waterstofbruggen van het proton hydratatiecomplex, wat tot gevolg heeft dat een watermolecuul losraakt van het complex. Dit tweede relaxatiekanaal leidt tot een reductie van de absorptie van de O–H strekvibraties. Deze reductie van de absorptie van de O–H strekvibraties van het gedissocieerde complex heeft een hoge geassocieerde anisotropiewaarde, omdat de excitatiekans van het proton hydratatiecomplex, en dus de kans op predissociatie, intrinsiek afhankelijkheid is van de relatieve oriëntaties en van de overgangsdipoolmomenten van de O–H strekvibraties van het complex ten opzichte van de polarisatie van de pomppuls.

Een vergelijkbare predissociatie van proton hydratatiecomplexen nemen we waar in *hoofdstuk 7*. In dit hoofdstuk onderzoeken we de dynamica van de buigvibratie van hydronium (H_3O^+) in gehydrateerde Nafion membranen. De geëxciteerde buigvibratie relaxeert via twee relaxatie paden. De grootste fractie vervalt naar een tussenliggende toestand met een tijdsconstante T_1 van 175

fs. Deze toestand correspondeert met een zeer sterke lokale verhitting van het proton hydratatiecomplex. Vervolgens koelt het complex en stelt zich een thermisch evenwicht in. Dit proces vindt plaats met een tijdsconstante T_{eq} van 1.53 ps. Een kleine fractie van de geëxciteerde buigvibraties relaxeert via predissociatie van één van de waterstofbruggen van het complex. Dit proces leidt tot een lang-levende bleking van de absorptieband van de buigvibratie. Omdat de kans op excitatie en dus predissociatie afhangt van de oriëntatie van het overgangsdipoolmoment van het complex ten opzichte van de polarisatie van de pomppuls,.heeft dit blekingssignaal een hoge geassocieerde anisotropie. Deze anisotropie vervalt met een lange tijdsconstante van 38±4 ps, waarschijnlijk door structurele relaxatie van het proton hydratatiecomplex in de Nafion nanokanalen.

In hoofdstuk 9 gebruiken we vibrationele oppervlakte som-frequentie generatie (VSFG) spectroscopie om de vibrationele respons van de hydratatieschillen van hydrofobe anionen zoals triflaat ($CF_3SO_3^-$), ethaansulfonaat ($C_2H_5SO_3^-$), en butaansulfonaat ($C_4H_9SO_3^-$) te bestuderen. De toevoeging van deze ionen heeft een groot effect op het VSFG spectrum van de watermoleculen aan het oppervlak van de oplossing. Dit effect is heel anders voor oplossingen in H_2O dan in D_2O. Voor oplossingen in H_2O leidt het toevoegen van deze hydrofobe ionen tot een sterke blauwverschuiving van de VSFG band van de waterstofgebrugde O–H strekvibraties. De amplitude van deze band verandert echter weinig. Voor oplossingen in D_2O leidt het toevoegen van deze ionen tot een hele kleine verschuiving van de VSFG band van de de waterstofgebrugde O–D strekvibraties, maar wel tot een sterke toename van de amplitude van deze band. Dit resultaat kan worden verklaard uit een sterk isotoop effect op de intra- en intermoleculaire menging van de O–H/O–D strekvibraties in de hydratatieschillen van de hydrofobe anionen. De mate waarin de O–H strekvibraties mengen hangt af van de sterkte van de dipool-dipool koppeling en het intrinsieke frequentieverschil van de ongekoppelde vibraties. Voor de onderzochte hydrofobe anionen bestaat er een groot verschil in frequentie tussen de O–H vibraties die waterstofgebrugd zijn aan de anionische groep en de O–H vibraties die zich in de nabijheid van het hydrofobe deel van het anion bevinden. Voor H_2O is de dipool-dipool koppeling $\sim$2 keer zo sterk als voor D_2O, terwijl het frequentieverschil slechts $\sim\sqrt{2}$ keer zo groot is als voor D_2O. De sterke dipool-dipool koppeling tussen O–H strekvibraties leidt ertoe dat voor hydrofobe anionen in H_2O de O–H vibraties rond het anion gemengd en gedelocaliseerd zijn. Voor D_2O is de koppeling zwakker en hebben de O–D vibraties bij de anionische groep en de hydrofobe groep een veel meer lokaal karakter. Dit isotoopeffect wordt niet waargenomen voor andere ionen zoals perchloraat (ClO_4^-), doordat voor deze ionen er een veel kleiner frequentieverschil bestaat tussen de water hydroxylgroepen die waterstofgebrugd zijn aan de anionische groep, en de water hydroxylgroepen die waterstofgebrugd zijn aan andere water moleculen. Dit heeft tot gevolg dat de hydroxylstrekvibraties in de hydratatieschil van ClO_4^- zowel in H_2O als in D_2O een sterk gemengd en gedelokaliseerd karakter bezitten.

Acknowledgement

All the work presented in this thesis would not have been done without support from many people, my colleagues, friends and family and also all the reviewers. I would like to take this opportunity to express my gratitude to all of you.

First of all I truly thank my supervisor Prof. Huib J. Bakker for his supervision with patience and inspiration. Thank you, Huib, for your countless work from the explanations and discussions on the experiment results to the tireless correction of the manuscripts and thesis. I have learned a lot from you not only about knowledge but also the way of getting things done.

There are a group of people I would like to thank for the pleasant cooperations on different projects: Niklas for the collaboration on proton clusters in acetontrile. Stephan for the work on hydronium bending mode. Johannes for the collaboration on the vibrational dynamics of hydroxide hydration shell. Simona for the observation of isotope effect of O-H/O-D vibrations around hydrophobic ions at the water interface. I would like to thank Ellen and Sietse for all the detailed explanations, instructions and direct help with setups at the beginning of my PhD. Hinco, a guy who makes impossible possible, for all the technical support, specially all kinds of sample cells. Jan for keeping the laser systems always alive and direct help on optics.

I would like to thank all the members in Bakker group and Rezus group for never letting me down when I needed help, discussions and suggestions, no matter if it was about work or life. The last five years I spent in the ultrafast spectroscopy group is about more than science. I have experienced the atmosphere within the group as very warm and pleasant, specially during tea/coffee breaks, lunch club, group uitje, drinks in Friday evenings with all of you: Artem, Carien, Giulia, Hinco, Jan, Janneke, Klaas-Jan, Konrad, Lianne, Łukasz, Marcin, Niels, Niklas, Oleg, Roel, Simona, Stephan, Yves and Wilbert. Special thanks go to the Sinterklaas party organizers, Ellen and Niklas. My former office mates Łukasz and Sietse, thank you for the office concert and discussion which helped me to integrate to the new environment. Simona, we had so much good time together in and out of office. Stephan, thank you for all the discussions, answers and understanding.

It is hard to thank everyone in limited words. So thank you to everyone who

has helped me and contributed to the thesis. My life in the Netherlands has always been accompanied by Chinese friends. I would like to thank all of you for the taste of China and Spring Festival.

Of course, I would like to thank AMOLF for the motivational atmosphere on research and the excellent support team for all the help on softwares, electronics and chemicals. Thanks to the Bonn group and Woutersen group for the inspirational work discussions.

Finally I would like to thank my family. Dear Family, all my love goes for you. It is your confidence, encouragement and support that has brought me this far. Mom, Dad and Lida I missed you so much, now I am back. 爸妈和程，我回来了。公公和婆婆，感谢你们对我的支持和鼓励。 Dear Peihan, my sweetheart, Mom loves you forever. And Zhe, my love, I promise what you promised.